Master's thesis

NTNU
Norwegian University of Science and Technology
Faculty of Engineering
Department of Structural Engineering

Yahya Muhyiddin

Sample preparation and the pilot testing of an oxygen consumption test that assesses the extent of pyrrhotite oxidation in sulfide-bearing concrete aggregates

Master's thesis in Civil and Environmental Engineering
Supervisor: Klaartje De Weerdt
Co-supervisor: Jan Lindgård, Nikolas Oberhardt, Mahsa Bagheri
June 2023

NTNU
Norwegian University of
Science and Technology

Yahya Muhyiddin

Sample preparation and the pilot testing of an oxygen consumption test that assesses the extent of pyrrhotite oxidation in sulfide-bearing concrete aggregates

Master's thesis in Civil and Environmental Engineering
Supervisor: Klaartje De Weerdt
Co-supervisor: Jan Lindgård, Nikolas Oberhardt, Mahsa Bagheri
June 2023

Norwegian University of Science and Technology
Faculty of Engineering
Department of Structural Engineering

NTNU
Norwegian University of
Science and Technology

Department of Structural Engineering
Faculty of Engineering
NTNU- Norwegian University of Science and Technology

ACCESSIBILITY

OPEN

MASTER THESIS 2023

SUBJECT AREA:	DATE:	NO. OF PAGES:
Concrete Technology	27.06.2023	141

TITLE:

Sample preparation and the pilot testing of an oxygen consumption test that assesses the extent of pyrrhotite oxidation in sulfide-bearing concrete aggregates

Oppredning av tilslag og pilot-testing av en oxygen consumption test som evalurerer oksidasjonspotensialet til magnetkis i sulfidholdige betongtilslag

BY:

Yahya Muhyiddin

SUMMARY:
The presence of pyrrhotite, a mineral consisting of iron and sulfur, in concrete aggregates can cause considerable damage to concrete structures. In 2016, a Canadian testing protocol was introduced, the aim of which was to investigate whether sulfide-bearing aggregates can be safely used in concrete.
This master's thesis focused on the second step of the Canadian testing protocol, the oxygen consumption test (OCT). This test measures the oxygen consumption of aggregate material in a hermetically closed cell over three hours. Samples from four aggregates, two Norwegian and two Canadian, were prepared and then tested with the OCT as part of this study.
The OCT setup at the SINTEF Concrete Laboratory is fully operative. One sample preparation process involving steel and tungsten carbide equipment was preliminarily found to be efficient and free of iron contamination.
The OCT results (oxygen consumption) seem reasonable, particularly for the Norwegian aggregates. However, the results for the two Canadian aggregates were significantly lower than the oxygen consumption reported by earlier work on the OCT in Canada. This might be due to a systematic source of error that requires further investigation.
A detailed procedure for the oxygen consumption testing in Norway, including a sample preparation process, was developed based on the existing literature on the OCT and the experience acquired through the work on the master's thesis.

RESPONSIBLE TEACHER: Klaartje De Weerdt

SUPERVISOR(S): Klaartje De Weerdt. Jan Lindgård. Nikolas Oberhardt. Mahsa Bagheri.

CARRIED OUT AT: Department of Structural Engineering, NTNU

Preface

This master's thesis is written as part of the 5-year master's program of Civil and Environmental Engineering at the Norwegian University of Science and Technology. The thesis was written during the spring of 2023 over a period of twenty-two weeks. Thirty ECTS are awarded upon successfully completing the master's thesis.

The thesis is a part of Work package 2 (WP2) of the Norwegian R&D project on pyrrhotite. The aim of the project is to better understand how pyrrhotite contributes to the degradation of concrete and to ensure that sulfide-bearing aggregates can be safely used in concrete. The project is led by NTNU, with partners including SINTEF, the Norwegian Public Roads Administration, BaneNOR, and Heidelberg-Cement Northern Europe. This thesis is a continuation of my specialization project [1] (TKT4550 Konstruksjonsteknikk fordypningsprosjekt) titled "*Discussion of the test parameters for an oxygen consumption test used to measure the pyrrhotite reactivity of sulfide-bearing aggregates"*. The specialization project was completed in the fall of 2022.

I would like to thank Dr. Jan Lindgård for his exemplary support and guidance which made this master's thesis an incredibly fulfilling educational journey. I am greatly indebted to PhD candidate Nikolas Oberhardt for his exceptional feedback and mentorship. Gratitude is also due to Professor Klaartje De Weerdt for introducing me to this interesting topic and for encouraging me to be part of the research project. I would as well like to thank Dr. Mahsa Bagheri, Associate Professor Kurt Aasly and Professor Rolf Arne Kleiv for providing me with great suggestions during discussions on the master's thesis.

Furthermore, my deepest gratitude goes to the technical staff at NTNU (Kornel Mateusz Tobiczyk) and SINTEF (Jonny Tverdal, Milos Duric, Frode Dalsaune, Odne Oksavik, Egil Rognvik, Daniel Lossius Voll, Joakim Eggen) who did not hesitate to offer me assistance and advice throughout this research endeavor. Moreover, I am thankful to the help from researchers Tobias Danner and Marit Haugen from SINTEF. Finally, I would like to thank Dr. Andreia Rodrigues who happily answered my countless questions.

I am also grateful to have had the opportunity to participate in the Canada-Norway workshop on pyrrhotite in Reykjavik, Iceland in May 2023. The experience was educationally and socially enriching.

Trondheim, spring 2023

Yahya Muhyiddin

Abstract

The presence of pyrrhotite, a mineral consisting of iron and sulfur, in concrete aggregates can cause considerable damage to concrete structures. In 2016, a Canadian testing protocol was introduced, the aim of which was to investigate whether sulfide-bearing aggregates can be safely used in concrete.

This master's thesis focused on the second step of the Canadian testing protocol, the oxygen consumption test (OCT). This test measures the oxygen consumption of aggregate material in a hermetically closed cell over three hours. Samples from four aggregates, two Norwegian and two Canadian, were prepared and then tested with the OCT as part of this study. The focus was to help establish the experimental setup of the OCT in Norway and to assess whether that the obtained results are reasonable. The process of sample preparation, in particular, was investigated, and the aim was to develop a methodology that was both efficient and contamination-free.

The OCT setup at the SINTEF Concrete Laboratory is fully operative. One sample preparation process involving steel and tungsten carbide equipment was preliminarily found to be efficient and free of iron contamination.

The particle size of the aggregate material is one of the parameters of the OCT. The particle size of test samples was determined both by sieving and by laser scattering (optical technique). The two methods gave significantly different particle size distributions.

The OCT results (oxygen consumption) seem reasonable, particularly for the Norwegian aggregates. However, the results for the two Canadian aggregates were significantly lower than the oxygen consumption reported by earlier work on the OCT in Canada. This might be due to a systematic source of error that requires further investigation.

Testing on one of the Norwegian aggregates preliminarily showed that increasing the duration of the OCT (to 16.7h) can lead to significantly higher oxygen consumption.

A detailed procedure for the oxygen consumption testing in Norway, including the sample preparation process, was developed based on the existing literature on the OCT and the experience acquired through the work on the master's thesis.

Sammendrag

Når betongtilslag inneholder magnetkis, et mineral som består av jern og svovel, kan dette føre til betydelige skader på betongkonstruksjoner. I 2016 ble en kanadisk testprosedyre introdusert. Målet med denne testprosedyren er å finne ut hvilke sulfidholdige tilslag som eventuelt kan brukes i betong.

Denne masteroppgaven har fokus på trinn to i den kanadiske testprosedyren, nemlig the oxygen consumption test, «OCT». Testen måler hvor mye oksygen som forbrukes av tilslagsmaterialet i en hermetisk lukket reaksjonscelle (beholder) i løpet av tre timer. Prøver fra fire tilslagstyper, to fra Norge og to fra Canada, ble preparert og etterpå testet med OCT som en del av denne oppgaven. Fokuset var å bidra til å bygge opp et eksperimentelt oppsett for OCT i Norge, samt vurdere om resultatene man får er fornuftige. Oppredningen av tilslag var spesielt satt i fokus, og målet var å utvikle en oppredningsprosedyre som både er effektiv og fri for kontaminering.

Det eksperimentelle oppsettet hos SINTEF Betonglaboratoriet er fult operativt. En oppredningsprosedyre som kombinerer wolfram- og stålutstyr, er funnet å være effektiv og med lav risiko for kontaminering av prøver.

Partikkelstørrelsen til tilslagsmaterialet er en av de viktigste parameterne til OCT. Partikkelstørrelsen til testprøvene ble bestemt gjennom sikting og gjennom en optisk metode (laser scattering). Store forskjeller mellom de to metodene ble avdekket, spesielt siden den optiske metoden viser større antall partikler <75 μm og >150 μm.

Alt i alt, resultatene fra OCT virker rimelige, spesielt for de norske tilslagene. Resultatene for de kanadiske tilslagene var mye lavere enn referanseverdiene i Canada, noe som kan tyde på en systematisk feilkilde som kunne ha påvirket resultatene fra pilot-testingen. En mulig feilkilde burde derfor undersøkes nærmere.

Et av de norske tilslagene ble testet i OCT med en lengere testperiode (16.7h sammenlignet med 3.5h). Den nye testperioden førte til betydelig høyere oksygenforbruk i reaksjonscellen.

Gjennom erfaringen fra denne masteroppgaven, og litteraturstudiet om OCT, ble det mulig å utvikle en norsk OCT-prosedyre som inkluderer oppredning av tilslagsmaterialet.

List of abbreviations

[OCT] Oxygen consumption test

[AMBT] Accelerated mortar bar expansion test

[NTNU] Norwegian University of Science and Technology

[SINTEF] Stiftelsen for industriell og teknisk forskning (English: The Foundation for Industrial and Technical Research)

[NPRA] Norwegian Public Road Administration

[IGP] Department of Geoscience and Petroleum

[NBTL] Norsk Betong og Tilslagslaboratorium (English: Norwegian concrete and aggregate laboratory)

[ULaval] Laval University (Université Laval)

[ERDC] The U.S. Army Engineer Research and Development Center

[DTA] Differential thermal analysis

[SEM] Scanning electron microscopy

[XRD] X-ray diffraction

[XRF] X-ray fluorescence

[XPS] X-ray photoelectron spectroscopy

[MSK] Maskimo aggregate from Trois-Rivières, Quebec, Canada

[BBM-C] Sample preparation methodology involving a bench ball mill with ceramic balls

[BBM-S] Sample preparation methodology involving a bench ball mill with steel balls

[VDM-S] Sample preparation methodology involving a vibratory disk mill with a steel grinding set

Table of Contents

1 Introduction

1.1 Motivation

Sulfide-bearing aggregates are responsible for severe concrete deterioration in cases mainly observed in the US and Canada. The deterioration of concrete seems to be driven by the oxidation of the iron-sulfide pyrrhotite, which in turn causes an internal sulfate attack in concrete. The result is deleterious expansion, cracking and potential collapse of the structures made from the affected concrete.

Currently, there are no fully developed tests that can reliably identify potentially deleterious sulfide-bearing aggregates. However, a three-step Canadian testing procedure is currently under development. This testing procedure was introduced by Rodrigues et al. [2] in 2016 and involves one chemical test (Step I – total sulfur content) and two performance tests (an oxidation test and an accelerated mortar bar test – Steps II and III).

The goal of the Norwegian research project on pyrrhotite is to investigate whether the current limit values for sulfide-bearing aggregates (regulations concerning the total sulfur content) need to be challenged. Part of the research project is therefore about the development of new test methods that can identify deleterious sulfide-bearing aggregates. To reach that end, SINTEF is carrying out the pilot testing of the two performances tests (Steps II and III) of the Canadian testing protocol. The pilot testing of Step III of the protocol (the accelerated mortar bar expansion test - AMBT) was initiated at the end of 2021. In recommendations for further work, my specialization project [1] written last semester (fall 2022) provided an early suggestion on how the pilot testing of Step II (the oxygen consumption test – OCT) should be conducted, in addition to suggestions on the parameter study. This master's thesis focuses on planning, preparing samples for, and carrying out the pilot testing of the OCT during the spring of 2023.

The OCT was first developed to test sulfide oxidation in mine tailings [3]. As part of the Canadian testing protocol, the test was modified to quantify the potential of sulfide oxidation in sulfide-bearing aggregates. If the oxidation potential (i.e., oxygen consumption in the test) is above a certain critical limit, the aggregate should be subjected to further testing (accelerated mortar bar expansion test) [2].

1.2 Objectives

The main objective of this thesis is to perform and contribute to a successful pilot testing with the OCT in Norway. More specifically, the thesis aims at the following:

- To ensure that the OCT setup in Norway is operating successfully.
- To ensure that the OCT results are properly corrected for changes in the testing environment (temperature and relative humidity).
- To test Norwegian aggregates with the OCT, thereby contributing to develop critical oxygen consumption thresholds that apply to Norwegian aggregates.
- To develop a detailed test procedure for the OCT with a focus on sample preparation.
- To vary some of the parameters of the OCT and achieve a better understanding of how these parameters affect the oxygen consumption results.
- To test Canadian aggregates and compare results with the Canadian research team.

1.3 Approach and structure of the thesis

The work on the master's thesis started by reviewing literature on pyrrhotite's role in concrete deterioration and, more specifically, on the OCT. A literature review on the OCT was conducted as part of the specialization project [1] (TKT4550 Konstruksjonsteknikk fordypningsprosjekt) in the fall of 2022. During the early stages of work on the master's thesis, additional literature on pyrrhotite and the OCT was reviewed, with the aim to focus on these topics not previously discussed (or only briefly mentioned) in the specialization project.

The background of the M.Sc. study is presented in **Chapter** 2. This Chapter is necessary to understand the context of the problem the OCT is attempting to solve. After all, the OCT is not a stand-alone test; it is rather a step in a larger test procedure that aims to detect deleterious sulfide-bearing aggregates.

Section 2.1 presents the deterioration cases observed in Canada and in the US. The section then introduces pyrrhotite, explains how it attacks concrete and summarizes the factors affecting its oxidation. In **Section** 2.2, the Norwegian and Canadian research projects on pyrrhotite are introduced. The section also provides details on relevant regulations. **Section** 2.3 introduces the oxygen consumption test and summarizes the procedure mentioned in the 2019 Annex P of the Canadian concrete standard (CSA A23.1:19/A23.2:19). **Section** 2.4 is entirely taken from the specialization project [1] (from the course Konstruksjonsteknikk fordypningsprosjekt, TKT4550) carried out last semester. The section describes the parameters of the OCT and reviews the literature discussing these parameters.

Chapter 3 outlines the stepwise manner by which the laboratory work and the pilot testing was conducted. **Chapter** 4 introduces the aggregate types prepared and tested as part of the present work. **Chapter** 5 presents and discusses the test matrix. For the pilot testing to be successful, proper understanding of the equipment used is necessary. Information about the equipment is summarized in **Chapter** 6.

Discussion of the sample preparation and the pilot testing methodologies are presented in **Chapter** 7. Results obtained from sample preparation and the oxygen consumption testing are outlined in **Chapter** 8, and these results are discussed in **Chapter** 9. The main findings are summarized in **Chapter** 10, and recommendations for further work are described in **Chapter** 11.

1.4 Scope and limitations

At the beginning of the present study, the focus was mainly on conducting many oxygen consumption tests with various aggregates and experiment with different test parameters (see Appendix A Table A.1). However, aggregate preparation took significantly longer time than anticipated, and this caused the scope of the thesis to slightly change. The new scope involved a stronger focus on sample preparation and on developing a reliable and efficient sample preparation procedure for the OCT. Several oxygen consumption tests were carried out, but significantly less than originally planned. Appendix A Table A.2 presents the revised test matrix.

Time and costs were two limitations affecting this study. As mentioned before, sample preparation was time-consuming. Towards the start of the M.Sc. study, sample preparation took place mostly at the IGP Mineral Processing Laboratory. The equipment at the Mineral Processing Laboratory was not always available because it could be booked by other students or projects. Later during the laboratory work, the preparation of samples was carried out by the technical staff at the SINTEF Rock Laboratory. However, there were limitations to the availability of the technical staff given that they had other projects and responsibilities.

Sample preparation was also cost intensive. An hourly fee for using the laboratory was charged to the research project, in addition to the labor cost when SINTEF employees carried out sample preparation. Cost limitations due to expensive sample preparation was one of the reasons behind limiting the number of oxygen consumption tests to be carried out.

Another limitation was the availability of one the Canadian aggregates (MSK 0.9) tested in this study. Only a limited amount of this aggregate was available (only 2.5 kg), and only one OCT test could be carried out. Had more of the aggregate material been available, more tests could have been performed, and that would have helped especially with the interpretation of the results.

2 Background

2.1 Degradation of concrete due to sulfide-bearing aggregates

2.1.1 Cases of pyrrhotite degradation

The earliest documented case of concrete degradation due to sulfide-bearing aggregates was found in Oslo, Norway [4] (1959). Since then, concrete deterioration due to sulfide-bearing aggregates has also been observed in the UK [5], Spain [6], Switzerland [7] and most recently in Canada [8] and the Eastern United States [9]. The PhD thesis of A. Rodrigues [10] and the work of Jana [11] provide a comprehensive overview of the cases of concrete degradation due to iron sulfides. Most cases of degradation can be linked to pyrrhotite, with only a few cases associated with pyrite. This section will focus on the recent cases in North America.

2.1.1.1 Cases of degradation in the Trois-Rivières region in Quebec, Canada

The concrete foundations of 900+ commercial and residential buildings in the Trois-Rivières region in Quebec suffered substantial damages due to iron sulfides between 1996 and 2008 [8, 12]. The damage often occurred less than five years after construction [8]. The aggregate materials were supplied by the Saint-Boniface quarry located in the Trois-Rivières region. The observed damages included map cracking of house foundations with yellowish coloration of the nearby surface. Rust, open cracks and pop-outs of aggregates were also observed [8]. See Figure 2.1 (pictures A and B) for examples of observed damages in Quebec [12]. Rodrigues et al. [8] reported that, in some cases the severity of the concrete degradation was so high that it constituted a significant structural threat to the house, ultimately causing the need to replace the foundation of the house. The macroscopic and stereomicroscopic examination of cores from damaged house foundations in Quebec concluded that pyrrhotite oxidized while pyrite did not [8].

Figure 2.1: (A) and (B) examples of damage from the Trois-Rivières region. (C) damaged house foundation in Connecticut, USA. Figure taken from [12] and modified.

2.1.1.2 Cases of degradation in Connecticut and Massachusetts, USA

The concrete foundations of thousands of residential and commercial buildings suffered from damages due to sulfide-bearing aggregates in Northeastern Connecticut (CT), USA, with more than 34,000 house at risk [9, 11]. 10,000 house foundations in Massachusetts are also be affected to various degrees [13]. Damages were seen between 10 and 20 years after construction, substantially longer compared to the cases in Eastern Canada. The deterioration of concrete caused map cracking with large amounts of whitish powder forming near the cracks. Reddish-brown stains (rust stains) were also observed in the vicinity of cracks [9, 11]. See Figure 2.1 (picture C) for examples of damages in CT, USA [12].

The majority of deterioration cases in the US ("the pyrrhotite epidemic" as called by Jana [11]) can be traced to aggregates supplied from Becker's quarry in Willington, CT [13]. Metamorphic rocks that contain substantial amounts of pyrrhotite can be found in the vicinity of the quarry [13]. Figure 2.2, taken from [14], shows a map of pyrrhotite occurrence in the continental US.

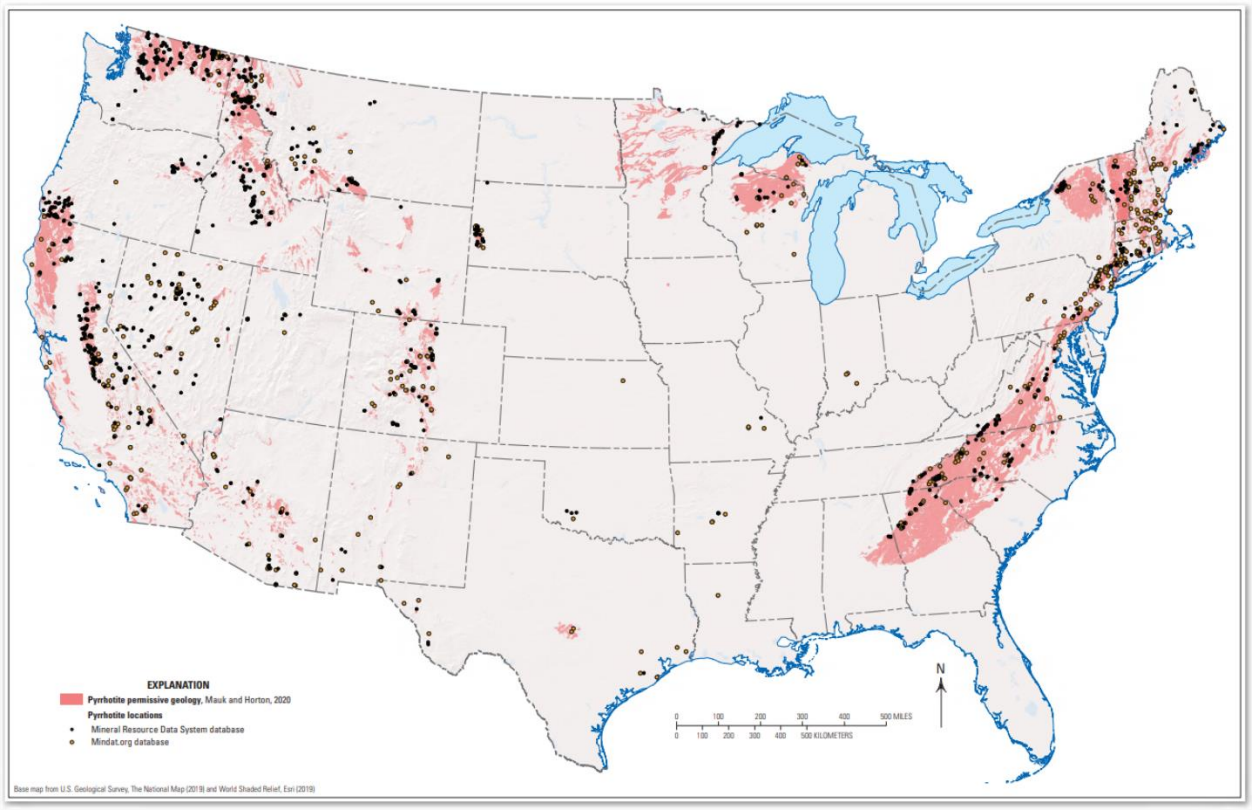

Figure 2.2: A map of the contintential US by the US Geological Survey (USGS). The map shows areas where pyrrhotite can occur (shaded with pink) and areas where pyrrhotite has been found (black and dark yellow dots). The data sources in the map are geolocial databases (shown in the figure) and [15]. Figure taken from [14].

2.1.2 Characteristics of pyrrhotite

Pyrrhotite is one of the most prevalent iron sulfide minerals, second only to pyrite, FeS_2 [16]. Pyrrhotite has a non-stoichiometric composition expressed in the formula $Fe_{1-x}S$ (with the value of x between 0 and 0.125) [16]. Because of this non-stoichiometry, pyrrhotite can have different crystal structures, ranging from pure monoclinic (pseudohexagonal) to pure hexagonal [17, p. 590]. The crystal structure of pyrrhotite is a function of the iron deficiency of pyrrhotite [17, p. 591]. Monoclinic structures arise when pyrrhotite is most iron-deficient, while hexagonal structures are the result of fewer iron deficiencies [18, 19]. Pyrrhotite with structure FeS (i.e., x=0) is called troilite, and this form of pyrrhotite is non-magnetic (antiferromagnetic) [17, p. 590].

Pyrrhotite exists in a wide variety of rocks, especially those of the volcanic and the mafic intrusive types [16]. Pyrrhotite is often found together with other (iron) sulfide minerals including pyrite and chalcopyrite [16]. In the host rocks, pyrrhotite typically forms bands that have a plate-like structure [20]. The distribution of pyrrhotite is often inhomogeneous in the host rock [12].

2.1.3 Mechanism of attack

The deterioration mechanism associated with pyrrhotite damage consists of two steps [8]. The first step involves the oxidation of pyrrhotite, resulting in the formation of sulfuric acid (see equation 1). Various forms of rust are also produced, including iron hydroxides and oxyhydroxides [16]. The second step is an internal sulfur attack: sulfuric acid reacts with portlandite forming gypsum, ettringite and potentially thaumasite (see equations 3, 4 and 5). Deterioration occurs because of the expansive nature of both these steps [8, 21]. Figure 2.3 shows a schematic view of the concrete degradation mechanism caused by pyrrhotite.

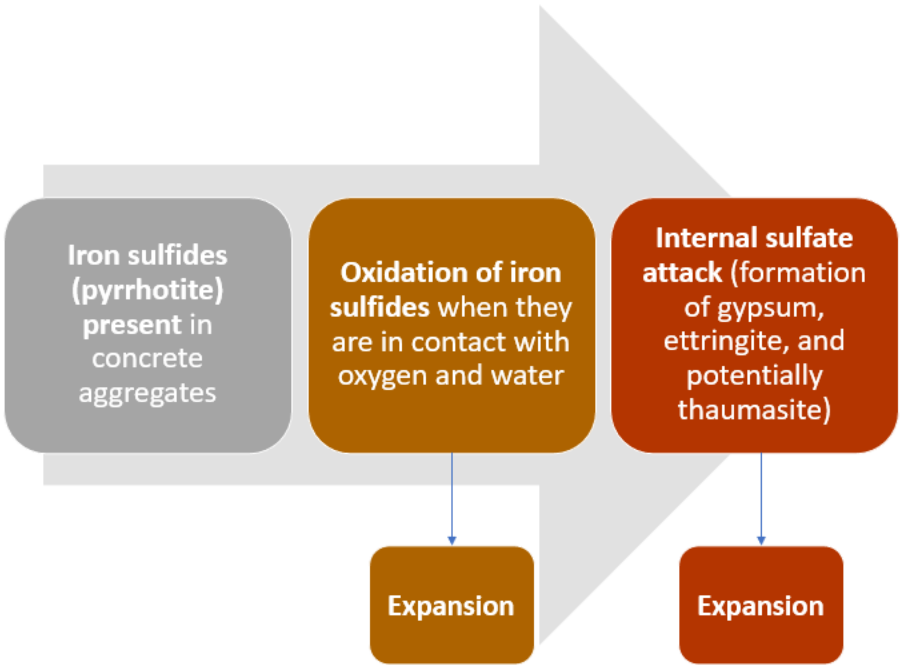

Figure 2.3: The figure illustrates the pyrrhotite degradation mechanism. Figure was created based on [8, 21].

According to Nicholson and Scharer [22], pyrrhotite oxidizes when it reacts with water and oxygen according to the following equation :

$$Fe_{1-x}S + \left(2 - \frac{1}{2}x\right)O_2 + xH_2O \rightarrow (1-x)Fe^{2+} + SO_4^{2-} + 2xH^+ \qquad (1)$$

Ferrous ions (Fe^{2+}) are produced in equation 1, the pyrrhotite oxidation reaction. These ferrous ions can oxidize to ferric ions (Fe^{3+}). When the pH is above 3.5, the precipitation of ferric hydroxide (rust) can occur [8, 16]:

$$Fe^{3+} + 3H_2O \rightarrow Fe(OH)_3 + 3H^+ \quad (2)$$

Further reactions of ferrous and ferric iron can lead to multiple forms of rust, including ferrihydrite and goethite [12, 16]. The formation of ferric ions (Fe^{3+}) also leads to further oxidation of pyrrhotite [16].

The sulfuric acid formed from the oxidation of pyrrhotite (equation 1) may initiate a reaction chain causing an internal sulfate attack in the concrete [8]. Gypsum can be produced when the sulfuric acid and portlandite react [23]:

$$H_2SO_4 + Ca(OH)_2 \rightarrow CaSO_4 \cdot 2H_2O \quad (3)$$

Gypsum ($CaSO_4 \cdot 2H_2O$) may react with aluminate (C_3A), which is one of the components of Portland cement, forming secondary ettringite ($C_3A \cdot 3CaSO_4 \cdot H_{32}$) according to the following equation [8, 10]:

$$3(CaSO_4 \cdot 2H_2O) + C_3A + 26H_2O \rightarrow C_3A \cdot 3CaSO_4 \cdot H_{32} \quad (4)$$

Rodrigues et al. [8] examined concrete cores from the damaged foundations in Quebec and showed the presence of not only gypsum and ettringite, but also thaumasite, in these cores. The formation of thaumasite ($CaSiO_3 \cdot CaCO_3 \cdot CaSO_4 \cdot 15H_2O$), especially at temperatures (5 ˚C) [24], can take place as part of the internal sulfate attack according to the following equation [8, 10, 25],:

$$\begin{aligned} 2CaCO_3 + 2SiO_2 \cdot H_2O + 2(CaSO_4 \cdot 2H_2O) + 2Ca(OH)_2 + 23H_2O \\ \rightarrow 2(CaSiO_3 \cdot CaCO_3 \cdot CaSO_4 \cdot 15H_2O) \end{aligned} \quad (5)$$

Although the first step of the deterioration mechanism is expansive (pyrrhotite oxidation reaction, see equation 1), the second step (internal sulfate attack, see equations 3, 4 and 5) is responsible for much larger expansion [8, 21].

2.1.4 Factors affecting pyrrhotite oxidation

In the Canadian testing protocol, the OCT provides an intermediate step before possibly starting the mortar bar expansion test for an aggregate where pyrrhotite is present. The duration of the mortar bar expansion test is 180 days [2]. If the OCT can discriminate well between deleterious and non-deleterious aggregates, then a significant amount of time and money can be saved [1].

Current chemical and petrographic techniques used to characterize iron sulfides struggle with multiple limitations. Some techniques can only provide the total sulfur content (Step I in the Canadian testing protocol), others only the content of iron sulfides (without distinguishing each iron sulfide) [12]. For

example, micro X-ray fluorescence (μXRF) cannot quantify pyrite and pyrrhotite content individually and provides only information about the total iron sulfide content [12, 26].

There are a few techniques that can quantify the content of pyrrhotite, but those techniques have serious limitations. Petrographic techniques (such as through a reflected light polarizing microscope) combined with total sulfur content measurements can be used to estimate the content of pyrrhotite in an aggregate sample [12]. However, the calculation remains theoretical, and the sample analyzed in the petrographic technique is small. Limitation of sample size also affects spectroscopic techniques such as XPS (X-ray photoelectron spectroscopy) [12, 26]. Another example is X-ray diffraction which can also differentiate between the content of pyrrhotite and pyrite in an aggregate sample. However, the high sensitivity limit in this technique represents a serious limitation [3].

The complexity of the pyrrhotite oxidation process makes it difficult to predict the oxidation potential of aggregates containing pyrrhotite purely based on total sulfur content, or even total pyrrhotite content. In 2020, Jana [11] summarized the cases of pyrrhotite and pyrite-related attack that are documented in the literature. He found that total sulfur content as SO_3 was in the range from 0.2% to 6% and pyrrhotite content (as a percentage of the volume of total iron sulfides) from <5% to 75%. Jana's findings further prove that quantification of total sulfur or pyrrhotite content might not be sufficient to find the oxidation potential of sulfide-bearing aggregates.

In addition to pyrrhotite content, the pyrrhotite oxidation process depends on many other factors. An overview of these factors is outlined in Janzen et al. (2000) [18], Belzile et al. (2004) [16] and in the PhD thesis of Andreia Rodrigues (2016) [10]. A summary of the most important factors is outlined below (the specific surface area of pyrrhotite, and by extension the particle size, has a very important effect on pyrrhotite oxidation but it is not listed here as it is discussed in detail later in Section 2.4.4 taken from the specialization project [1])

2.1.4.1 Access to oxygen and humidity

Pyrrhotite can be oxidized by oxygen (pH>4) and by ferric iron (pH<4) [16, 27]. As shown in Section 2.1.3, the pyrrhotite oxygen reaction requires both oxygen and water. Experimentally, the necessity of oxygen for pyrrhotite oxidation is demonstrated by the work of Knipe et al. [28].

2.1.4.2 Crystal structure's effect on pyrrhotite reactivity

Different pyrrhotite structures have different levels of reactivity (i.e., oxidation) [12, 18]. The reactivity of different pyrrhotite crystal structures is the subject of disagreement [18, 29]. However, there are indications that monoclinic (magnetic) pyrrhotite with large iron deficiencies is more reactive than hexagonal (non-

magnetic) pyrrhotite [12, 29]. One of the reasons is that the ratio of ferric iron to total iron is higher in monoclinic pyrrhotite compared to hexagonal pyrrhotite [18, 29]. Ferric ions are one of the two oxidants of pyrrhotite [18].

2.1.4.3 Temperature

Pyrrhotite oxidation increases with increasing temperature [30]. In their study on the oxidation kinetics of 12 pyrrhotite samples, Janzen et al. [18] found that the oxidation rate of pyrrhotite by oxygen almost doubled for every 10°C increase in temperature. The measurements of the pyrrhotite oxidation rate took place at three different temperature 25, 35 and 45°C. Kwong [31] also reported a doubling of the pyrrhotite oxidation rate between 25 and 35°C. An earlier work by Janzen [32] shows an increasing rate of oxidation as temperature increases. All these works indicate that the oxidation of pyrrhotite follows Arrhenius behavior (which describes the dependence of the reaction rate on temperature).

2.1.4.4 Electrochemical interactions

Galvanic contact between two sulfide minerals can significantly enhance the oxidation rate [33]. Such interactions between pyrite and pyrrhotite were the subject of further research questions posed by Rodrigues in her PhD thesis [10]. Galvanic interactions between pyrrhotite and pyrite occur because of their rest potentials, which is a measure of their electrochemical stability [34, 35]. Pyrite is characterized by a higher rest potential compared to pyrrhotite [36]. Therefore, when pyrite and pyrrhotite are present in the same aggregate, and where electrochemical contact is established between them, pyrite becomes an anode, and pyrrhotite a cathode [33]. Pyrrhotite is therefore consumed, and the oxidation rate significantly increases. In fact, in Appendix II of the NPRA report [37] on pyrrhotite, Per Hagelia argues that the galvanic interactions between pyrite and pyrrhotite might be the main oxidation mechanism responsible for the damage seen in Trois-Rivières region (as opposed to the oxidation of pyrrhotite on its own without galvanic interactions with pyrite).

2.2 Testing protocols, research, and regulations

2.2.1 The Canadian testing protocol

The cases of deleterious expansion and cracking of concrete that occurred in the Trois-Rivières region highlight the need for testing protocols that are capable of ensuring that no deleterious sulfide-bearing aggregates are used as concrete aggregates.

Rodrigues et al. [2] (2016) presented a testing program for sulfide-bearing aggregates consisting of three steps. The first Step of the testing protocol is to measure the total sulfur content, while Steps II and III reflect the two steps of the degradation mechanism: the oxidation of pyrrhotite followed by an internal sulfate attack [2].

The original protocol as proposed by Rodrigues et al. [2] in 2016 will be presented and summarized first. Proposed modifications to the testing protocol will then be outlined.

Firstly, the total sulfur content of aggregates by mass (S_T, wt. %) is found through chemical techniques (Step I) [2]. Aggregates with total sulfur content exceeding 1 wt. % are automatically rejected. Those with sulfur content below 0.1 wt. % are automatically accepted as concrete aggregates. If the total sulfur content of the aggregate is between 0.1 and 1 wt. %, then aggregate samples are petrographically examined. If petrographic techniques find traces of pyrrhotite, the aggregate moves to Step II of the testing protocol. The total sulfur content limits, in addition to the focus on the indication of pyrrhotite, were proposed by Rodrigues et al. [2] based on the relevant Canadian standards (as will be outlined in Section 2.2.4).

In Step II, aggregates samples are tested with an accelerated oxidation test (oxygen consumption test, OCT) [2]. The goal is to measure how reactive (i.e., vulnerable to oxidation) the iron sulfide minerals in these aggregates are. The test lasts 3.5h and the extent of the sulfide mineral oxidation is quantified based on the oxygen consumption of ground aggregate material (with a certain mass of deionized water mixed in) in a sealed reaction cell [3]. If the oxygen consumption in Step II is higher than 5%, aggregates are then with Step III.

Step III, first introduced by Rodrigues et al. [38] (2015), is an accelerated mortar bar expansion test (AMBT) that consists of two phases [2, 38]. The first phase aims to create conditions suitable for internal sulfate attack in the mortar bars. If the mortar bars expand more than 0.10% in the first phase (90 days), they are rejected. Otherwise, the aggregate is tested in the second phase (90 days), which was found ideal for thaumasite formation. If an increase in the expansion is observed in the second phase, then the aggregate is

rejected, otherwise the aggregate can be used in concrete. The phases of the mortar bar expansion test are outlined in Table 2.1 (based on the work of Rodrigues et al. [38]).

A flowchart of the testing protocol published in 2016 is shown in Figure 2.4.

Table 2.1: Phases of Step III in the Canadian testing protocol, the mortar bar expansion test according to the 2015 work by Rodrigues et al. [38]. Modifications to the test have been suggested.

	Phase 1	**Phase 2**
Purpose	"Conventional" internal sulfate attack (gypsum & ettringite)	Thaumsite formation (requires carbonate source)
Temperature	80°C	4°C
Relative humidity	80%	100%
Wetting cycles	Two cycles (3 h) per week in a 6% bleach solution	Two cycles (3 h) per week in a 6% bleach solution
Effect on aggregates containing sulfide minerals	Expansion	Rapid regain of expansion followed by potential destruction of samples
Effect on control aggregates	No effect	No effect

Annex P [39] of the Canadian standard (2019) for concrete (CSA A23.1:19/A23.2:19) includes a modified version of the testing protocol. The limits for total sulfur content of Step I were modified to 0.15 and 1 wt. %. Annex P [39] also includes a more conservative limit value for Step II (4% oxygen consumption) and revised limit values for Step III (no limit value after phase 1 and 0.10% expansion in phase 2). Figure 2.5, originally taken from [12] and modified in the specialization project [1], shows this modified version of the testing protocol. It should be noted that the limit values of the protocol are still subject to revisions and modifications based on new research and results. New critical limits for the expansion of mortar bars in the AMBT were suggested by El-Mosallamy and Shehata in 2016 [40].

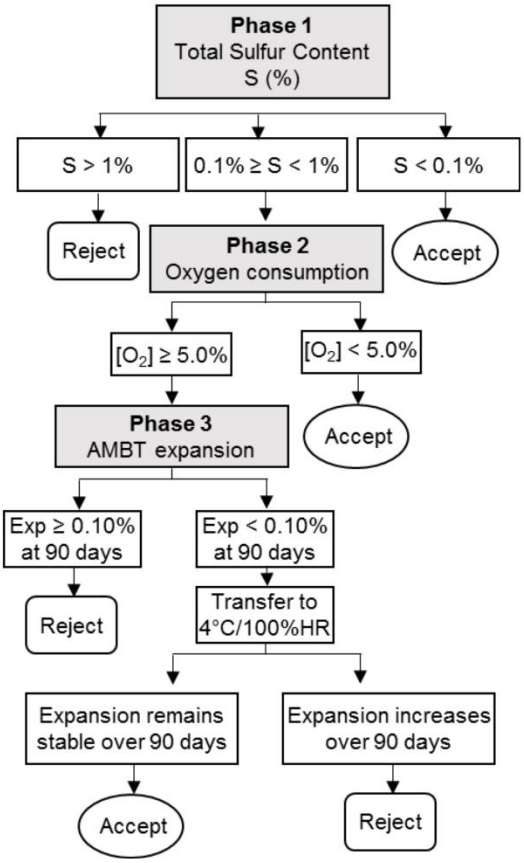

Figure 2.4: Flowchart of the Canadian testing protocol as proposed by Rodrigues et al. [2] in 2016. The figure is taken from [41].

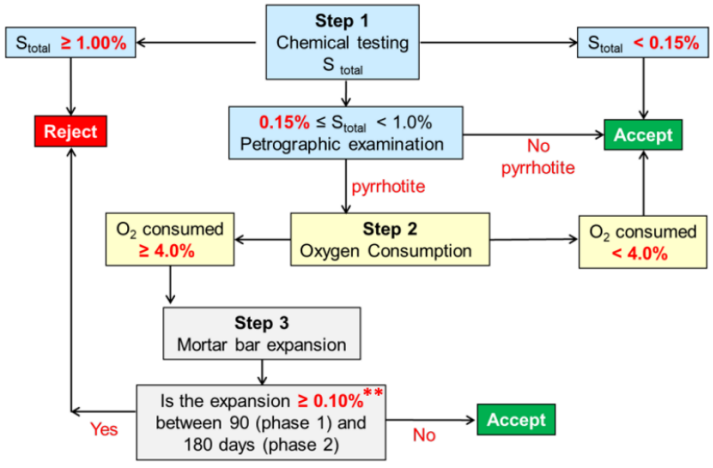

Figure 2.5: Schematic view of the modified Canadian testing protocol in 2019 (as included in Annex P [39]). Original figure taken from [12]. Modified figure taken from the Specialization project [1]. ** During the Canada-Norway workshop on pyrrhotite (held in October, 2022), a new threshold of 0.15% was proposed.

2.2.2 The American testing protocol

In 2018, the U.S. Army Engineer Research and Development Center (ERDC) published what it called "a phased approach" [42] to test concrete aggregates for pyrrhotite-related degradation. Jana [11] combined the recommendations by the ERDC with the Canadian testing protocol by Rodrigues et al. [2] and proposed a testing program consisting of the 5 steps described in the following paragraphs.

Step 1 involves petrographic examination (according to U.S. standard ASTM C295 [43]) of rock cores to look for evidence of iron sulfides. If iron sulfides are not found, then the aggregate is accepted for use as a concrete aggregate. If iron sulfides are found, Step 2 of the procedure is carried out.

Step 2 of the procedure involves chemical testing of rock samples for total sulfur (as SO_3). The ERDC recommends that the total sulfur analysis be carried out using XRF (X-ray fluorescence) or LECO infra-red combustion [42]. If the total sulfur is between 0.10 and 1%, the aggregate is tested with Step 3 of the protocol. Otherwise, the aggregate is either rejected (if S_T > 1 wt. %) or accepted (if S_T <0.1 wt. %) for use as a concrete aggregate.

In Step 3, aggregate samples are tested with XRD (X-ray diffraction) to quantify and characterize pyrrhotite and the other iron sulfides.

If pyrrhotite is found in Step 3, then a short-term oxidation test similar to the OCT is carried out. This oxidation test is based on the work of Wille and Zhong [9] and it involves subjecting ground aggregate material to a 35% solution of hydrogen peroxide. The oxidation potential of the aggregate material is measured by released sulfates (SO_4^{2-}).

If the sulfate release from the previous step is significantly elevated, a long-term performance test (similar to the accelerated mortar bar expansion test proposed by Rodrigues et al. [38]) is suggested. This long term is based on the American standard ASTM C157 [44] which includes a standard test method of length change of mortar bars.

Figure 2.6, taken from Jana [11], shows a flowchart illustrating the various steps of the protocol described above.

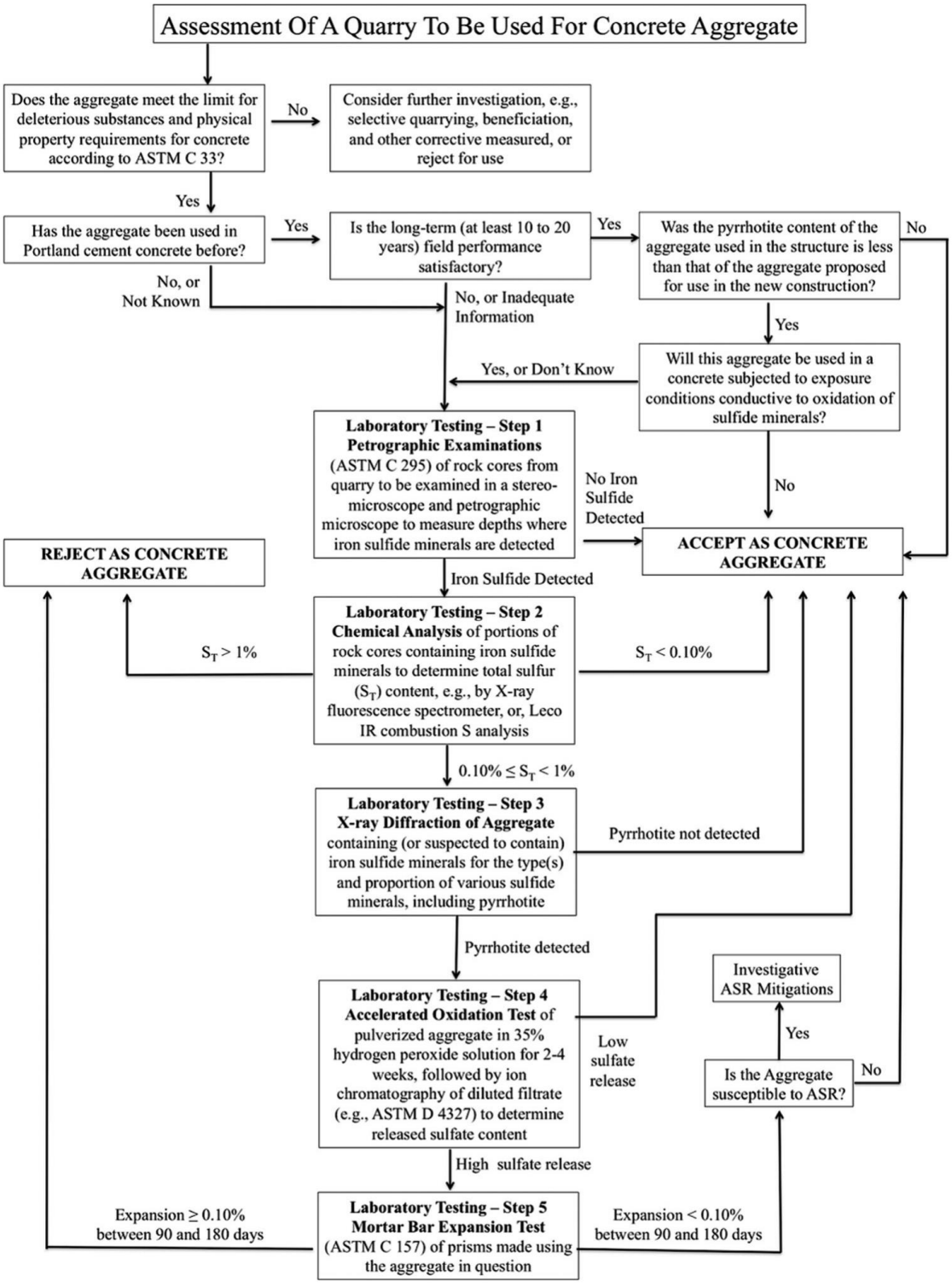

Figure 2.6: The flowchart shows a 5-step testing protocol proposed by Jana [11] based on the recommendations of the ERDC [42] and the Canadian testing protocol [2]. The flowchart is taken from Jana [11].

2.2.3 Norwegian research effort into pyrrhotite

Pyrrhotite became the subject of an important discussion in Norway because of the Follo Line project. According to Ytterdal (2018) [45], construction on the Follo Line project began in 2015. The aim was to use the aggregate masses from the TBM (tunnel boring machines) to produce the prefabricated concrete segments needed for the tunnel. Thus, a prefabricated concrete factory was built at the construction site. However, 30% of samples from the Follo Line project showed high sulfur content (>0.10 wt. %), and 60% contained traces of pyrrhotite [45]. The presence of pyrrhotite in samples with high sulfur content (>0.10 wt. %) resulted in the need to buy commercial aggregates and transport them to the construction site, which had huge economic and environmental consequences.

Following the challenges faced by the Follo Line project, a working group on the pyrrhotite problem was initiated in 2018 by the Norwegian Concrete Association (Norsk Betongforening, NB) [37]. As part of a pre-project, a workshop on the role of pyrrhotite in the degradation of concrete was held in Oslo in 2018, with participants from Norway, Canada, Finland, Switzerland, and the UK. In November 2019, the Norwegian Public Road Administration (NPRA) published a report [37] written by the participants in the pre-project on pyrrhotite-related damage in concrete. The report included an introduction on pyrrhotite and how it can damage concrete. The state-of-the-art report also included a comprehensive literature review on the topic, based on the PhD work of Rodriguez [10]. The proceedings and presentations of the 2018 workshop were also included in the NPRA report [37].

The main Norwegian pyrrhotite research project was started in 2020. The research program is divided into two main parts, work package 1 (WP1) and work package 2 (WP2). The objective of the first work package (WP1) is to quantify and characterize sulfide minerals (particularly pyrrhotite) and achieve a better understanding of the presence of pyrrhotite in Norwegian aggregates. This work package is led by Associate Professor Kurt Aasly at the Department of Geoscience and Petroleum (IGP) at NTNU. Nikolas Oberhardt from the NPRA is the public sector PhD candidate in this project. In addition to his work on sulfide minerals, N. Oberhardt is looking into the methods for measuring the total sulfur content in aggregate samples and how to increase the accuracy of such methods [46]. In 2021, Øystein Fure wrote his master's thesis [47] on the use of conventional and SEM-based techniques for better characterization and understanding of aggregates from Follo Line project in Norway and Trois-Rivières in Canada.

The aim of the second work package (WP2) is establishing test methods and corresponding critical limits that enable the use of sulfide-bearing aggregates in concrete safely. More specifically, WP2 includes the pilot testing of Steps II and III of the Canadian testing protocol at the SINTEF Concrete Laboratories in Norway [48]. WP2 is led by the Department of Structural Engineering at NTNU. The pilot testing of Step

III (mortar bar expansion test) is currently ongoing. Hallvard Lindstad wrote his specialization project [46] and his master's thesis as part of WP2. His master's thesis focused on the pilot testing of the mortar bar expansion test in Norway, including the effect of bleach type on the resulting expansion of the mortar bars. This M.Sc. study is part of the Norwegian research project on pyrrhotite, and it focuses on the pilot testing of Step II (the OCT).

The participants in the Norwegian research project are NTNU, SINTEF, the NPRA, BaneNOR and Heidelberg-Cement Northern Europe. Moreover, the project has close international cooperation with Université Laval (ULaval) in Canada. In October of 2022, a workshop on pyrrhotite-related concrete degradation was held in Quebec City. Another Canada-Norway workshop on pyrrhotite was held in Reykjavik, Iceland in May of 2023. The two workshops were attended by representatives from the Norwegian research project, ULaval, and other Canadian institutions. The workshop consisted of presentations and discussions on most aspects related to pyrrhotite degradation covering the scope of both WP1 and WP2 of the Norwegian research program.

The Norwegian research project is participating in the interlaboratory study launched by ULaval in the early winter-spring of 2023. The study focuses on the interlaboratory testing of the total sulfur analysis and the oxygen consumption test. Aggregate material and necessary equipment for this testing was shipped from ULaval to Norway. In addition, three documents with general guidelines [49], total sulfur determination procedure [50] and oxygen consumption procedure [51] were distributed by ULaval to the participating institutions as part of the interlaboratory study.

2.2.4 Overview of relevant regulations

The European standard EN12620 [52] sets the maximum limit of the total sulfur content allowed in concrete aggregates at 1 wt. %. If pyrrhotite is detected in the aggregate material, the standard mandates an upper limit for the total sulfur content (S_T, wt. %) of 0.1 wt. %. In Norway, the presence of any pyrrhotite is detected by the use of a differential thermal analysis (DTA) [53].

In the 2014 edition of the Canadian concrete standard CSA A23.1 [54], a new Annex P was included, and it mandated new rules similar to those found in the European standard EN12620. When the total sulfur content exceeds 1.0 wt. %, the material cannot be used as aggregate material for concrete. If the sulfur content exceeds 0.10 wt. %, and traces of pyrrhotite are detected, then the material cannot be used for concrete. These rules are to be applied for sources of concrete aggregates that are new or not previously used in concrete.

There is a subtle difference between the previously mentioned Canadian (from 2014) and European limits. With the presence of pyrrhotite, the allowed total sulfur content by mass is 0.1 wt. % in the European standards compared 0.10 wt. % in the 2014 Canadian standard. The European limits are less conservative and practically allow for 0.144 wt. % sulfur content by mass.

In Canada, a modified version of the Canadian testing protocol is included in the new Annex P of the 2019 edition of the Canadian concrete standard CSA A23.1:19/A23.2:19. Annex P is currently only informative (compliance is not mandatory). In the new (2019) Annex P, the total sulfur content is kept at 1.0 wt. %, while the content of allowed sulfur in the presence of pyrrhotite is set at 0.15 wt. % [39] (i.e., almost identical to the European limit).

There are no limits on sulfur content in the relevant American standards. However, the 2019 American standard ASTM C294-19 mentions iron sulfides and their potentially deleterious effects on concrete: "*Marcasite and certain forms of pyrite and pyrrhotite are reactive in mortar and concrete, producing a brown stain accompanied by a volume increase that has been reported as one source of popouts in concrete."* [55]. There are however no indications in the standard on the minimum amount of pyrrhotite that can cause damage in concrete [11].

2.3 The oxygen consumption test (OCT)

2.3.1 Introduction to the OCT

The OCT is the second step of the Canadian testing protocol (see Figure 2.4). The aim of the OCT is to accelerate the oxidation of pyrrhotite. The OCT provides the two reactants necessary for pyrrhotite oxidation (oxygen and water, see equation 1). The oxidation potential of the aggregate material is measured by the consumption of one of the reactants (oxygen). The higher the oxygen consumption, the higher the oxidation potential of the aggregate.

The aggregate material is prepared to a fine particle size (typically <150 µm) and then mixed with a certain amount of water [3, 39]. The mixture is placed in a hermetically sealed plexiglass reaction cell (typically 200 mm in height) with an oxygen sensor mounted on top of the cell (shown in Figure 2.7). The test measures how much oxygen is consumed during 3.5h (the first 0.5h is for the stabilization of the oxygen sensor).

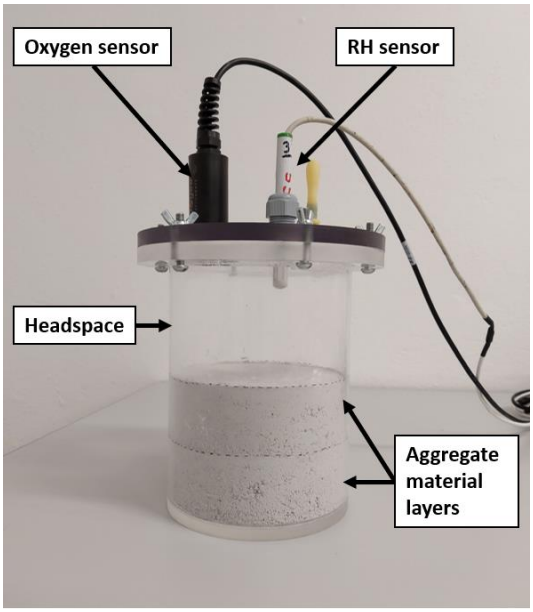

Figure 2.7: The figure shows one of the reaction cells used in the pilot testing with the OCT. The RH sensor shown in the picture is not required by the 2019 Annex P [39] of the Canadian standard (CSA A23.1:19/A23.2:19). The height of the cells purchased from Canada for the pilot testing in Norway is 200 mm and the internal diameter is 146.5 mm.

2.3.2 Development of the OCT

The test was first presented in 2016 in the work of Rodrigues et al. [3]. The test built on the work of Elberling and coworkers [56] and Elberling and Nicholson [57] where oxygen consumption was used as a

method of measuring the extent of sulfide mineral oxidation (particularly that of pyrrhotite) in mine tailings. The transport mechanism considered was the diffusion of oxygen into the mine tailings. The oxygen consumption was calculated based on Fick's second law and assuming steady state conditions [56, 57]. The conclusion was that oxygen consumption through Fick's second law can be used to estimate the oxidation rate of sulfide minerals. Measuring the rate of pyrrhotite oxidation was done to prevent acid rock drainage (toxic waste from mines). Mine tailings typically have a fine grain size (100—200 μm) [57].

The early development of the OCT was done in cooperation with the research team of Professor Bruno Bussière at UQAT (Université du Québec en Abitibi-Témiscamingue) [3].

2.3.3 Test procedure

This section is mainly based on the 2019 Annex P [39] of the Canadian standard of concrete (CSA A23.1:19/A23.2:19). The 2019 Annex P will be hereinafter referred to as Annex P. A much shorter summary of the Annex P procedure was included in the specialization project on the OCT developed last semester [1]. The following summary is more detailed and includes modifications to the procedure proposed during the 2022 Canada-Norway workshop, the 2023 Canada-Norway workshop on pyrrhotite and by the procedure of the interlaboratory study initiated by ULaval in the spring of 2023 [49, 51].

2.3.3.1 OCT setup

The main apparatus of the oxygen consumption test is composed of the three main components [3, 39]:

1. **Reaction cell** (Figure 2.7): plexiglas circular column. The height of the cell is 200 ± 2 mm with an internal diameter of 142 ± 2 mm (146.5 mm for the cell purchased from Canada for the pilot testing). The wall thickness should be 10 mm. During the OCT, the volume of the reaction cell will mainly consist of the aggregate material layers and the headspace (the air-filled volume between the aggregate material and the lid of the reaction cell).
   The cell used by Rodrigues et al. [3] in 2016 had an internal diameter of 141.7 mm and a height of 200 mm.
2. **Data logger** (Figure 2.8a): used for the collection of measurements from the oxygen sensor. Rodrigues et al. [3] used the quad-volt data logger OM-CP-IFC200. A 4-channel HOBO logger is used in the interlaboratory study [51].
3. **Galvanic-cell oxygen sensor** (Figure 2.8b): this oxygen sensor measures the concentration of oxygen inside the reaction cell during the OCT. Rodrigues et al. [3] used the Apogee SO-100 & 200 series (see Figure 2.8).

(a) (b)

Figure 2.8: (a) An example of a data logger that can be used for the OCT. The photo is taken at Ulaval by Dr. Jan Lindgård. (b) Oxygen sensor (Apogee SO-200 Series), picture taken from [58].

2.3.3.2 Sample preparation

The key objective of this step is to ensure that the aggregate material used in the OCT is representative, especially because iron sulfides are often not homogenously distributed in the host rock [11, 12]. To ensure representative samples, the minimum mass of both the subsample and the field sample are included in Annex P (from the standard CSA A23.2-1A). In the Annex P [39] terminology, the subsample is the aggregate mass that is first subjected to crushing. A test specimen (2.5 kg) for the OCT is then obtained in a representative way from the subsample. The test specimen is subsequently subjected to grinding.

More specifically, the subsample is crushed to pass the 2.5 mm sieve, while the subsample is ground to the target size <160 μm. No specific proportion of the material fraction <80 μm is required by Annex P, but it is recommended to avoid the production of too much fine material [39]. However, during the 2022 Canada-Norway workshop on pyrrhotite, it was informed that the following revised particle size is desired for the OCT [59]:

- 50% between 80—160 μm
- 50% between 0—80 μm

The above particle size distribution is also used in the procedure for the interlaboratory study which was circulated by ULaval [49, 51]. The Annex P procedure from 2019 is thus slightly modified, and the test specimen is also sieved over an 80 μm sieve to control the percentage of the fraction <80 μm at 50%.

Note that in Annex P [39] and in the OCT literature [3, 40, 60], the particle size of the aggregate material used in the OCT is determined by sieving (through amount of material passing or retained over a specific sieve opening). The particle size shown for the samples prepared in this M.Sc. study is also determined by sieving unless otherwise specified.

2.3.3.3 Testing room

The room required for testing should comply with the following conditions [39]:

- The OCT is to be carried out in room temperature of 23 ± 2 °C
- The relative humidity in the room cannot decrease below 50%
- The test is to be conducted at atmospheric pressure (see Rodrigues et al. [3])

2.3.3.4 Test setup

The aggregate material layers in the reaction cell (see Figure 2.7) are composed of a mixture of aggregate material and distilled/deionized water, with the necessary mass of each component calculated according to equations 6 and 7, respectively. When mixing the aggregate material with the added water, lumps should be broken down as they might affect the results [51], probably because they reduce the permeability of the aggregate layers to oxygen.

The mixture is added to the reaction cell in two layers, each with a thickness of 5 cm. Multiple compressions by the steel pestle are required to reach the necessary thickness. A video attached to the test procedure in the interlaboratory study provides a visual demonstration of the preparation of the reaction cell [51].

The reaction cell should be hermetically sealed. Thread seal tape and high vacuum grease (as shown in Figure 2.9) can be used to ensure that no oxygen gets in or out of the reaction cell.

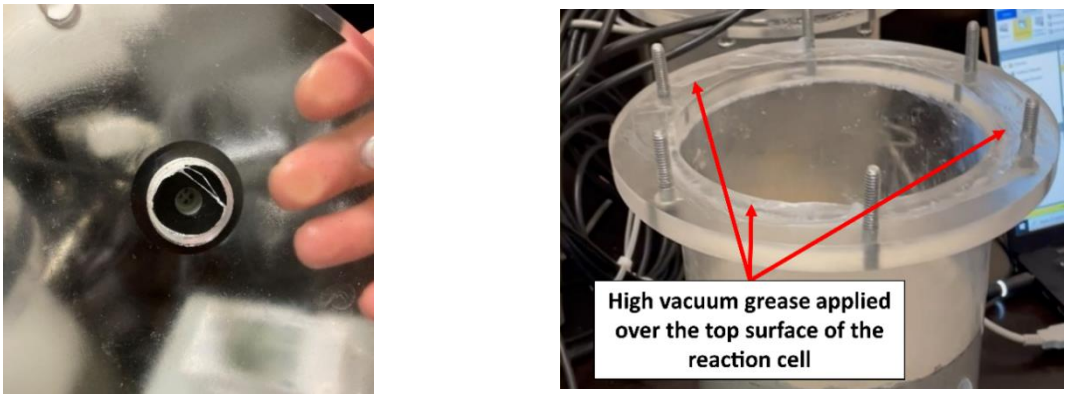

(a) (b)

Figure 2.9: (a) The figure shows the acrylic cap of the reaction cell. The oxygen sensor is inserted in the designated hole and sealed with thread seal tape (colored white). (b) Figure shows the reaction cell after the application of high vacuum grease to hermitically seal the cell (see red arrows). Photo credits (both photos): Dr. Jan Lindgård. Photos taken at Ulaval.

2.3.3.5 Necessary mass of aggregate material and added water

Annex P [39] shows how the amount of aggregate material and added water for each oxygen consumption test can be calculated. The specialization project [1] (TKT4550, fordypningsprosjekt) written last semester

briefly presented this calculation procedure found in Annex P. A new clearer and more structured outline of the Annex P calculation process is described below.

The required mass of water and of aggregate material for the OCT is based on two conditions [3, 39]:

1. **Porosity** (n_{gm}) of the aggregate material layers in the reaction cell (after compression by the steel pestle). This porosity is defined as the volume of air and added distilled/deionized water (ASTM D1193 Type IV) in the aggregate layers divided by the total volume of the compressed aggregate layers.
2. **Saturation level/degree** (S_{gm}) in the aggregate material layers in the reaction cell (after compression). This saturation level is defined as the volume of added water in the compressed aggregate layers divided by the volume of air and added water in these layers.

The following equation can be used to find the required aggregate mass so that the conditions above are met [3, 39]:

$$m_{aggregate} = [(1 - n_{gm}) \times V_{gm} \times \rho_{agg}] \quad (6)$$

As for required mass of added distilled/deionized water, the following equation can be utilized [3, 39]:

$$m_{added\ water} = [(V_{gm} \times n_{gm}) \times S_{gm} \times \rho_{w}] \quad (7)$$

where $m_{aggregate}$ and $m_{added\ water}$ is the required mass (g) of aggregate material and added water, respectively. These masses are calculated for the two layers of aggregate material in the reaction cell. Porosity (n_{gm}) is set at 50%. The volume of the ground material layers is V_{gm} (cm^3).

ρ_w (in g/cm^3) is the density of added water and can be assumed to be 1 g/cm^3 according to the procedure of the interlaboratory study [51]. ρ_{agg} (in g/cm^3) is defined by Annex P [39], the interlaboratory procedure [51] and Rodrigues et al. [3] as the "relative bulk (dry) density." Discussions during the 2023 Canada-Norway workshop concluded that the density referred to here is the particle density of the aggregate. Here the "particle density" refers to the density of the aggregate particles without considering inter-particle voids.

2.3.3.6 Oxygen consumption measurements

The OCT measures the percent reduction in the oxygen gas concentration over 3 hours. The total duration of the OCT is 3.5 h. The first 30 min is the stabilization period for the oxygen sensor.

Annex P [39] provides the following equation to calculate the oxygen consumption of the test specimen:

$$\text{Consumed oxygen (in \%)} = \frac{X - Y}{X} \times 100 \quad (8)$$

Where X is the oxygen level (in % O_2) at the end of the stabilization period (0.3h), and Y (in % O_2) is the oxygen level at the end of the total test period (3.5h).

2.4 Assessment of the OCT parameters (*taken from the specialization project, TKT4550*)

The following chapter is taken entirely from the specialization project [1] (from the course Konstruksjonsteknikk fordypningsprosjekt, TKT4550) written last semester. Only a few minor changes were made.

Table 2.2 shows a literature overview of the OCT and the variation in the test parameters. For each work of research, the parameters found by the authors to provide the highest consumed oxygen are highlighted. In addition, the test parameters recommended by Annex P are also included.

Rodrigues et al. [3] ran the OCT with different values of the test parameters. A complete list of these parameters and their combinations are presented in Figure 2.10. The purpose of these multiple runs of the OCT was to find the parameters (out of those shown in Figure 2.10) which would maximize oxygen consumption for deleterious aggregates, while maintaining low levels of oxygen consumption for non-reactive aggregates.

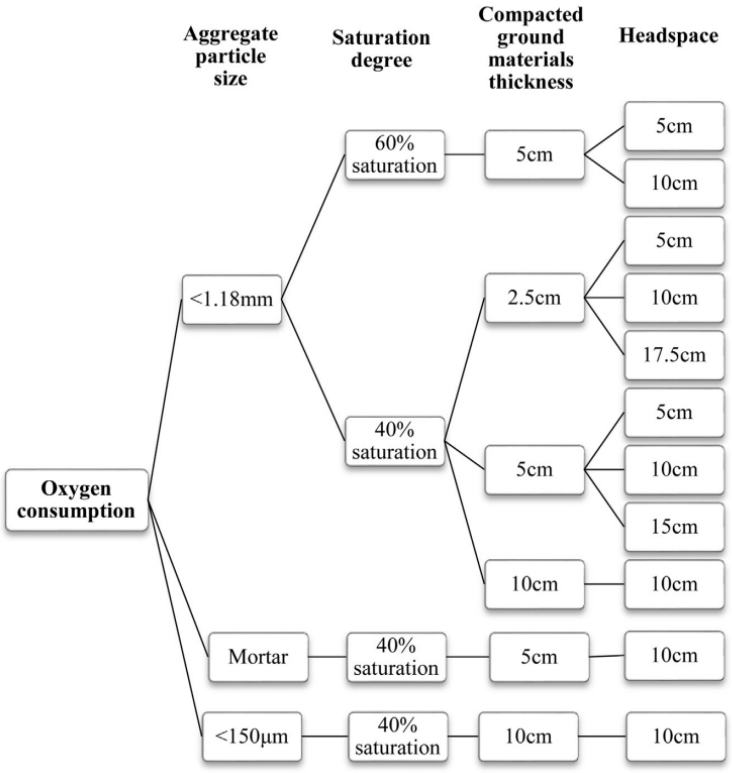

Figure 2.10: The figure shows the parameter values used for the OCT by Rodrigues et al. [3]. The mortar particle size, shown in the figure, is between 150 µm and 5 mm.

Table 2.2: Values of OCT test parameters in the reviewed literature. Parameter values that provide the highest oxygen consumption in their respective paper/work are bolded.

OCT test parameter	**Rodrigues et al., 2016 [3]**	**El-Mosallamy and Shehata, 2017 [60]**	**Annex P, 2019 [39]**	**El-Mosallamy and Shehata, 2020 [40]**	**Canada-Norway workshop, 2022 (Rodrigues [59])**
Aggregate type	Canadian aggregates. 10 aggregates (7 sulfide-bearing, 3 no/negligible sulfides)	Canadian aggregates. 6 aggregates with sulfur content (S_T, wt. %) between 0 and 14.5 wt. %	Requirements for labs to test a reference aggregate ("sulfide-bearing reactive control aggregate")	Canadian aggregates. 21 aggregates with no known sulfide-related issues, 3 sulfide-bearing reactive aggregates and 3 control non-sulfide bearing aggregates	MSK 0.9 (S_T = 0.9 wt. %), MSK 0.2, PKA (S_T = 0.04—0.06 wt. % [3])
Oxidizing agent	**Ambient air**	**Ambient air**	**Ambient air**	**Ambient air**	**Ambient air**
Crushing and grinding	Jaw crusher and roller crusher followed by a rod mill	Jaw crusher followed by either a pulverizer (ceramic vs. cast-iron plates) or a micro-deval apparatus	Crushing equipment (for example a jaw crusher) followed by grinding equipment (for example a pulverizer with ceramic plates)	Jaw crusher (cast-iron vs. manganese steel plates) followed by a pulverizer with ceramic plates	Annex P procedure (assumed)
Particle size (gradation level of samples)	**<150 µm**, <1.18 mm, and mortar particle size (5 mm—150 µm)	**75—150 µm**. Some aggregates were also tested with sizes: coarse (150—600 µm) and fine (75—300 µm)	**<160 µm** (with instructions to avoid excessive amounts of particles <80 µm)	**75—300 µm** (50%: 75—150 µm, 50%: 150—300 µm)	**<150 µm** (50% <75 µm sieve and 50% 75—150 µm), (75—300 µm) and (<300 µm)
Saturation level	**40%,** 60%	**40%**	**40%**	**40%**	20%, 25%, 30%, **35%, 40%**
Thickness of aggregate layer	25 mm, 50 mm, **100 mm**	**100 mm**	**100 mm**	**100 mm**	**100 mm**
Headspace	50 mm, **100 mm**, 150 mm, 175 mm	**100 mm**	**100 mm**	**100 mm**	**100 mm**
Total duration	**3.5 hours**	**16.5 hours**, 3.5 hours	**3.5 hours**	**16.5 hours**, 3.5 hours	**3.5 hours**

2.4.1 Type of aggregates

Types of aggregates tested using the OCT include both non-sulfide bearing aggregates and sulfide bearing reactive aggregates. In most cases multiple aggregates with a total sulfur content (S_T, wt. %) between 0.1 and 1 wt. % were also tested. Many of these aggregates had a history of good performance as concrete aggregates.

Rodrigues et al. [3] tested 10 types of aggregates, three of which were control aggregates containing no/negligible amounts of sulfide minerals. Among the sulfide-bearing aggregates, one mainly consisted of sulfide minerals, and the remaining aggregates had a total sulfur content (S_T, wt. %) between 0.05 and 4.2 wt. %.

El-Mosallamy and Shehata [60] tested six aggregates with a total sulfur content (S_T, wt. %) between 0 and 14.5 wt. %. A larger number of aggregates from Ontario, Canada were tested by El-Mosallamy and Shehata [40] including multiple carbonate aggregates, silicate-containing aggregates and three aggregates with a relatively high sulfur content (0.54—14 wt. %).

According to Annex P [39], laboratories that test aggregates using the OCT must regularly test a reference aggregate ("sulfide-bearing reactive control aggregate") in order to validate the laboratory's experimental setup. Annex P also provides the expected oxygen consumption for the sulfide-bearing MSK aggregate (taken from Rodrigues at al. [3]), indicating that this aggregate may be selected as a reference aggregate.

2.4.2 Oxidizing agent

In all reviewed research on the OCT, ambient air was used as the oxidizing agent. Although the use of pure oxygen might accelerate the oxidation process, it might make the test setup complicated and commercially suboptimal.

Alternative tests to the OCT use oxidizing solutions like hydrogen peroxide solutions [11, 61] and sodium hypochlorite solutions [62]. Such agents cannot be used in the OCT without significantly modifying the test, as it is more straightforward with these agents to measure the oxidation rate based on released sulfates in the solution as opposed to oxygen consumption (see Alternative Tests to the OCT, Chapter 2 in the specialization project [1]).

2.4.3 Crushing and grinding of samples

The equipment used by Rodrigues et al. [3] for crushing and grinding the samples consisted mainly of a jaw crusher, a roller crusher and a rod mill (to reach particle size <150 um). The equipment was mainly made from steel (Andreia Rodrigues, personal communication, April 2023).

The equipment used by El-Mosallamy and Shehata [60] included a jaw crusher, disk pulverizers (either cast-iron plates or ceramic plates) and a grinding mill with stainless steel balls (micro-deval apparatus). El-Mosallamy and Shehata [60] found that the use of cast-iron equipment to grind the samples led to iron contamination and resulted in overestimated levels of the oxygen consumption. Figure 2.11, which is taken from El-Mosallamy and Shehata [40], shows the oxygen consumption for a sulfide-free aggregate ground with disk pulverizers with different plate materials (cast-iron plates are compared to ceramic plates). The use of disk-pulverizers with cast-iron plates contaminated the samples with iron, which got oxidized and consumed additional oxygen during the OCT.

Annex P [39] does not elaborate on the exact material of the crushing/grinding equipment but specifies that ceramic plates must be used when using disk pulverizers (with possible contamination mentioned as a consequence of using cast-iron plates).

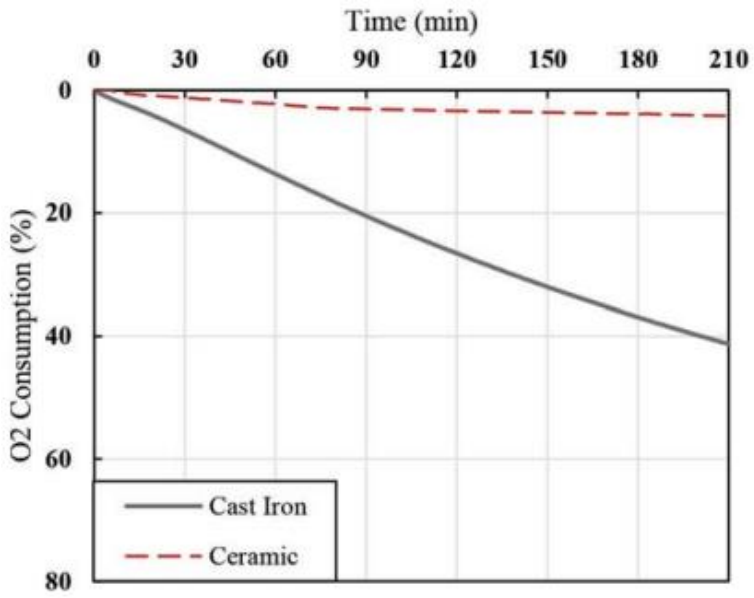

Figure 2.11: Oxygen consumption levels for samples ground with desk pulverizers with either ceramic or cast-iron plates. The aggregate tested is non-reactive. The figure is reproduced in [40] on the basis of experimental data from [60].

In a later research, El-Mosallamy and Shehata [40] investigated whether the use of a jaw crusher with cast-iron plates can also lead to contamination of aggregate samples. Samples were prepared by using two jaw crushers each having plates with different materials. Figure 2.12 shows the oxygen consumption obtained when preparing the aggregate samples with a jaw crusher with either cast-iron plates or manganese steel plates.

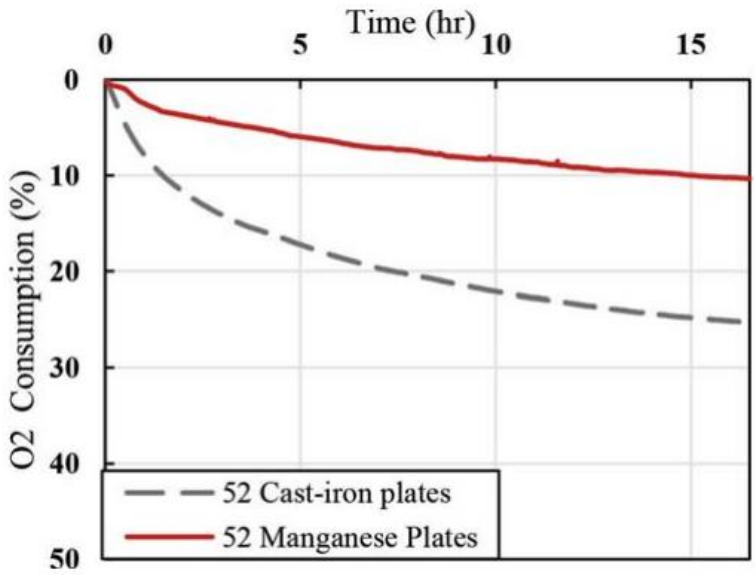

Figure 2.12: The figure shows how oxygen consumption changes depending on the plate material of the jaw crusher. Cast-iron plates are compared to manganese steel plates. The aggregate tested is named "52" in the figure and has a total sulfur content (S_T, wt. %) of 0.54 wt. %. Taken from El-Mosallamy and Shehata [40]

As Figure 2.12 shows, the use of a jaw crusher with cast-iron plates leads to increased oxygen consumption, hinting at probable contamination of the samples. The results in Figure 2.12 are also consistent with the results from other aggregates tested by El-Mosallamy and Shehata [40]. It is interesting to note that Annex P [39] of the Canadian concrete standard does not prohibit the use of cast-iron plates for a jaw crusher (only for pulverizers). The lack of specification on the type of jaw crushers in Annex P is likely because of the time difference as the Annex was published in 2019, while research regarding the importance of the plate material of jaw crushers by El-Mosallamy and Shehata [40] was published the year after, in 2020. Therefore, it is probable that further limitations on the type of jaw crushers for the OCT will be introduced in the next edition of the standard.

2.4.4 Particle size

Results from Marcelino et al. [61] indicate that pyrrhotite samples with a smaller particle size are linked to higher rates of oxidation. According to Janzen et al. [18], a significant increase in the specific surface area of pyrrhotite (i.e., surface area per unit mass) is achieved at a smaller particle size, with the increase being much higher than the geometric relationship would indicate. This large increase in the specific surface area of smaller pyrrhotite particles is caused by the pyrrhotite's surface roughness and an increased number of fractures. Janzen et al. [18] further showed that the rate of pyrrhotite oxidation strongly increased for samples with higher specific surface area.

Rodrigues et al. [3] tested the following particle sizes:

- 5 mm to 150 µm (called "mortar particle size")
- <1.18 mm
- <150 µm (passing the 150 µm sieve)

Figure 2.13 shows the oxygen consumption levels for 8 aggregates (6 reactive and 2 non-reactive aggregates) as a function of the three sample gradation levels shown above. Figure 2.13 is reproduced from Rodrigues et al. [3]. The finer sample sizes are correlated with higher levels of oxygen consumption, both for control non-reactive aggregates (PKA and DLS) and for the sulfide-bearing aggregates (the remaining aggregates in Figure 2.13). The finest particle size (<150 µm) resulted in the highest amount of consumed oxygen for all aggregate samples.

In 2017, El-Mosallamy and Shehata [60] prepared the aggregate sample with a particle size distribution (75—150 µm), i.e. particles were retained on the 75 µm sieve, but passed through the 150 µm sieve. Two aggregates (C20 and MSK) were tested with two other particle size distributions; the *coarse size fraction* (50%: 300—600 µm, 50%: 150—300 µm) and the *fine size fraction* (50%: 150—300 µm, 50%: 75—150 µm).

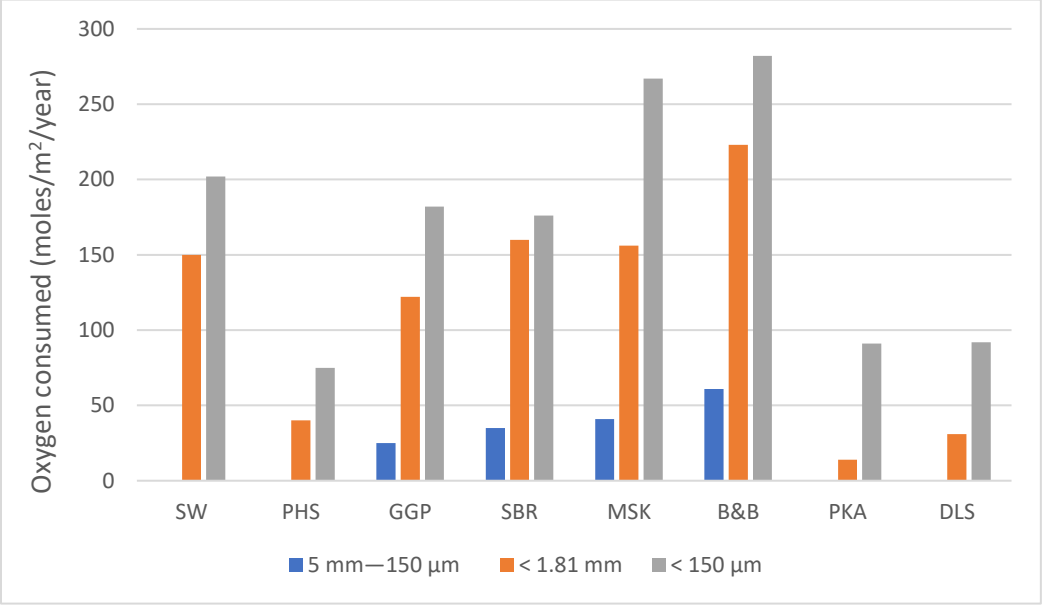

Figure 2.13: Effect of particle size on the level of oxygen consumption in the OCT. PKA and DLS aggregates are control aggregates containing negligible amounts of sulfides (S_T <0.12 wt. %), while the other aggregates are sulfide-bearing aggregates (total sulfur content between 0.05 and 4.22 wt. %). Reproduced from Rodrigues et al. [3]

Figure 2.14, reproduced from El-Mosallamy and Shehata [60] based on results from [3, 60], shows the O_2 consumption for the following aggregates, C1 and MSK, as a function of the particle size distribution. The

particle size varies in total between 75 and 600 µm. For the MSK aggregate, the fine sample gradation (75—300 µm) gave higher oxygen consumption compared to the size fraction of (<150 µm). For the C1 aggregate, oxygen consumption was higher for the particle size distribution (75—150 µm) compared to the particle size (<150 µm).

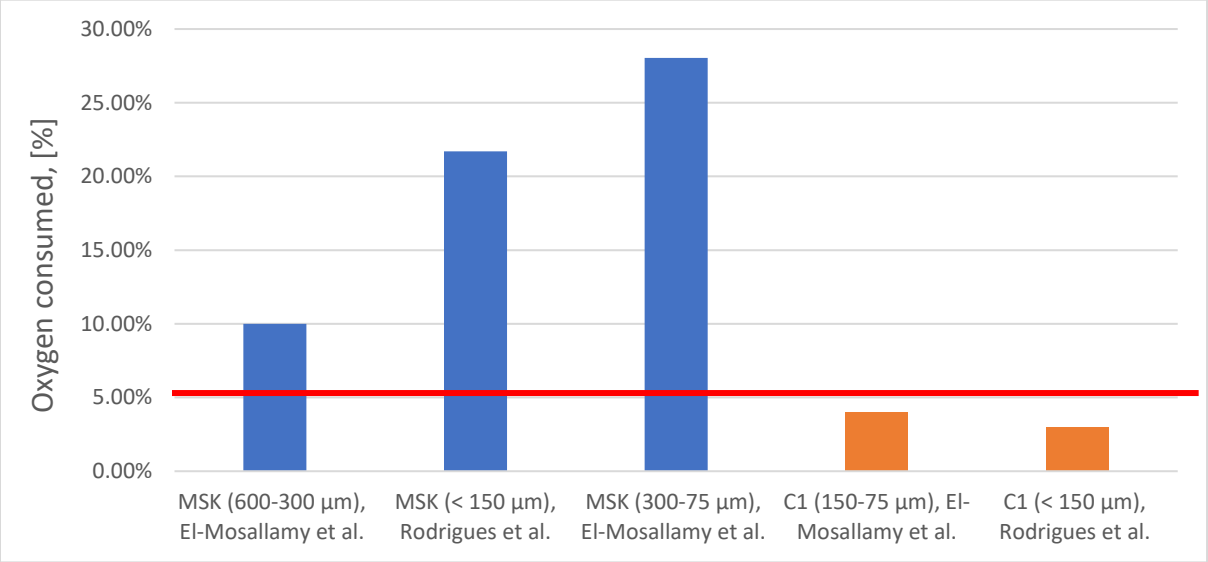

Figure 2.14: Oxygen consumption in (%) as a function of aggregate type and particle size distribution. The test duration is 3.5h. The results for the MSK sample are in blue, and for the C1 sample (S_T =0.09 wt. %) are in orange color. The horizontal red line indicates the oxygen consumption threshold (5%) proposed by Rodrigues et al. [3] in 2016. Reproduced from [3, 60].

Figure 2.14 then indicates that the correlation between the higher pyrrhotite oxidation rate and smaller particle sizes (as Marcelino's results indicated [61]) does not hold for particle size distributions in the range 300—75 µm. At very fine particle sizes (<75 µm), there seems to be a slight reduction in the oxidation rate of pyrrhotite. No definitive reason was given in the reviewed literature on this slight reduction in the oxidation rate [40, 60]. Perhaps, this slight reduction is merely due to variation in the specific surface area of pyrrhotite samples. Janzen et al. [18] noted that pyrrhotite samples of the same size might have significantly different specific surface area values.

Annex P [39] emphasizes that the aggregate samples must pass through the 160 µm sieve, which is close to the particle size distribution proposed by Rodrigues et al. [3] in 2016. Taking the recommendations of El-Mosallamy and Shehata [60] into consideration, Annex P recommends many steps during the OCT test procedure whose purpose is to limit the amount of very fine particles (<80 µm).

During the Canada-Norway workshop on the durability issues caused by pyrrhotite held in October 2022, Rodrigues [59] presented the oxygen consumption levels for the MSK 0.9 aggregate (estimated total sulfur content of 0.9 wt. %) with the following particle sizes:

- <150 µm (50% <75 µm, 50% 75—150 µm)
- <300 µm (33% <75 µm, 33% 75—150 µm, 33% 150—300 µm)
- 75—300 µm (50% 75—150 µm, 50% 150—300 µm)

Figure 2.15, reproduced from [59], shows the oxygen consumption for the MSK 0.9 aggregate as a function of the these three particle size distributions. The particle size distribution (50% <75 µm, 50% 75—150 µm) provides higher levels of oxygen consumption compared to the other two. The reason could be that this particle size distribution results in a good balance between limiting the fraction of very fine particles (<75 µm) to only 50% while still maintaining an overall fine particle size (<150 µm).

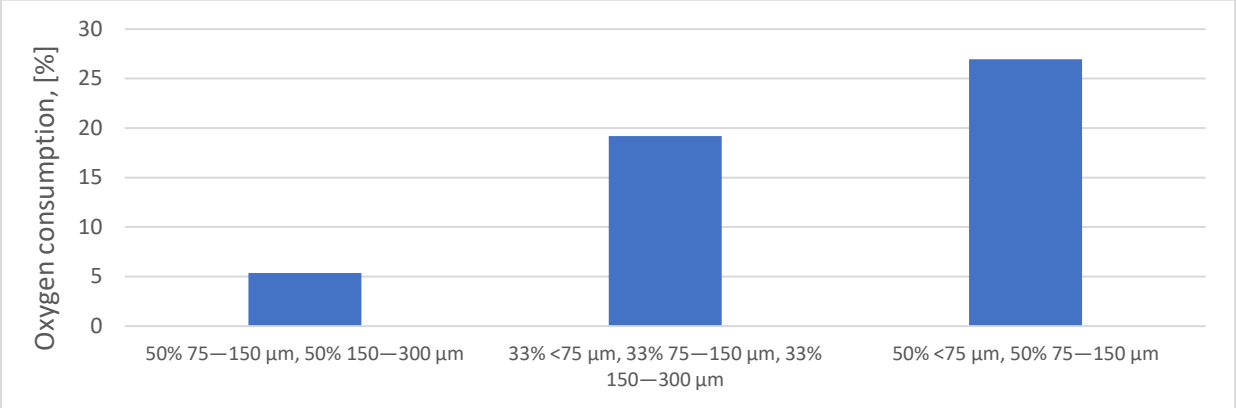

Figure 2.15: Oxygen consumption in the OCT for aggregate MSK 0.9 as a function of the particle size distribution. Except for the particle size, the test parameters values are as recommended by Annex P. Figure reproduced from [59].

Overall, for particle size >300 µm, there is a correlation between higher oxygen consumption and finer particle size distributions. For particle size <300 µm, it is important to control the amount of very fine particles (<75 µm) while maintaining an overall fine particle distribution (preferably <150 µm).

2.4.5 Saturation level

The saturation level is the extent to which the void-space volume between the aggregate particles in the ground material layers (after compaction) is filled with water. The void-space is defined as the volume in the ground material layers that is filled with water and air [3].

Two levels of saturation were tested by Rodrigues et al. in 2016 [3], 40% and 60%. Figure 2.16 shows the oxygen consumption as a function of the saturation level for a given combination of the headspace and the total ground material thickness. The figure is reproduced from Rodrigues et al. [3].

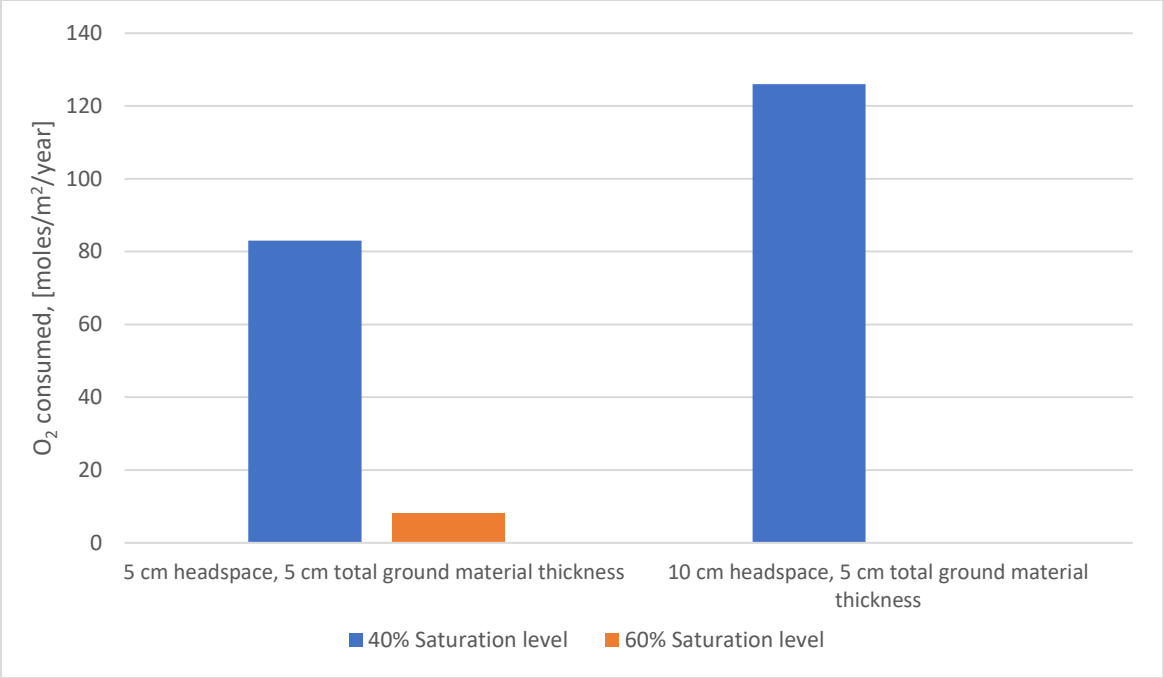

Figure 2.16: Oxygen consumption (MSK aggregate) as a function of the saturation level for two combinations of headspace and total ground material thickness. For 10 cm headspace and 5 cm ground material thickness at 60% saturation, no oxygen is consumed. Figure reproduced from [3].

When comparing the saturation levels at the same combination of headspace and ground material thickness, oxygen consumption is highest at the 40% saturation level. At the 60% level, a water film forms on the surface of the sample stopping or significantly slowing down the oxidation reaction [3]. Annex P of the Canadian standard also specifies a saturation level of 40% [39].

Note that the two combinations of the saturation level and the ground material thickness included in Figure 2.16 are the only two combinations tested with 60% saturation by Rodrigues et al. [3] in 2016.

Results for other saturation levels were presented by Rodrigues [59] at the Canada-Norway workshop on pyrrhotite held in October 2022. Figure 2.17 shows the oxygen consumption for the MSK 0.9 aggregate at different saturation levels (in the range 20—40%). Most oxygen is consumed at 35% saturation (only slightly higher than for the 40% saturation level). The oxygen consumption levels for 25% saturation are also quite close to the values for 40% saturation. These close values highlight the need to test more aggregates with saturation levels between 20—40%.

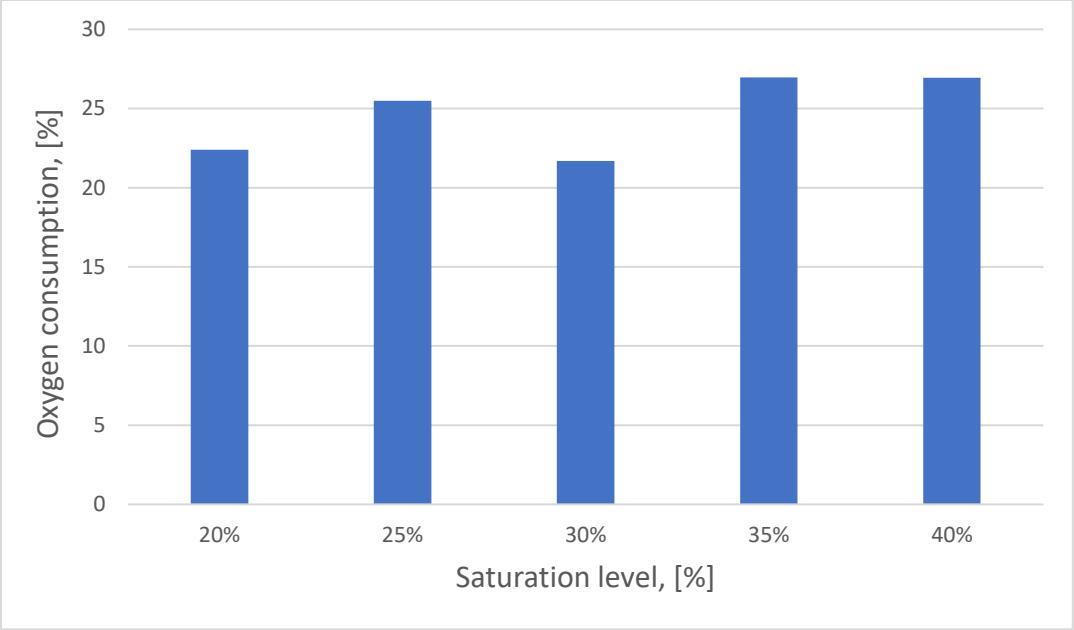

Figure 2.17: Oxygen consumption for the MSK 0.9 aggregate as a function of the saturation level. Apart from the saturation level, the test parameter values are as recommended by Annex P. Figure is reproduced from [59].

2.4.6 Thickness of the headspace and the ground material layers

The headspace is that section of the reaction cell that lays between the ground material layers and the acrylic cap (see Figure 2.7). The ground material thickness is the thickness of the aggregate sample layers (after mixing with water followed by compaction) towards the bottom of the reaction cell. The fixed height of the reaction cell (200 mm) limits the combinations of headspace and ground material thickness.

Figure 2.10 shows the combinations of headspace and ground material thickness tested by Rodrigues et al. [3]. A headspace of 10 cm and a ground material thickness of the same value were found to be the combination resulting in the highest oxygen consumption (with 40% saturation). Later work by El-Mosallamy and Shehata [40, 60] also used these values. Consequently, these are also the values included in the OCT's test setup in Annex P [39]

2.4.7 Duration of the test

Rodrigues et al. [3] did not experiment with different durations of the OCT, but rather all samples were tested with a duration of 3 hours (in addition to half an hour to stabilize the probes of the oxygen sensor). On the other hand, El-Mosallamy and Shehata [40, 60] experimented with a test duration of 16 hours to investigate whether the increased duration will lead to higher oxygen consumption or not.

Figure 2.18, taken from El-Mosallamy and Shehata [40], shows the oxygen consumption levels for 21 aggregates (2 reactive and 19 non-reactive aggregates). The aggregates samples were tested with a total duration of 3.5 hours and 16.5 hours (including the probe stabilization period). The aggregate samples tested for 16.5 hours showed consistently higher, and in many cases, more than double the oxygen consumption compared to aggregates tested with a duration of 3.5 hours. The increase in oxygen consumption is seen both for reactive aggregates (MSK) and non-sulfide bearing aggregates (C1, "crushed quarried limestone" as an example).

However, the increase in the oxygen consumption given the increased duration (16.5h) is not linear. For example, the non-reactive aggregates 1043 and 1047 (in Figure 2.18) had similar levels of oxygen consumption with an OCT duration of 3.5 hours. When the duration changes to 16.5 hours, the increase in oxygen consumption for aggregate 1047 is more than double the increase for aggregate 1043.

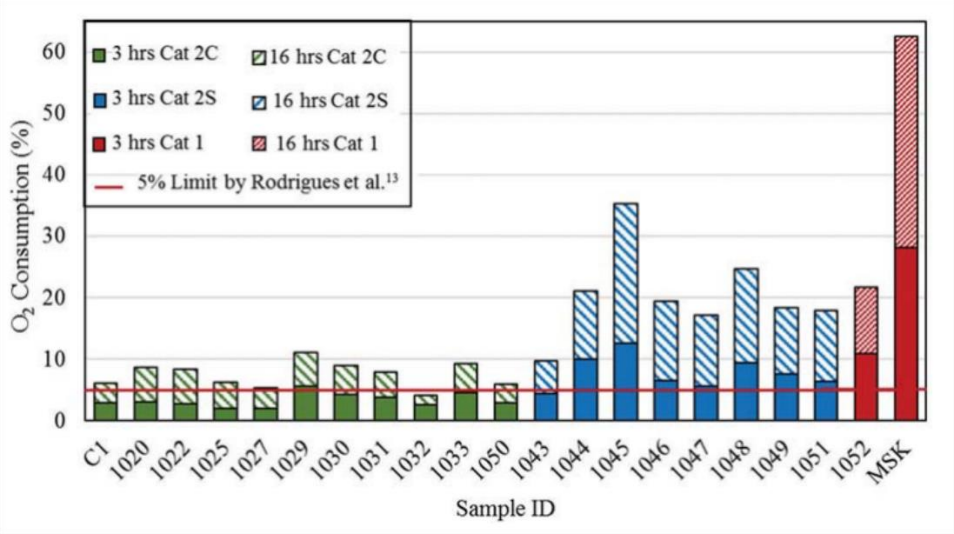

Figure 2.18: Oxygen consumption for different aggregates as a function of the OCT duration. Results for reactive aggregates are colored red. The other aggregates are non-reactive (carbonate-containing aggregates are colored blue, while aggregates with silicates are colored green). Taken from [40].

In the work of Elberling et al. [56] on mine tailings, the oxidation rate of different sulfide minerals (mostly pyrite and pyrrhotite) was measured. Even though these experiments provide the intellectual basis for the later development of the OCT, they are still significantly different from the OCT. For example, the length of the Plexiglass reaction cell used in these experiments is 1 m while the height of the reaction cell in the OCT is 0.2 m. However, these experiments can provide some valuable insights regarding how the oxidation rate of pyrrhotite changes with time.

Figure 2.19 is taken from [56] and shows the oxidation rate of pyrrhotite as a function of time (both on the basis of consumed oxygen and on sulfate production). The figure shows how the oxidation rate, based on

the consumed oxygen, increases significantly during the first 2 days, and then remains constant for the rest of the testing period.

Given that the experimental setup of Elberling et al. [56] is different, care should be taken when applying conclusions derived from this setup to the OCT. However, combined with the results from El-Mosallamy and Shehata [40], Figure 2.19 gives a further indication of the importance of varying the OCT duration, perhaps experimenting with longer durations as a means of potentially achieving higher levels of oxygen consumption. However, prolonged testing time requires a revised (increased) critical acceptance threshold of oxygen consumption.

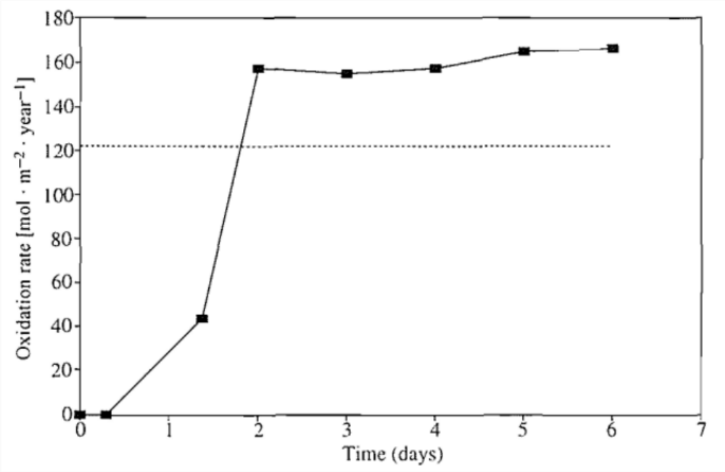

Figure 2.19: The oxidation rate of pyrrhotite as a function of the test duration. Method based on sulfate production (dashed line). Method based on oxygen consumption (solid line with black squares). The results for the method based on sulfate production are taken as a mean value over the testing period. Figure is taken from [56].

2.4.8 Oxygen consumption threshold

In the work of Rodrigues et al. [3], the oxygen consumption for all the non-sulfide bearing aggregates was less than 3% of the initial oxygen concentration, and therefore, a 5% threshold value was proposed. The 5% threshold value was also used by El-Mosallamy and Shehata [40] even though a total test duration of 16.5h was considered, indicating the conservative nature of the 5% limit. Likely to be on the safe side, a 4% limit was proposed in Annex P [39].

El-Mosallamy and Shehata [40] found that many aggregates with silicates had high levels of oxygen consumption (above the 5% threshold) even though their total sulfur content was very low. Figure 2.18, taken from [40], illustrates the finding: carbonate aggregates (Cat 2C) and aggregates with silicates (Cat 2S) have similarly low total sulfur content, but the Cat 2S aggregates show substantially higher oxygen consumption. El-Mosallamy and Shehata attributed these results partly to contamination from the crushing equipment (even when using a jaw crusher with manganese steel plates) and partly to the possible oxidation

of other phases such as biotite. These results highlight the impact of material composition on the OCT results and indicate the potential need for a separate oxygen consumption threshold for aggregates with silicates. El-Mosallamy and Shehata [40] have indeed recommended separate critical thresholds for carbonate aggregates and aggregates with silicates for the mortar bar expansion test (given that aggregates with silicates underwent more significant expansion).

3 Overview of laboratory work and pilot testing

To achieve the objectives of this M.Sc. Study as outlined in Section 1.2, the laboratory work and pilot testing were performed in a stepwise manner. The steps are outlined in the following sections.

3.1 Step A: Preliminary tests

At the beginning of this step, SINTEF installed and calibrated the oxygen and relative humidity sensors needed for the OCT. SINTEF also created the software necessary to log and extract the data produced by the sensors.

The purpose of this step was to ensure that the OCT setup is operating as intended. To achieve this goal, three non-representative aggregate samples were reduced to a particle size <150 μm or similar with either all steel or all tungsten pulverizing equipment. These samples were then tested with the OCT. The necessary training to use the equipment for sample preparation was carried out during this step.

Another purpose for this step was to ensure that the oxygen sensors provided reliable measurements. Therefore, this step was used to determine whether the sensor measurements needed to be corrected for ambient conditions (particularly RH). The necessary corrections were implemented in the OCT software by SINTEF.

3.2 Step B: Effect of sample preparation on oxygen consumption

The objectives of this step were (1) to preliminarily check whether using steel in sample preparation can lead to contamination, and (2) to determine whether the use of steel can improve the efficiency of the sample preparation process. To achieve these objectives, samples from a soft and a hard aggregate were prepared with three different sample preparation pathways (i.e., methodologies); two pathways involving steel grinding equipment, and one with only ceramic/tungsten equipment. Then, the oxygen consumption, the efficiency of sample preparation and the full particle size distribution curves were compared for these samples.

At least one sample from each aggregate was prepared with each pathway and then tested with the OCT using the standard test parameters outlined in Annex P [39] (see Table 2.2). In addition, a small parameter study was conducted to investigate how the saturation level and the test duration affect oxygen consumption. To that end, one test was carried out with 60% saturation, and the oxygen consumption for two other tests was taken after 3.5 and 16.7 hours.

3.3 Step C: Benchmarking against the Canadian test results

Two Canadian sulfide-bearing aggregate samples were tested with the OCT using the standard test parameters outlined in Annex P [39]. One of the aggregate samples was prepared with the "optimal" sample preparation pathway (with respect to time and cost efficiency) from Step B, while the other aggregate sample was already prepared with ceramic/tungsten equipment before the start of the present study. The oxygen consumption results from these two samples were compared to the Canadian reference values.

In this step, one of the Canadian aggregates was mixed with one of the Norwegian aggregates from Step B at a fixed percentage. Two parallel oxygen consumption tests with this aggregate mixture were carried out, each with a different oxygen sensor. The primary goals were to examine whether results similar to those in Canada could be obtained, and to check whether the reaction cells and the corresponding sensors gave identical results.

Based on the results from the three steps, a recommended detailed procedure for both sample preparation and OCT testing was proposed.

4 Aggregate types

Four aggregates were selected for testing with the OCT during this M.Sc. study. The aggregates were selected based on their content of total sulfur (relevance), availability, the recommendations of the specialization project [1] for the pilot testing, and further discussion and deliberation during the master's thesis. These aggregates include a pure limestone from Norway, a Norwegian sulfide-bearing aggregate (referred to as SM1) and two sulfide-bearing Canadian aggregates (referred to as MSK) with varying total sulfur content. The properties of these aggregates are outlined in Table 4.1.

Table 4.1: An overview of the aggregates tested with the OCT, including their rock type, total sulfur content and particle density.

Aggregate	Rock type	Total sulfur, wt. % S_T		Particle density [g/cm3]
		Estimate	LECO (performed by NBTL)	
Limestone	Pure limestone	-	0.02 wt. %	2.72
SM1	Granitic gneiss	-	0.45 wt. %	2.72 (CE-declaration)
MSK 0.9	Norite or a hypersthene gabbro [3]	0.9 wt. %	1.05 wt. % (freshly ground material)	2.86 (Pierre-Luc Fecteau, personal communication, March 2023)
MSK Rich	Norite or a hypersthene gabbro [3]	1.8 wt. %	1.84 wt. % (freshly ground material)	2.93 (Andreia Rodrigues, personal communication, May 2023)

The limestone aggregate is an almost pure calcite from the Verdal municipality in Norway. The aggregate is a stable non-alkali reactive form of limestone and is not expected to contain pyrrhotite. The total sulfur content of this aggregate was found to be 0.02 wt. % (performed at NBTL). This aggregate was selected because it is non-sulfide-bearing and is therefore not expected to have any significant consumption in the OCT.

At the start of the M.Sc. study, it was planned to mix the limestone aggregate with the Canadian sulfide-bearing aggregates for many test samples (see the original test matrix, Appendix A Table A.1) and test these samples with the OCT. However, the change of focus from OCT testing to sample preparation later in the M.Sc. study meant that limestone was only mixed in with one of the Canadian aggregates for only two OCT test samples (see the revised test matrix, Appendix A Table A.2).

SM1 is a Norwegian aggregate. The origin of SM1 is confidential (requirement from the producer). According to the CE-declaration of the material, simplified petrographic analysis shows that the aggregate is primarily gneissic/granitic in origin with inclusions of dark rocks. Simple stereographic screening was

performed by N. Oberhardt on handpicked particles to validate the analysis in the CE-declaration. The screening showed that the particles consisted of a gneissic rock that is rich with feldspar and biotite. Some inclusions of iron oxides were also found. In the CE-declaration the total sulfur content is given to be 0.15 wt. %. Statistics from 2004—2018 show a variation of the total sulfur content (S_T, wt. %) between 0.01 and 1.13 wt. % (SINTEF Community, Restricted test report 2019:00168). During the M.Sc. study, the total sulfur measured for this aggregate was 0.45 wt. % (performed at NBTL). In addition, testing on this material (DTA) has shown an indication of pyrrhotite.

SM1 was selected for the pilot testing because it might contain pyrrhotite that reacts under the conditions of the OCT. The aggregate has a total sulfur content by mass that exceeds the EN12620 [52] limit (<0.144 wt. % if pyrrhotite is found in the aggregate).

MSK is a Canadian sulfide-bearing aggregate that contains significant amounts of various iron sulfides, including pyrite and pyrrhotite [3]. According to Rodrigues et al. [3], the type of rock in the MSK aggregate can be norite or a hypersthene gabbro.

Two variants (MSK 0.9 and MSK Rich) of this aggregate with varying sulfur content are tested in the OCT as part of this study. Freshly prepared (crushed and ground) MSK 0.9 and MSK Rich showed a total sulfur content of 1.05 wt. % and 1.84 wt. %, respectively (performed at NBTL). The MSK aggregate is the aggregate responsible for the damages to house foundations in the Trois-Rivières region in Quebec, Canada.

The MSK aggregate is selected for the pilot testing in Norway because it is a sulfide-bearing aggregate with an expected high oxygen consumption in the OCT. As argued in the specialization process [1], The aggregate was tested extensively in Canada at ULaval [3, 59, 63] and at Toronto Metropolitan University [40, 60], making it possible to compare the oxygen consumption obtained in Norway for this aggregate to the results obtained in Canada..

As mentioned before, one of the limitations of the pilot testing was the availability of the Canadian aggregate MSK 0.9. The MSK aggregate material arrived in Norway in October of 2021. Table 4.2 shows an overview of the particle size distribution and the available amounts of the Canadian MSK aggregates before the start of the pilot testing with the OCT. Only MSK 0.9 and MSK Rich were tested with the OCT (see the revised test matrix, Appendix A Table A.2). Furthermore, the MSK aggregate variant MSK 0.2 was also available for the pilot testing (see Table 4.2), however, it was prioritized to test the MSK Rich and 0.9 aggregates because of their expected higher oxygen consumption in the OCT in addition to time limitations.

Table 4.2: Overview of Canadian aggregate availability for pilot testing with the OCT. Only aggregates that have a total mass > 1 kg available are considered.

Aggregate type	Particle size [mm]	Available mass [kg]	Mass available for the OCT [kg]	Condition of aggregate before the start of this study
MSK 0.9	0—0.147	2.5	2.5	Washed and dried[1)]
MSK 0.2	5/14	20.1	15[2)]	To be washed and dried
MSK Rich	5/20	18.2	13.7[2)]	Washed and dried

1) Prepared by SINTEF. Leftover material from the accelerated mortar bar test (AMBT) in 2022 (stored in a plastic bag).
2) Some material is kept for later AMBT testing.

5 Test matrix

The test matrix shown in Appendix A Table A.1 was the original test matrix planned at the beginning of the present study. The plan was to test 6 aggregates (limestone, SM1, norite, MSK 0.2, MSK 0.9 and MSK Rich) with the OCT. The test matrix focused on varying the test parameters (particularly the saturation level and particle size) in addition to combining the MSK aggregates with limestone. The aggregates were to be prepared with only tungsten or ceramic grinding equipment. However, the inefficiency of the sample preparation process meant that the original test matrix was no longer realistic. There was a need to investigate other equipment that can pulverize the aggregate samples more effectively, including steel equipment. Thus, the focus of the present study shifted towards finding a sample preparation procedure that is more effective without causing any iron contamination in the samples. Appendix A Table A.2 shows the revised test matrix that includes all the oxygen consumption tests carried out throughout the M.Sc. study.

The OCT parameters chosen for the tests in the revised test matrix (Table A.2) are the standard Annex P [39] test parameters (shown in Table 2.2 in Section 2.4). Only the test duration and the saturation level were varied for a few tests to study the effect on oxygen consumption. The particle size <147 μm was used, and the fraction <75 μm was kept at a maximum of 50% of the end particle size distribution.

6 Equipment

6.1 Equipment for sample preparation

6.1.1 Equipment for crushing and grinding

The following sections outline the type of comminution equipment used for sample preparation in this study. Crushing/grinding equipment used solely for preliminary testing is not listed in this section (this equipment is mentioned in Table 8.1). All comminution processes were performed dry.

6.1.1.1 Crushing equipment

The rushing of aggregate material was achieved using jaw and disk crushers. The properties of both crushers are outlined in the following paragraphs.

Figure 6.1 shows a picture of the *RETSCH BB100* jaw crusher (hereafter referred to only as "jaw crusher"). For the purposes of this master's thesis, the jaw crusher has only been used with tungsten carbide plates. The opening can be adjusted from 0 to 20 mm. This jaw crusher was used to reduce the particle size of coarse samples (with fractions such as 4/20, 8/16 mm) down to a particle size of 1—3 mm.

Figure 6.1: The figure shows the **RETSCH BB100** jaw crusher used for sample preparation.

Figure 6.2 shows a picture of the *FRITSCH Disk Mill PULVERISETTE 13* (hereafter referred to only as "disk crusher"). The disk crusher was only used with tungsten grinding disks to crush the material from a D_{max} of 2—3 mm down to a particle size of approximately 300—1000 μm.

(a) (b)

Figure 6.2: The figure shows the **FRITSCH Disk Mill PULVERISETTE 13**. Picture (a) shows how the machine looks from the outside and picture (b) shows the disks (steel disks are shown in the picture, but tungsten disks were used in sample preparation for this thesis).

The material can be fed to the disk crusher continuously. As for the jaw crusher, the material has to be fed batchwise as the feed size is controlled by the capacity of the removeable collector at the bottom of the jaw crusher (shown at the bottom left of Figure 6.1).

6.1.1.2 Grinding equipment

A bench ball mill (see Figure 6.3) was used to grind aggregate materials from a D_{max} of 1—3 mm to a particle size distribution below 150 μm. The mill shell (the black cylinder in Figure 6.3) rotates, and the grinding media are small balls. The type of balls used were either all steel (6 mm in diameter) or all ceramic (9—12 mm in diameter). The charge of the mill is subjected to strong pulverization forces due to a combination of abrasion (“cascading”) and impact (“cataracting”) [64, p. 148].

Figure 6.3: The figure shows **the bench ball mill** used for further grinding of OCT samples.

During sample preparation, the maximum feed size of the ball mill (excluding the weight of the grinding balls) was 600 g. The mill was filled to its maximum feed size whenever possible. The speed of the mill

was set to 85% of the critical speed (which is the speed at which centrifugal forces arise in the shell [64, p. 148]).

The *RETSCH RS 200* vibratory disk mill (see Figure 6.4) was also used. This disk mill grinds the sample material by pressure and friction [65]. The grinding set (see Figure 6.5, taken from [65]) consists of a small container, ring, and puck (disk). The steel grinding set was used for this study, and it had a capacity of 100 ml. For this type of grinding set, the RPM can be manually changed from 700 to 1500. The duration of each round can also be selected.

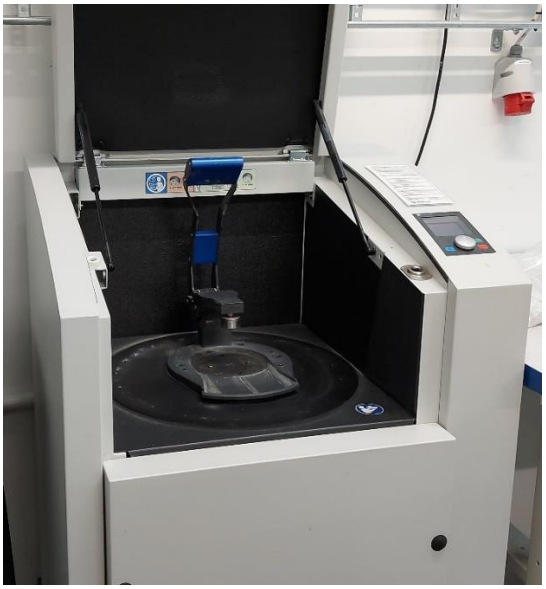

Figure 6.4: The figure shows the vibratory disk mill (**RETSCH RS 200**).

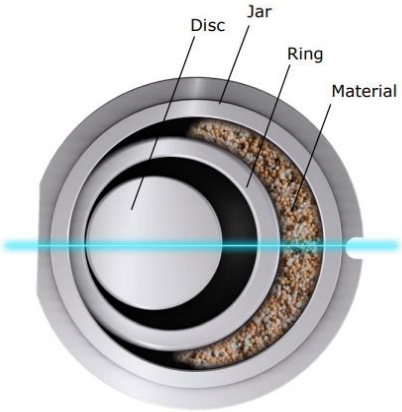

Figure 6.5: The figure shows the steel grinding set of the vibratory disk mill (**RETSCH RS 200**). Figure taken from [65].

A planetary ball mill (*FRITSCH Planetary Mono Mill PULVERISETTE 6.* See Figure 6.6) was used to grind small quantities of aggregate materials (<80 g) to a particle size distribution <142—147 μm. The mill, however, is often used for ultra-fine grinding (<15 μm). The grinding set (shown in Figure 6.7) consisted of tungsten balls and a tungsten-lined bowl. The grinding set rotates at high RPMs around the center of the mill, thus generating high gravitational, centrifugal and Coriolis forces that pulverize the aggregate material [66].

Figure 6.6: The figure shows the planetary mill **FRITSCH Planetary Mono Mill PULVERISETTE 6**.

Figure 6.7: The figure shows the grinding set (tungsten-lined bowl and tungsten balls) of the planetary mill.

6.1.2 Sieving equipment

The four different methods of sieving employed in the present study were:

1. SWECO Separator/Vibrating screen
2. RO-TAP RX-29 Sieve Shaker
3. RETSCH AS 300 Vibratory Sieve Shaker
4. Sieving by hand

All sieving operations in the present study were performed dry.

The *SWECO Separator* (Figure 6.8) was often used when preparing a subsample with a mass ≥ 6 kg. The maximum load of material placed over the *SWECO Separator* at any given time was approximately 2 kg for a minimum sieve time of ca. 50s before more material is added. Usually, however, smaller loads of material and longer sieving durations were used.

Figure 6.8: The figure shows the **SWECO Seperator** with a sieve tower consiting of the 142 µm and 77 µm sieves.

During sample preparation, these sieves (all 42.2 cm in diameter) with the following openings were exclusively used with the *SWECO Separator*: 77 µm, 142 µm, 4 mm and 20 mm.

The *RO-TAP RX-29* Sieve Shakers (see Figure 6.9) subject the material inside the sieving tower to swinging and tapping motions to enhance sieving efficiency. These sieve shakers have a capacity of ca. 200 g.

Different run times are possible. A sieve run time of 5 min was usually selected. These sieve shakers were used with the 75 and 147 μm sieves during sample preparation.

The *RETSCH AS 300 Vibratory Sieve Shaker* (see Figure 6.10) subjects the material and the sieves to a swinging motion. Different sieve cycle times are also possible. Here also a sieve time of 5 min was usually selected.

Hand sieving was used for some samples. The duration of hand-sieving was approximately 2—3 min.

Figure 6.9: The picture shows the **RO-TAP RX-29 Sieve Shakers.**

Figure 6.10: The picture shows the **RETSCH AS 300 Vibratory Sieve Shaker**.

6.1.3 Sampling equipment

4 splitters were used during the present study, including one rotary splitter, two riffle splitters and one small half-splitter. The riffle splitters had openings of 40 and 50 mm, while the opening of the small splitter was 25 mm.

Figure 6.11 shows the 10-chamber rotary splitter used. The splitter is of the type *MACSALAB Cascade Rotary Splitter*. The material is fed inside the cone shown in Figure 6.11. The material then passes to the feeder which vibrates the material and feeds it to the rotating sampling cups. The speed of the vibrating feeder can be adjusted. It was ensured that the speed remains as constant as possible when dividing samples with this splitter.

Figure 6.11: The figure shows the 10-chamber *MACSALAB Cascade rotary splitter*.

6.1.4 Equipment for determination of particle size distribution

The *Horiba LA-960 Laser Particle Size Analyzer* (shown in Figure 6.12) was used to determine the full particle size distribution of the prepared aggregate samples. The working principle involves a laser scattering optical technique to determine the particle size.

The sample size needed for each test was 1—3 g (see Section 7.1). A wet measurement regime was used, and the samples were dissolved in water as opposed to ethanol. Ultrasound (30 seconds) was employed to avoid the formation of lumps.

Figure 6.12: The picture shows *Horiba LA-960* (otherwise known as the *Laser Scattering Particle Size Distribution Analyzer*).

6.2 Equipment for the OCT pilot testing

6.2.1 Reaction cells

Two reaction cells were shipped from Canada to Norway for the pilot testing. The reaction cells were received in January 2023. The reaction cells had an internal diameter of 146.5 mm, height of 200 mm and wall thickness of 10 mm. The two reaction cells (Figure 6.13) were manufactured at the same machine shop as the cells used by Rodrigues et al. [3]. Before the cells were shipped to Norway, they were preliminarily tested and approved by Dr. Andreia Rodrigues at ULaval.

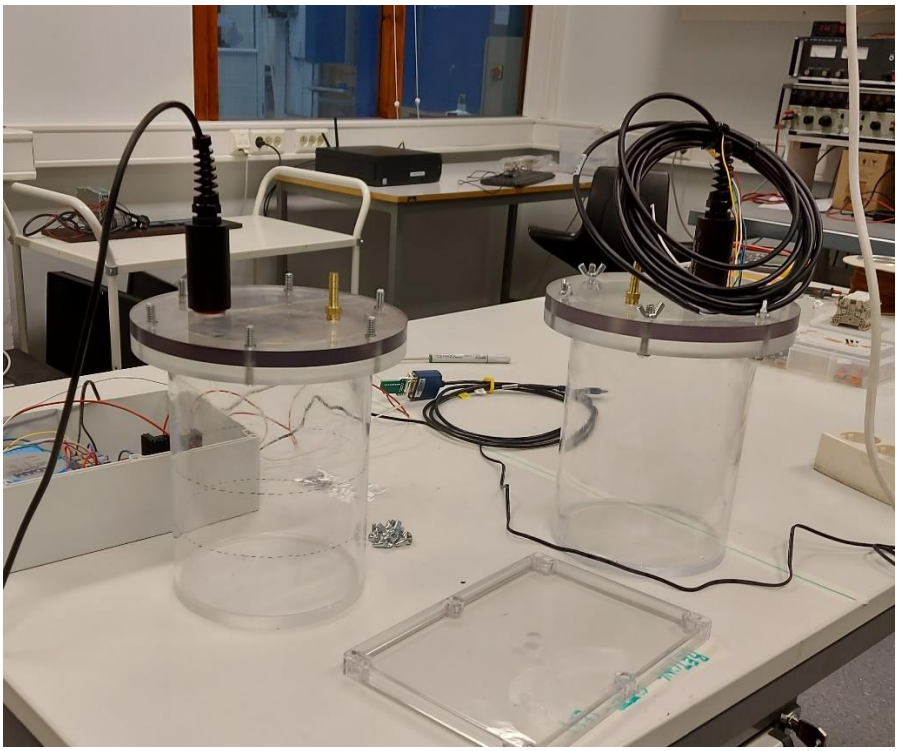

Figure 6.13: The picture shows the two reaction cells shortly after they arrived in Trondheim.

6.2.2 OCT software

SINTEF developed the OCT software used in the pilot testing. The interface of the software is shown in Figure 6.14. Time (relative and absolute), RH, temperature, and O_2 concentration from each test is automatically logged onto an Excel file.

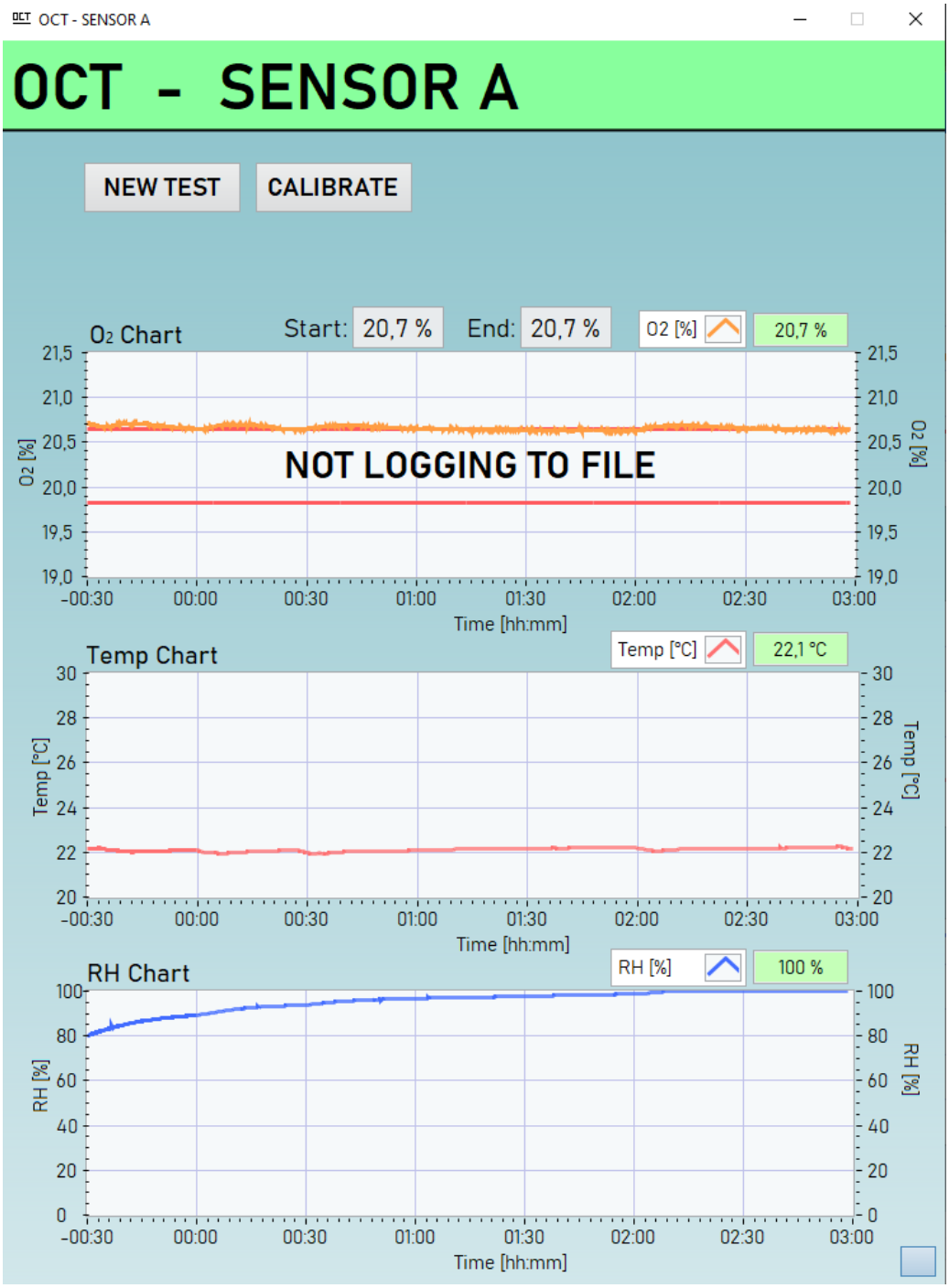

Figure 6.14: The interface of the OCT software used in the pilot testing.

6.2.3 Oxygen sensor

Two oxygen sensors of the type Apogee SO-110 were purchased by SINTEF. The sensors are part of the Apogee SO-100 series recommended by Annex P [39]. Understanding how the sensors work, and how they account for changes in temperature, pressure and relative humidity is vital in obtaining reliable results.

According to the product manual of the sensor [67], this galvanic-cell type sensor produces a voltage signal. This signal is linearly proportional to the absolute oxygen concentration. Table 6.1, modified from the product manual [67], outlines the specifications of the oxygen sensor.

Table 6.1: Table shows the specifications of the oxygen sensor SO-110. Modified from the product manual [67].

Parameter	**Oxygen sensor performance**
Response Time (time required to read 90% of saturated response)	60 s
Measurement Range	0 to 100% O_2
Sensitivity (at sea level, 101.3 kPa)	52-58 mV in 21% O_2; 2.6 mV per % O_2; 26 µV per 0.01% O_2
Measurement Repeatability	Less than 0.1% of mV output at 20.95% O_2
Non-linearity	Less than 1%
Signal Decrease per Year	1.8% per year (1 mV per year)
Operating Environment	-20 to 60 °C; 0 to 100% relative humidity (non-condensing); 60 to 140 kPa
Input Voltage Requirement	12 V DC continuous (for heater); 2.5 V DC excitation (for thermistor)

The calibration of the sensor and the corrections for temperature, pressure, and relative humidity have been performed by SINTEF in close cooperation with the author of this study. The following paragraphs focus on why these corrections are needed and how they are implemented in the OCT software. The sections are mainly based on the information provided in the product manual of the oxygen sensor [67].

6.2.3.1 Calibration of sensor

According to the product manual [67], the user should calibrate the sensor before its use for the first time. The calibration is mostly of the typical (linear) type. Although the sensor measures the absolute concentration of oxygen, it is possible to convert this measurement to a relative oxygen concentration (e.g., amount of O_2 relative to the amount of air). SINTEF carried out the calibration process. Both oxygen sensors were calibrated in an environment with 100% RH (see Section 6.2.3.4).

According to the oxygen sensor manual [67], the absolute concentration of oxygen is a function of temperature and absolute pressure according to the ideal gas law. When pressure or temperature change, the absolute O_2 concentration changes, but the relative O_2 concentration remains the same. The relative O_2 concentration is the amount of O_2 relative to the amount of air, and this ratio does not change when temperature or pressure fluctuate [39, 67]. However, the signal output of the oxygen sensor is a function

of the absolute, not relative, O_2 concentration [67]. Therefore, the measured relative O_2 concentration from the sensor must be corrected for changes in temperature and pressure.

6.2.3.2 Pressure corrections

According to the product manual [67], when the pressure increases by 1 kPa (compared to sea level), the sensor measures an increase (with a ratio of 0.987%) in the *relative* O_2 concentration. However, the increase in pressure should only affect the *absolute* amount of oxygen, not its relative concentration.

The OCT does not require the exact O_2 concentration at a given point in time, but rather the percentage reduction in the relative O_2 concentration over 3 hours. No significant change in atmospheric pressure is expected over that short period of time. Pressure corrections were nonetheless implemented because they are needed for the RH corrections (see Section 6.2.3.4). Pressure corrections can be calculated based on the equations described in the sensor manual [67]. In the OCT software, pressure values were taken for Trondheim at sea level from the website (yr.no) and then corrected for the elevation of the SINTEF Concrete Laboratory.

6.2.3.3 Temperature corrections

According the ideal gas law, when the temperature increases by 1°C (from 20°C), the *measured* relative concentration of oxygen will incorrectly decrease by a ratio of 0.341% [67]. The electronic systems of the sensor can also affect the sensor's response to changes in temperature.

The following empirical equation from the product manual [67] accounts for both of these effects, and is based on measurements performed in a dry atmosphere:

$$O_2\ [\text{in } \%] = O_{2M} + C_3 T_S^3 + C_2 T_S^2 + C_1 T_S + C_0 \qquad (9)$$

where T_S is the temperature measurement by the sensor. The coefficient C_0 can be calculated according to the following equation:

$$C_0 = -(C_3 T_C^3 + C_2 T_C^2 + C_1 T_C) \qquad (10)$$

where T_C is temperature measurement by the sensor during the calibration process.

Figure 6.15, taken from the manual [67], shows the behavior of the sensor SO-110 (according to equations 9 and 10) across a wide range of temperatures.

During the Norwegian pilot testing, the temperature is maintained at 20 °C (± 2 °C) in the room where the OCT is carried out. Even if no temperature corrections are carried out, Figure 6.15 shows that the measured

relative oxygen concentration for the Apogee SO-110 is almost constant in the temperature range 18—30˚C. Nonetheless, to be on the safe side, temperature corrections (equations 9 and 10) were included in the OCT software developed for the Norwegian pilot testing. The chosen coefficient values for the equations are as shown in Figure 6.15.

Temperature corrections (as shown by equations 9 and 10) require the temperature measured by the sensor (T_S). The OCT software records all the sensor temperature measurements throughout the test duration. These measurements are both presented visually by the software (see Figure 6.14) and written onto the Excel file.

The temperature might change temporarily if the door to the testing room is constantly opened and closed. Although the expected change in temperature is expected to be small, the reaction cell was placed in a polystyrene case (see Figure 6.16) to minimize the effects of any changes in the room temperature.

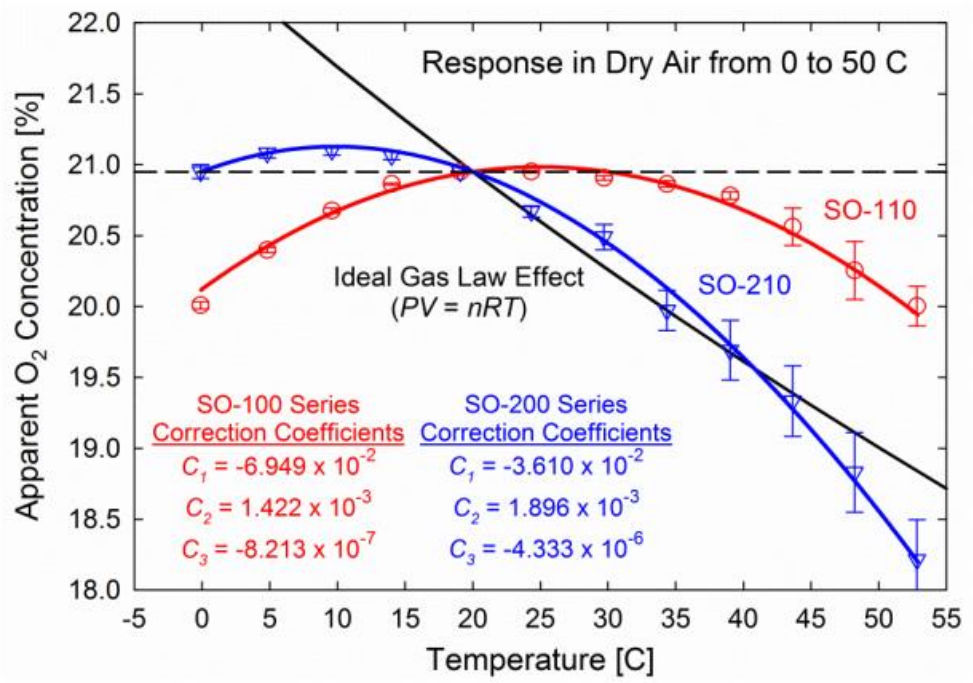

Figure 6.15: The figure shows the uncorrected ("apparent" [67]) oxygen concentration as a funciton of temperature. The correct relative oxygen concentration is 20.95%. The red line shows the expected behavior for the SO-110 sensor used in the present study (according to the eq. 9 and 10). The coefficients seen in the lower left part of the figure are to be used in equation eq. 9 and 10. The figure is taken from O_2 sensor manual [67].

To avoid further changes in temperature during the test, the water mixed with the aggregate material during preparation of the reaction cell will be at room temperature.

Figure 6.16: The picture shows the polystyrene case used to keep the reaction cell in an environment of constant temperature.

6.2.3.4 Relative humidity corrections

Changes in relative humidity cause a change in the *absolute and relative* concentration of oxygen because oxygen gas becomes diluted by the water vapor molecules [67]. Figure 6.17, taken from the product manual [67], shows the effect of decreasing oxygen concentration with increasing relative humidity values at both constant (A) and variable temperature (B).

When performing measurements in an atmosphere with high RH, it is possible to calculate the relative oxygen concentration given a dry environment (i.e., cancel the effect of high relative humidity) through the following equations [67]:

$$O_2\ [\text{in } \%] = O_{2M}\frac{P_C + (e_{AM} - e_{AC})}{P_C} \tag{11}$$

where O_{2M} is the oxygen concentration measured by the sensor. P_C is the calibration pressure [kPa]. e_{AM} and e_{AC} is the measured and the calibration vapor pressures, respectively. The vapor pressure can be found from the following equation [67]:

$$e_A = e_S\frac{RH}{100} \tag{12}$$

e_S is the saturation vapor pressure and is a function of air temperature (T_A) as shown by the following equation [67]:

$$e_S = 0.61121 \exp\left(\frac{T_A\left(18.678 - \frac{T_A}{234.5}\right)}{257.14 + T_A}\right) \quad (13)$$

As for the effects of condensation, the oxygen sensor has an internal heater which prevents condensation from occurring on the sensor probe [67]. Otherwise, the sensor would give faulty measurements if water vapor condensed on its surface.

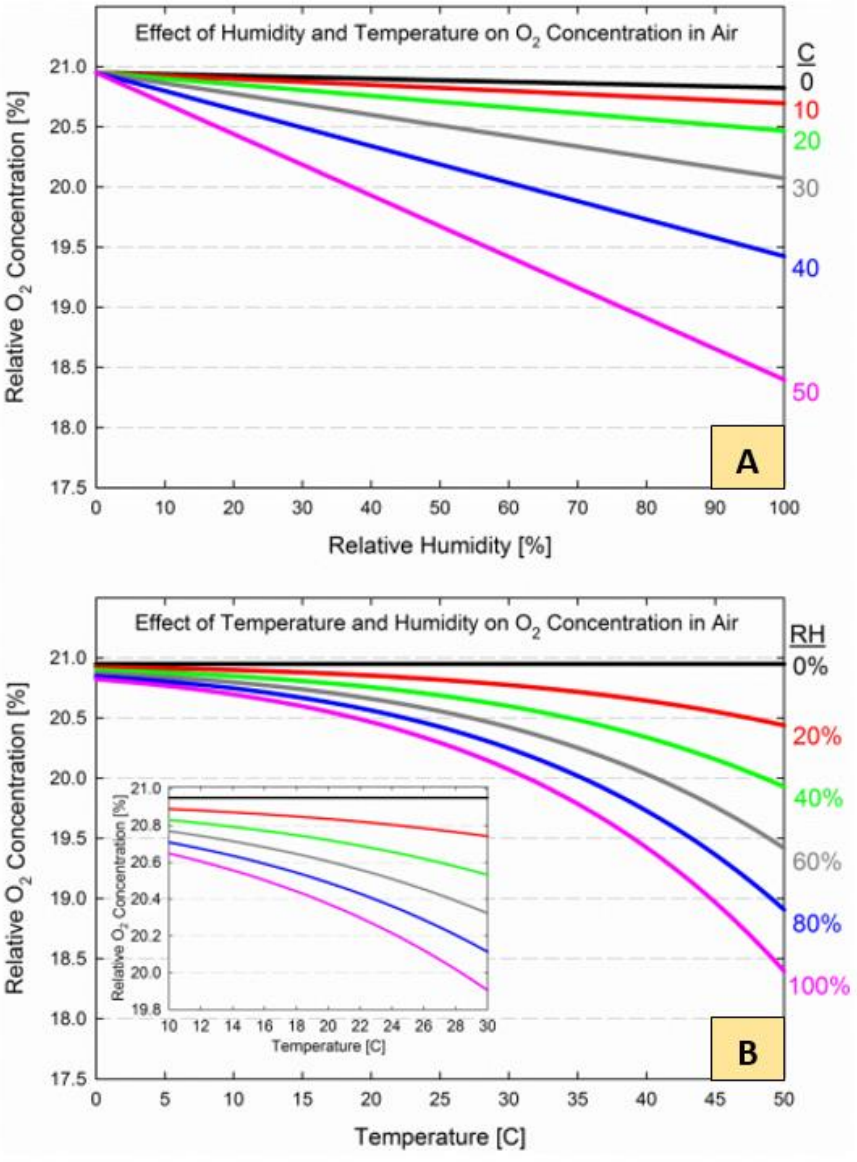

Figure 6.17: The two figures show the relationship between temperature, relative humidity and the relative oxygen concentration. Figure (A) shows the effect of relative humidity on relative oxygen concentration at constant temperature. Figure (B) illustrates the effect of temperature on relative oxygen concentration at constant relative humidity. The two figures are taken from manual [67] and modified.

Equations 11, 12 and 13 were implemented in the OCT software to produce oxygen concentration measurements that are corrected for changes in RH. One of the variables in equation 12 is RH. Measurements of RH are provided by an RH sensor (see the following section). The temperature measured by the sensor is used as an approximation for air temperature.

The Excel file produced by the OCT software provides oxygen concentration values both with and without RH corrections.

6.2.4 RH sensors

The Apogee oxygen sensor cannot measure relative humidity. Therefore, a sensor of the type E+E Elektronik EE06 series was installed by SINTEF in each of the reaction cells. This sensor is capable of measuring temperature in the range (-40 to 60 ˚C) and relative humidity in the range (0—100%). Due to the limited number of channels in the signal converter (see Section 6.2.5), only RH measurements are taken with this sensor. The RH sensors were calibrated prior to use by SINTEF. The calibration equations were added to the OCT software such that the corrected (true) RH values would appear on the user interface of the OCT software (in Figure 6.14) and in automatically produced the Excel file.

The accuracy of the sensor's measurements is ± 3% for RH in the range 10—90%. For RH higher than 90%, the accuracy decreases to ± 5% [68].

6.2.5 Analogue-to-digital signal converter and power unit

The signal that the Apogee SO-110 oxygen sensor outputs is an analogue signal that needs to be converted to a digital signal. This signal conversion is done by a data acquisition module of the type ADAM-4017 (see Figure 6.18). A power unit is also needed because each oxygen sensor requires 12.5 V for the heater (DC continuous) and 2.5 V for the thermistor (DC excitation) [67].

The technical staff at SINTEF made a compact box (shown in Figure 6.18) where the power unit and the data acquisition model are placed. The two oxygen sensors are connected to this compact box. A computer can be connected to the box via USB-cable.

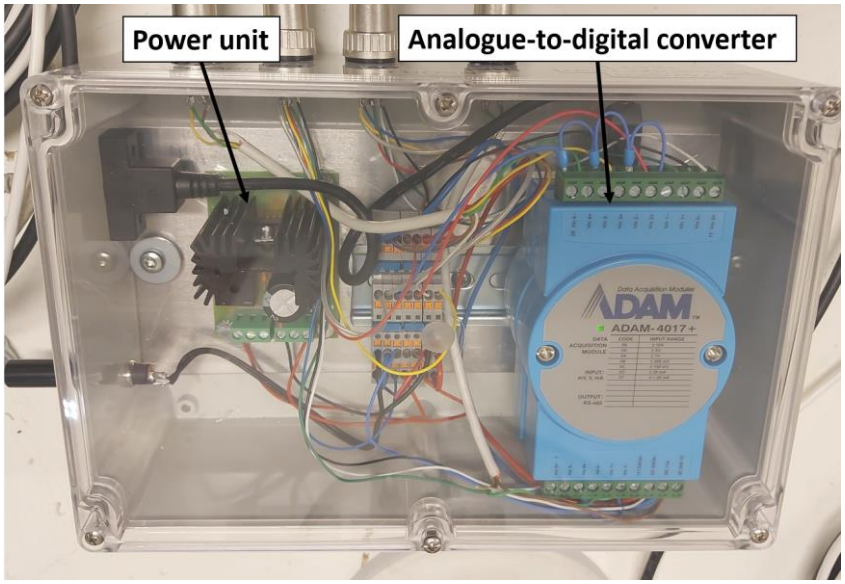

Figure 6.18: The picture shows the compact box that contains the data acquisition unit (right) and the power unit (left). The compact box was created by the technical staff at SINTEF.

7 Methods

7.1 Sample preparation

The preparation of samples to be tested in 1) the OCT, 2) for total sulfur analysis and 3) for particle size distribution by laser scattering is described in this section. The sample preparation process adopted in the present study was broadly based on the recommendations of Annex P [39]. Figure 7.1 shows a a general flowchart of the sample preparation methodology adopted for this study.

The general flowchart in Figure 7.1 starts with the field sample. If the D_{max} of the field sample exceeded 20 mm, the field sample was preliminarily crushed to the particle size 4/20 mm. The field sample was then divided (*Splitting I* in Figure 7.1) to obtain a representative subsample. To do this, the field sample was spread as a monolayer on the ground and quartered according to a modified procedure based on the internal procedure developed by N. Oberhardt (the modified procedure is shown in Appendix G1). Possible half-splitting by a riffle splitter was sometimes also necessary to obtain the representative subsample. Note that the term "subsample" in this thesis refers in general to the aggregate mass (washed or unwashed) before it was subsequently crushed and ground. To wash the subsample, the aggregate material was spread on a sieve and washed by water spray (*Washing* in Figure 7.1). The opening of the sieve used during washing is shown in Table 7.1. After washing, the washed subsample was dried to constant mass in a ventilated oven (at 105 or 110 °C) for 12 hours (*Drying* in Figure 7.1).

The particle size of the washed and dried subsample was then reduced by consecutive crushing and grinding (*Crushing* and *Grinding* in Figure 7.1). First coarse crushing was carried out using a jaw crusher to reduce the particle size to a D_{max} of 1—3 mm. Second, a disk crusher was used to reduce the particle size to a D_{max} of 300—1000 µm. Further processing of the crushed material was carried out according to one of the pathways (methodologies) presented in Figure 7.2. The material was processed by either the vibratory disk mill with a steel grinding set (**VDM-S** pathway in Figure 7.2) or the bench ball mill and planetary mill until the entire aggregate material passed the 147 µm sieve. Grinding with the bench ball mill was carried out using ceramic (pathway **BBM-C**) or steel (pathway **BBM-S**) balls.

Each washed and dried subsample was crushed/ground in several stages. After almost each pass through the crushing/grinding equipment, the processed material was sieved over the 75 and 147 µm sieves (*Sieving* in Figure 7.1). However, subsamples SM1-2 and MSK-Rich-1 were first sieved over the 2.5 mm and the 3.353 mm sieve, respectively, until the entire material passed the sieve. Then further crushing and sieving (over the 147 and 75 µm sieves) were carried out for these two subsamples. In general, after sieving the

processed material, only the oversize material retained on the sieve with the largest opening would then be crushed/ground further in the comminution process.

The individual fractions (0—75 µm and 75—147 µm) were sometimes divided by a splitter (*Splitting II* in Figure 7.1). This process was mostly used to obtain bulk samples for total sulfur analysis from the 0—75 µm fraction. Most of the obtained bulk test samples from the 0—75 µm fraction were tested with LECO at NBTL (Norwegian concrete and aggregate laboratory).

Following the splitting process, the two fractions were then mixed by hand to homogenize the subsample. Later in the pilot testing (for MSK Rich), the homogenization process was performed by passing the material through a riffle splitter five times as recommended by Andreia Rodrigues (personal communication, April 2023). For the two OCT test samples where MSK Rich was mixed in with limestone, the mixture of the two aggregates was also passed through a riffle splitter five times.

After the two fractions (<75 µm, 75—147 µm) were mixed, a 10-chamber rotary splitter was used to divide the mixed material to obtain an OCT test sample (2.3—2.55 kg) and a test sample for particle size distribution analysis by laser scattering (10—20 g). The process is shown as *Splitting III* in Figure 7.1. Note that the term "test sample" in this thesis refers to the crushed and ground aggregate mass ready to be tested in the OCT, for total sulfur content or for particle size analysis by laser scattering.

Limestone and SM1 test samples were analyzed with *Horiba LA-960* to investigate whether the particle size determined by sieving reflects the actual particle size of the sample. With *Horiba LA-960*, it is also possible to determine the full particle size distribution curve of the test sample. The test sample for particle size determination (10—20 g), obtained in the process *Splitting III* in Figure 7.1, was first mixed properly by a small stainless-steel spoon before using the spoon to extract a specimen of 1—3 g from each test sample. The 1—3 g specimen was then tested in *Horiba LA-960*. In total, three 1—3 g specimens from each limestone and SM1 test sample (10—20 g) were analyzed. To examine the reproducibility of the results, multiple measurements of the same specimen were often taken.

Table 7.1 shows an overview of all the subsamples prepared in this study. At the beginning of laboratory work, three limestone subsamples were prepared to be used in preliminary OCT testing. These subsamples were partially used to receive training on the use of the crushing equipment. The general procedure illustrated in Figure 7.1 was not therefore followed for these subsamples, as they were obtained in a non-representative manner and then directly crushed without washing or drying. Table 8.1 describes the equipment used for the crushing of these subsamples.

In Steps B and C of laboratory work, five subsamples were prepared, including two subsamples of limestone, two of SM1 and one subsample of MSK Rich. Appendix B includes detailed flowcharts showing how the general procedure in Figure 7.1 was adapted for each subsample.

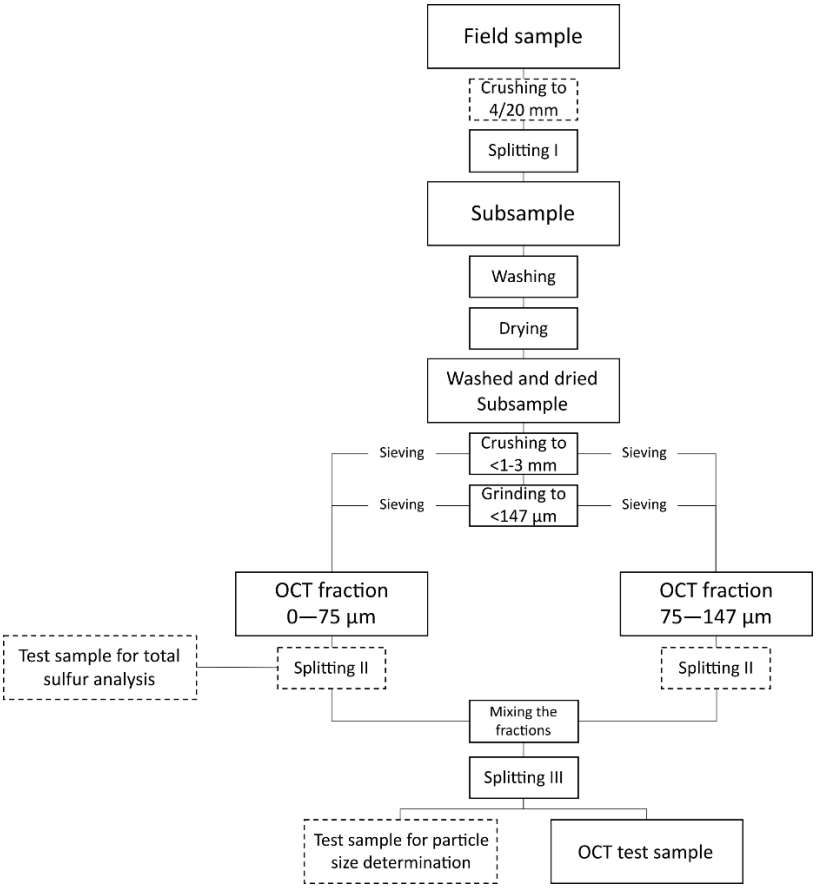

Figure 7.1: The general flowchart of sample preparation adopted in the present study. This methodology was in a broad sense based on Annex P [39]. The detailed flowchart for the preparation of each subsample is shown in Appendix B. Dashed boxes/processes were not always carried out.

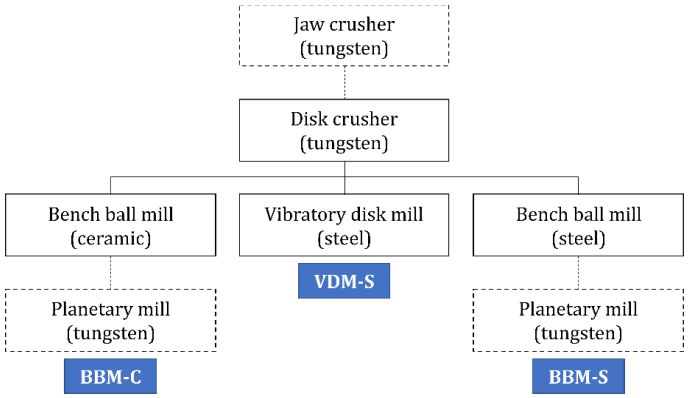

Figure 7.2: The three pathways of sample preparation. The abbreviation for each pathway is colored blue. The suffix (S) denotes that steel grinding equipment were involved in sample preparation, while the suffix (C) indicates that only tungsten/ceramic equipment were used. Dashed equipment was not always used in sample preparation.

Table 7.1: Overview of the subsamples prepared during the laboratory work. The MSK 0.9 sample tested with the OCT was prepared before the start of this M.Sc. study.

Subsample	Aggregate	Starting fraction [mm]	Starting mass [kg]	Sieve used in washing	Final particle size (by sieving)	Pathway in Figure 7.2	Sieving method	Flowchart in Appendix B
PreLim-1	Limestone	4/16	5	-	50% <77 µm 50% 77—142 µm	-	*SWECO vibrating screen*	-
PreLim-2	Limestone	4/16	ca. 5	-	<125 µm	-	Hand sieving	-
PreLim-3	Limestone	4/16	3	-	20% <77 µm 80% 77—142 µm	-	*SWECO vibrating screen*	-
Lim-1	Limestone	4/16	24	ca. 2.5 mm	27% <77 µm 73% 77—142 µm	BBM-C	*SWECO vibrating screen*	Figure B.1
Lim-2A	Limestone	4/16	6.6	2.8 mm	44% <75 µm 56% 75—147 µm	VDM-S	*RETSCH AS 300* sieve shaker	Figure B.2 Figure B.3
Lim-2B					50% <75 µm 50% 75—147 µm	BBM-S	*RO-TAP* and *RETSCH AS 300* sieve shakers	Figure B.2 Figure B.4
SM1-1	SM1	4/20	6.4	4 mm	37% <77 µm 63% 77—142 µm	BBM-C	Mostly *SWECO vibrating screen*	Figure B.5 Figure B.6
SM1-2A	SM1	4/20	5.6 (estimated)	4 mm	44% <75 µm 56% 75—147 µm	VDM-S	Hand sieving	Figure B.5 Figure B.7 Figure B.8
SM1-2B					46% <75 µm 54% 75—147 µm	BBM-S	Hand sieving	Figure B.5 Figure B.7 Figure B.9
MSK-Rich-1	MSK Rich	5/20	4.65	-	50% <75 µm 50% 75—147 µm	VDM-S	Hand sieving	Figure B.10

7.2 OCT pilot testing

The OCT methodology adopted in the pilot testing is largely based on the recommendations of Annex P [39] (see Section 2.3.3 – Test procedure) in addition to a video from ULaval (circulated as part of the interlaboratory procedure) titled *Oxygen consumption test procedure* [51]. Photos and videos taken by Dr. Jan Lindgård from a demonstration of the OCT procedure during the 2022 Canada-Norway workshop on pyrrhotite proved very helpful as well.

After sample preparation and splitting, the OCT samples (2.3—2.55 kg) were placed in separate plastic bags to avoid the segregation of the different material fractions. The OCT sample to be tested was then placed in a stainless-steel tray and mixed thoroughly. The excess aggregate material was then removed by a stainless-steel spoon. See Table 7.2 for the needed amounts of water and aggregate material (calculated according to equations 6 and 7 in Section 2.3.3.5).

Table 7.2: The table shows the aggregate and deionized water mass needed for the OCT reaction cell. The water mass is calculated for 40% saturation.

Aggregate	Particle density [g/cm^3]	Aggregate mass needed [g]	Mass of deionized needed [g]
Limestone	2.72	2293	337
SM1	2.72	2293	337
MSK 0.9	2.86	2411	337
MSK Rich	2.93	2470	337

In Step C, in addition to testing pure MSK Rich aggregate, MSK Rich was mixed in with limestone at 25%. The mixing of these two aggregates was “by volume” (i.e., such that the MSK Rich particles would take up 25% of the total volume occupied by the aggregate particles in the reaction cell). Based on this calculation, the necessary mass of MSK Rich was 617 g and of limestone 1719 g. The amount of water needed was 337 g, as for the other tests.

In general, after deionized water (from the SINTEF Concrete Laboratory) was added to the aggregate material, the mixture was thoroughly homogenized (though mixing by hand) in a stainless-steel or plastic tray. The formation of lumps was avoided. The mixture was then placed in the reaction cell as described in Annex P (see Chapter 2 Section 2.3.3.4).

8 Results

8.1 Preliminary testing (Step A) results

By the end of the preliminary testing step, the OCT setup (reaction cell, sensors, and OCT software) was working as intended. The O_2 sensor measured an O_2 concentration around 20—21% at the start of preliminary tests. The range of RH values measured in the entire 3.5 hours of the OCT ranged between 50—100% (see Figure 8.1). Potential issues with the OCT software and the wiring of the sensors were fixed at the end of this step.

Three preliminary oxygen consumption tests with limestone were carried out. Table 8.1 provides a summary of the tests and their parameters. Because the purpose of preliminary testing was not to get accurate oxygen consumption results, the samples were not obtained in a representative manner and were neither washed nor dried. The oxygen consumption was 0% for one test and invalid for the two others.

Table 8.1: The table shows an overview over the preliminary tests carried out in Step A of laboratory work.

Subsample	Material	Particle size	Saturation	Density [g/cm^3]	Ground material height	Equipment for sample preparation	O_2 consumption
PreLim-1	Limestone (4/16 mm)	<142 µm	40%	2.65	ca. 10 cm	Tungsten equipment (Jaw crusher).	Invalid. Recording of O_2 concentration stopped after 100 min.
PreLim-2	Limestone (4/16 mm)	<125 µm	60%	2.65	Ca. 7.5 cm	Steel equipment. (*RETSCH BB250* jaw crusher and a disk mill)	Invalid. Signal to the OCT software was received from the wrong O_2 sensor.
PreLim-3	Limestone (4/16 mm)	<142 µm	40%	2.7	10 cm	Tungsten equipment (Jaw and disk crusher).	0%

The main purposes with preliminary testing were to gain experience with the OCT testing and to identify potential issues with the laboratory procedures and the OCT setup. The observed issues included:

- A mistake in the preparation of the reaction cell where more material was added to the top layer compared to the bottom layer due to a calculation mistake. This will decrease the porosity of the top layer and increase it for the bottom layer.
- The use of a wrong internal cell diameter. At the beginning of this step, it was assumed that the reaction cells sent to Norway from Canada had the same internal diameter (141.7 mm) as the cells used by Rodrigues et al. [3] in 2016. After manually measuring the diameter and checking again with the Canadian researchers, the correct cell diameter was found to be 146.5 mm.

- Slightly wrong density values were used. The correct density value for limestone is 2.72 g/cm^3. The correct density was used for later ("proper") testing.

These issues imply that the saturation level for the preliminary tests will be slightly different from the values in Table 8.1. However, these values still reflect the amount of water added in each test (see Section 2.3.3.5).

Another challenge encountered during this step was that subsample PreLim-3 got contaminated by iron from the jaw crusher due to a miscommunication where the jaw crusher was not cleaned prior to use. During "proper" testing (Steps B and C), it was ensured that all machines and equipment were cleaned with water and/or compressed air before and after use.

Figure 8.1 illustrates how RH changes during the OCT for the preliminary test at 60% saturation (subsample PreLim-2 in Table 8.1) and at 40% (PreLim-3). RH increases as time progresses, and 100% RH is reached at 95 min for 60% saturation and at 162 min for 40% saturation.

In the preliminary test planned at 60% saturation level, a thin film was observed on top of the aggregate material layers (see Figure 8.2). This thin film was reported by Rodrigues et al. [3] in 2016 when testing aggregate material with a 60% saturation level.

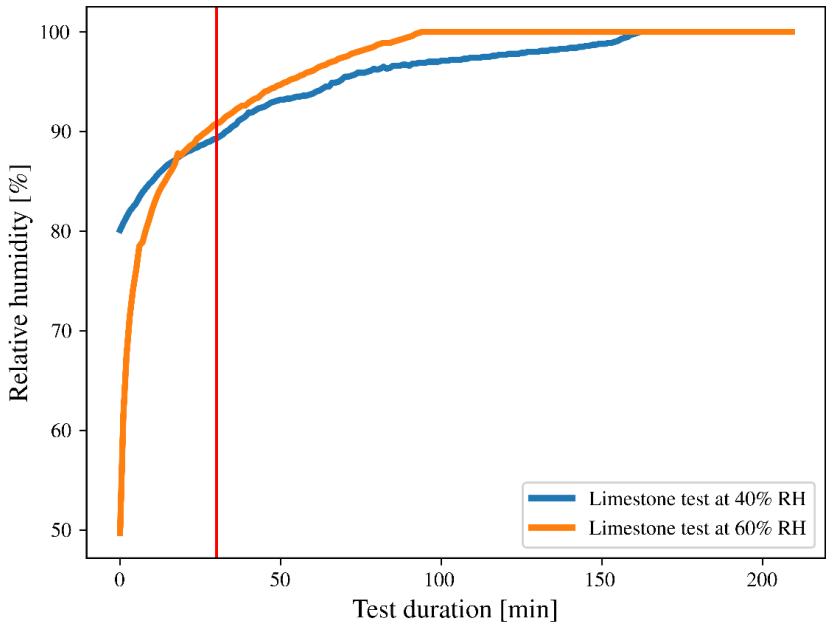

Figure 8.1: The figure shows how RH changes during the OCT. The tested material is limestone at 60% saturation (subsample PreLim-2 in Table 8.1) and at 40% (PreLim-3). The vertical red line marks the end of the stabilization period (0.5h) of the OCT.

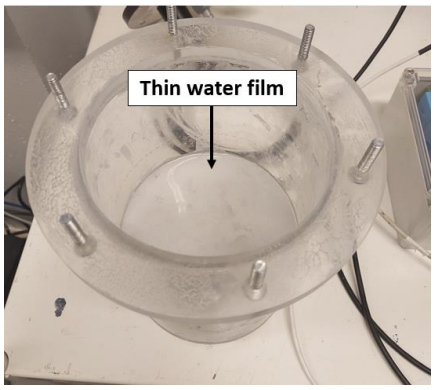

Figure 8.2: The figure shows the thin water film that appeared when testing the aggregate sample PreLim-2 with 60% saturation level.

8.2 Sample preparation results

Table C.1 in Appendix C presents a rough estimate of time spent on the preparation of each subsample in this study after preliminary testing. The durations recorded include the total time spent on aggregate preparation (crushing, grinding, and sieving), including time for cleaning, and setting up the equipment. However, the durations do not include time spent on splitting, washing, or drying of the aggregate.

To better explain Table C.1, the preparation of subsample Lim-1 will be illustrated in the following points:

- Subsample Lim-1 had a washed and dried mass of **21.2** kg (4/16 mm). Through crushing with the jaw crusher, 5.6 kg passed the 142 µm sieve. **15.6** kg were retained on the sieve and had a particle size of ca. <2.5 mm. This step took 3h (rough estimate).
- The mass (**15.6** kg) retained on the 142 µm sieve after processing with the jaw crusher was introduced to the disk crusher (through several passings) and **3** kg remained with a particle size >142 µm sieve (i.e., 12.6 kg were reduced to the particle size <142 µm). This step took 3h (estimated).
- The remaining mass (**3** kg) with an estimated particle size of <1 mm was ground with the bench ball mill with ceramic balls (BBM-C pathway) until the entire material was reduced to the particle size <142 µm. This step was the most time-consuming, taking an estimated 17.5h to be completed.

As shown by the preparation of the subsample Lim-1, grinding was the most time-consuming part of sample preparation. Moreover, the preparation of the harder SM1 aggregate took significantly more time compared to the limestone aggregate (see Table C.1).

As shown in Figure 7.2, the pathways (BBM-C, VDM-S and BBM-S) use the same equipment for crushing (jaw/disk crusher with tungsten plates) but are mainly different in the type of equipment (steel or ceramics)

used for grinding. It is therefore possible to compare the three different pathways by looking at the grinding steps in Table C.1. Table 8.2 below (summarizing the grinding steps in Table C.1) presents the time spent on grinding for each limestone and SM1 subsample. According to Table 8.2, grinding with steel equipment (BBM-S and VDM-S in Figure 7.2) is less time consuming than using ceramic equipment (pathway BBM-C). In fact, for limestone, it took 17.5h to reduce 3 kg of limestone to the target size <142 μm using pathway BBM-C, while it took only 4-5h to reduce 2.36 kg to the same target size using the pathway VDM-S. For SM1, it took roughly 24h to grind 3.17 kg with pathway BBM-C, and only 8-9h to grind 1.78 kg with pathway VDM-S.

Table 8.2: Time spent on grinding of each subsample. Summarized from Table C.1 in Appendix C.

Subsample	Mass with fraction >147 μm after crushing	Pathway in Figure 7.2	Time spent
Lim-1	3 kg	BBM-C	17.5h
Lim-2A	2.36 kg	VDM-S	4-5h
Lim-2B	1.4 kg	BBM-S	6-7h[1)]
SM1-1	3.17 kg	BBM-C	24h[2)]
SM1-2A	1.78 kg	VDM-S	8-9h
SM1-2B	0.86 kg	BBM-S	4h[3)]

1) 5-6h bench ball mill (steel balls) + 1h planetary mill (tungsten)
2) 23h bench ball mill (ceramic balls) + 1h planetary mill (tungsten)
3) 3h bench ball mill (steel balls) + 1h planetary mill (tungsten)

When preparing samples as described in Chapter 7, the particle size is determined by sieving. The fractions (0—75 μm) and (75—147 μm) for each prepared subsample is shown in Table 7.1 and in the test matrix, Appendix A Table A.2.

The particle size for test samples was also measured by laser scattering. Table 8.3 and Table 8.4 compare the particle size distribution produced by each pathway for the limestone and SM1 aggregates, respectively, as determined by laser scattering. Appendix D shows the full particle size distribution curves. As shown in Table 8.3 and Table 8.4, the results indicate significant differences compared to the desired particle size for the OCT and to the particle size found by sieving (shown in Table 7.1).

For all tested limestone samples (Table 8.3), ca. 10% of the sample had the particle size >150 μm. For the SM1 samples (Table 8.4), ca. 15—30% of the sample mass had the particle size >150 μm. Around 60—70% and 50—60% of the samples for limestone and SM1, respectively, had a particle size <77 μm. Around 40—50% of the samples of both aggregates had a particle size <39 μm. Therefore, for particle size >39 μm, the results show that limestone samples are crushed/ground to a finer particle size compared to the SM1 samples.

The grading of the limestone test samples (shown in Table 8.3 and Figure D.4 in Appendix D) is quite similar. The limestone test samples ground using the vibratory disk mill (pathway VDM-S in Figure 7.2) had a slightly coarser particle size (in the range ca. 20—116 µm) as determined by *Horiba LA-960* compared to the other two limestone samples.

The grading of SM1-2B (BBM-S) was slightly coarser than the other two SM1 samples (see Table 8.4 and Figure D.8). The particle size distribution for the SM1 test samples prepared with pathways VDM-S and BBM-C was more comparable (with the pathway VDM-S producing a slightly higher number of particles <3 µm, see Figure D.8).

Table 8.3: The particle size distribution for the three limestone test samples (with the pathway according to Figure 7.2 given in paranthesis) as found by laser scattering. For an overview of all the subsamples prepared in this thesis, see Table 7.1.

Particle size, [µm]	Cumulative percentage of test sample under given particle size						
	Desired particle size for the OCT	Lim-1 (BBM-C)		Lim-2A (VDM-S)		Lim-2B (BBM-S)	
		Average[1)]	σ[2)]	Average[1)]	σ[2)]	Average[1]	σ[2)]
10	-	13.3%	0.3%	14.7%	1.0%	13.9%	0.3%
39	-	43.8%	0.4%	41.6%	1.9%	47.5%	0.5%
77	ca. 50%	67.4%	1.2%	61.5%	2.0%	70.3%	0.5%
116	-	84.1%	0.8%	79.1%	1.4%	85.2%	0.5%
152	ca. 100%	92.3%	0.3%	89.3%	0.8%	92.6%	0.4%

1) Average of three tests
2) σ: standard deviation

Table 8.4: The particle size distribution for the three SM1 test samples (with the pathway according to Figure 7.2 given in paranthesis) as found by laser scattering.

Particle size, [µm]	Cumulative percentage of test sample under given particle size						
	Desired particle size for the OCT	SM1-1 (BBM-C)		SM1-2A (VDM-S)		SM1-2B (BBM-S)	
		Average[1)]	σ[2)]	Average[1)]	σ[2)]	Average[1]	σ[2)]
10	-	16.4%	2.4%	19.2%	1.0%	15.6%	0.9%
39	-	43.2%	2.4%	47.0%	2.1%	38.9%	3.3%
77	ca. 50%	60.8%	2.2%	60.2%	1.3%	50.2%	2.5%
116	-	75.8%	2.0%	71.7%	0.7%	61.4%	0.7%
152	ca. 100%	85.4%	1.5%	80.9%	0.3%	72.5%	0.8%

1) Average of three tests
2) σ: standard deviation

Note that when the percentages of fractions (<75 µm) and (75—147 µm) are provided for a sample elsewhere in this thesis, these percentages reflect the amount of material passing or retained on the 75 µm sieve and are not determined through particle size analysis using *Horiba LA-960* (laser scattering) unless explicitly stated.

8.3 OCT pilot testing results

In this section, the oxygen consumption results for the tested aggregates are presented. Oxygen consumption is shown after implementing corrections for ambient conditions (RH, temperature and pressure). Unless otherwise indicated, the standard Annex P [39] OCT test parameter values are used (shown in Table 2.2).

8.3.1 OCT results for Step B

To investigate the effect of sample preparation on oxygen consumption, limestone and the SM1 aggregate samples were prepared with steel grinding equipment (pathways VDM-S and BBM-S in Figure 7.2). These samples were then tested with the OCT. The results from these two pathways are compared with the results from pathway BBM-C (involving only ceramic/tungsten equipment).

The limestone test samples prepared with pathways BBM-C and BBM-S resulted in an oxygen consumption of 0%. However, oxygen consumption could be as high as 0.44% because the O_2 concentration was only recorded with one decimal place for these two tests. The accuracy was increased to two decimal places for all other tests in Steps B and C. The oxygen consumption for the limestone test sample prepared with the pathway VDM-S was 0.15%.

Figure 8.3 shows the oxygen consumption for the SM1 test samples. The oxygen consumption was 3.0% and 3.47% for the samples prepared with pathways VDM-S and BBM-S, respectively. The test sample prepared with pathway BBM-C had an oxygen consumption of 3.46%.

At the end of Step B, the RH sensor in one of the reaction cells was found to give strange results. The sensor was stable, but further calibration by SINTEF showed that the measured RH was 100% when the corrected (true) RH was only 91%. This error mainly affected the SM1 samples prepared with pathways BBM-C and BBM-S. The oxygen consumption for these tests might increase slightly (possibly by 0.26% oxygen consumed) if the sensor had measured the correct RH level. Both RH sensors were re-calibrated until they provided quite similar (RH vs time) plots during the OCT. The other RH sensor gave reasonable results before and after recalibration.

To study how a higher saturation level affects oxygen consumption, one limestone test was carried out at 60% saturation level. The remaining test parameters are as recommended in Annex P [39]. The test sample was prepared with only ceramic/tungsten equipment (pathway BBM-C in Figure 7.2). The oxygen consumption for the test was 0.35%.

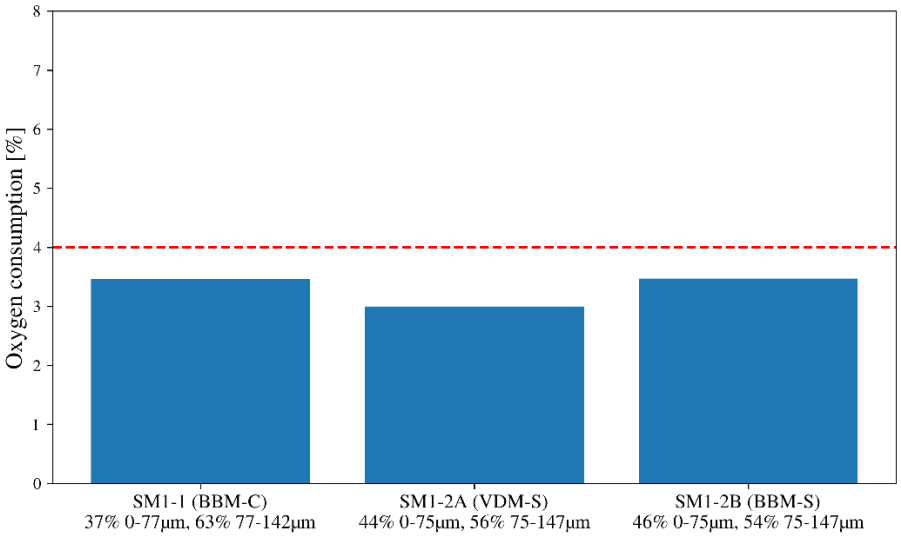

Figure 8.3: The oxygen consumption values for SM1 prepared with three sample preparation pathways. The particle size distribution (determined by sieving) for each test is shown. The red dashed line shows the 4% limit proposed in Annex P [39].

The effect of test duration was also investigated. The oxygen consumption results were taken after 16h 44min (16.7h) for the SM1 tests prepared with pathways VDM-S and BBM-S. These results are compared to those taken after 3.5h in Figure 8.4. The results show a significant increase in oxygen consumption with the longer test duration. The oxygen consumption after 16.7h was 8.5% and 8.6% for the tests prepared with VDM-S and BBM-S, respectively.

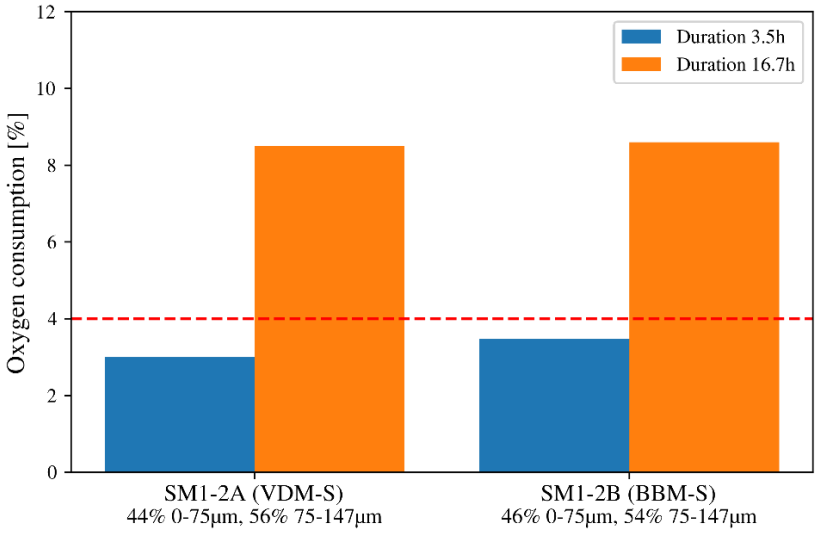

Figure 8.4: The figure shows the relationship between oxygen consumption and test duration (3.5h and 16.7h) for two SM1 tests prepared with two different pathways (BBM-S and VDM-S). All other test parameters were as recommended by Annex P [39]. The red dashed line shows the 4% limit proposed in Annex P [39].

8.3.2 OCT results for Step C

Figure 8.5 presents the oxygen consumption results obtained for aggregates MSK 0.9 and MSK Rich and compares them to the Canadian test results. The oxygen consumption was 8.75% and 7.41% for MSK 0.9 and MSK Rich, respectively.

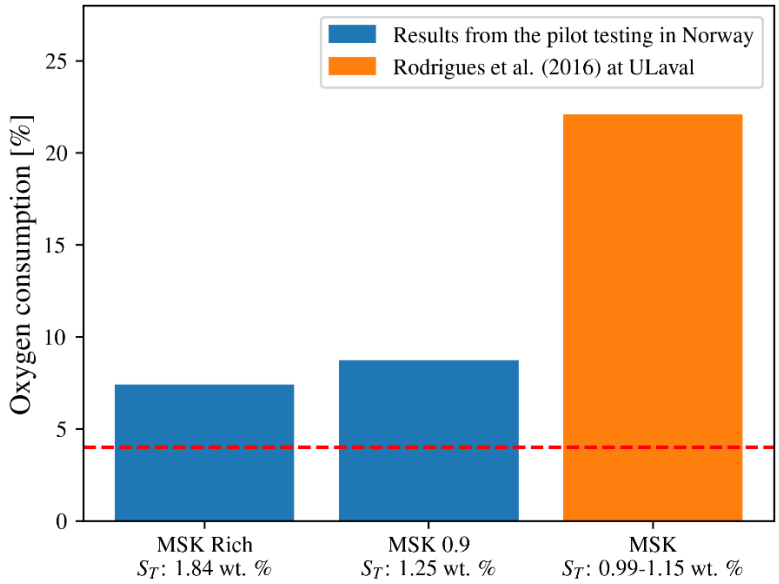

Figure 8.5: The figure shows the oxygen consumption for the Canadian MSK aggregate. The results from this present study are colored in blue, while the results from Rodrigues et al. [3] in Canada are highlighted in orange (average of six tests). The standard Annex P [39] parameters were used for all these tests. The red dashed line shows the 4% critical limit.

Two parallel tests with the aggregate mixture (25% MSK Rich, 75% limestone) were carried out as part of the Norwegian pilot testing. The results are presented in Table 8.5. The oxygen consumption was 2.20% and 2.18% respectively.

Table 8.5: The table presents the oxygen consumption for the MSK-limestone aggregate mixture.

Aggregate	Particle size	Saturation	O_2 sensor	Reaction cell	O_2 consumption [%]
25% MSK Rich., 75% limestone	33% <75 µm, 67% 75—147 µm	40%	Sensor A	Cell 1	2.20%
25% MSK Rich., 75% limestone	33% <75 µm, 67% 75—147 µm	40%	Sensor B	Cell 2	2.18%

9 Discussion

The focus of this M.Sc. study was both on the sample preparation process and on the pilot testing of aggregate samples in the OCT as shown by the objectives laid out in Section 1.2. Overall, the results show that these objectives were reasonably achieved.

First the results of the preliminary testing will be discussed. A discussion of sample preparation, particularly the efficiency of the process, particle size distribution and sample representativity will ensue. The results of each of the steps of the laboratory work and pilot testing outlined in Chapter 3 will then be thoroughly examined. Lastly, the proposed procedure for sample preparation and OCT testing will be analyzed.

9.1 Preliminary testing (Step A)

Step A was mainly focused on training and on trouble-shooting any potential issues that can arise during later "proper" testing. Despite the issues listed in Section 8.1, this step contributed to a better understanding of how RH changes in the reaction cell during the OCT. All preliminary tests (3 in total) showed that 100% RH is reached during the OCT, confirming the need for calibrating the oxygen sensor in an environment with 100% RH.

By the end of this step, the OCT setup was operating successfully (the RH sensors had to be re-calibrated during later testing, however, this did not affect the oxygen consumption results significantly – see Section 8.3.1).

9.2 Sample preparation

9.2.1 Time and cost efficiency

The inefficiency of the sample preparation process was one of the main challenges encountered during the pilot testing. The process was time consuming, partly due to a lack of experience with sample preparation, but also because the process was somewhat inherently lengthy (given that, for each oxygen consumption test, 2.6 kg are to be reduced in size from, for example, 4—20 mm to <150 µm). The available literature on the OCT does not provide information on the duration of sample preparation, except for a comment by El Mosallamy et al. [60] reporting that samples were processed for 8 hours in a micro-deval abrasion machine after introduction to the jaw crusher. However, at the Norway-Canada workshop on pyrrhotite in May 2023, the participants at Ulaval confirmed that sample preparation is indeed time-consuming.

At the start of the pilot testing, one of the early objectives was to avoid the use of steel pulverizing equipment during sample preparation due to possible iron contamination. However, the time spent on the process (see Table 8.2 and Appendix C Table C.1) using only ceramic/tungsten equipment necessitated looking into alternative ways of grinding the aggregates. The use of steel equipment was considered, and pathways BBM-S and VDM-S (see Figure 7.2 for the sample preparation pathways) were investigated.

The comparison presented in Table 8.2 shows that pathway BBM-C (grinding with the bench ball mill with ceramic balls) is more time-consuming compared to pathways VDM-S and BBM-S for both limestone and SM1. In general, it took more time to grind the SM1 aggregate material compared to limestone, indicating the importance of the aggregate's mineralogy and hardness on time spent on grinding.

In addition, there was a delay (due to mistake in mounting the *SWECO* vibrating screen used for sieving) that caused a slightly increased time consumption in the preparation of subsample SM1-1 with the pathway BBM-C. However, this error is unlikely to affect the results presented in Table 8.2 significantly.

When it comes to the effect of operator, it is possible to argue that my lack of experience with sample preparation led to increased time consumption. However, it is important to note that the trained laboratory technician from SINTEF also needed to familiarize himself with the sample preparation procedure (for example, the most appropriate sieving technique for this procedure had to be selected).

It is possible to calculate the time spent on the entire sample preparation process (crushing and grinding) for one OCT test sample (2.6 kg) from each of the subsamples listed in Table C.1. However, this does not provide a good comparison between the grinding pathways (VDM-S, BBM-C and BBM-S) mainly because of the effects of scale, especially on crushing (assuming equal efficiency of the equipment, less time is spent crushing/grinding 1 kg of material when a larger sample is prepared compared to a smaller sample). The subsamples listed in Table C.1 varied substantially in mass. Therefore, Table 8.2 (focusing on the grinding steps) provide a better comparison between the pathways partly because the aggregate masses listed (i.e., the material remaining >147 µm after crushing) were more comparable (the masses were in the range of ca. 1—3 kg).

As shown in Table 8.2, the time spent by pathways BBM-S and VDM-S is comparable for SM1. For limestone, pathway VDM-S is significantly more efficient at grinding limestone than pathway BBM-S (4-5h to grind 2.36 kg to <147 µm with VDM-S compared to 6-7h to grind 1.4 kg to the same target size with BBM-S). When considering cost efficiency based on time spent, pathway VDM-S is therefore more cost efficient, at least for softer aggregates like limestone. Cost efficiency in general can be dependent on other cost factors, including the cost of using laboratory facilities and labor cost, however, these factors are more

variable and might change in the future (for example, when a laboratory purchases a new piece of equipment).

9.2.2 Particle size

Another related challenge was the particle size distribution to be adopted in the pilot testing. The procedure in Annex P [39] requires a particle size distribution <160 μm. However, discussions taking place during the 2022 Canada-Norway workshop on pyrrhotite [59], in addition to the interlaboratory procedure proposed by ULaval [51], propose a particle size distribution of 50% 0—80 μm and 50% 80—160 μm. 100% of the material sample should reach the desired fractions at the precise percentages, otherwise, sample representativity might be reduced. Moreover, different aggregates respond differently to the same crushing/grinding process depending on the aggregate's hardness and grindability (evident by the longer time it took to grind SM1 compared to limestone in this study). To get exactly 50% of each of the fractions, the parameters of the crushing/grinding process will have to be adjusted for each aggregate, thus making the process tedious and likely even more cost intense.

Considering the above challenges, and after discussion with the Canadian research team, the samples in the pilot testing were comminuted to a target size of <147 μm (<142 μm for subsamples Lim-1 and SM1-1), keeping the fraction <75 μm (<77 μm for subsamples Lim-1 and SM1-1) at a maximum of 50% of the OCT sample mass. This adopted approach is conservative, as El-Mosallamy and Shehata [60] showed that the fine fraction (<75 μm) can slightly lower the oxygen consumption results (see Section 2.4.4). A possible reason for this reduction is that fine material (<75 μm) can be more closely packed, thus lowering the permeability of oxygen in the ground material layers.

However, it was suspected that the particle size determined by sieving over the 75 and 147 μm sieves might not fully reflect the actual particle size distribution of the test samples. For this reason, the particle size of test samples (10—20 g) of SM1 and limestone was analyzed in *Horiba LA-960 Particle Size Analyzer*. Although these test samples passed the 147 μm (or 142 μm) sieve, ca. 10—30% of the particles were >150 μm (as shown in Table 8.3 and Table 8.4). A possible explanation for the relatively large percentage of particles above 150 μm could be that the crushing procedure produced many elongated particles that pass through smaller sieve openings. A more homogenous crushing of particles can be achieved through a slower, stepwise reduction scheme (as discussed later in this section).

As shown in Table 8.3 and Table 8.4, for most samples, the fraction of fine particles (<75 μm) was significantly higher than 50% (in the range 50—70%). Even more unexpected was the percentage of particles finer than 39 μm which was around 40—50% for all tested samples. Although a higher percentage of fine particles can be somewhat expected given that these fractions can get stuck on the surfaces of larger

particles, these unusually high percentages are more likely caused by rapid inhomogeneous crushing and/or quite inefficient sieving. Wet sieving can increase sieving efficiency, however, contact with water would peroxidize the particles.

As mentioned in Section 7.1, a larger proportion of the limestone samples were in the range 39—150 µm compared to the SM1 samples (i.e., in the particle size range >39 µm, limestone is crushed/ground finer than SM1) indicating that the aggregate mineralogy and hardness plays an important role in the particle size produced when crushing and grinding.

Except for the relatively small differences mentioned in Section 7.1, for limestone, the different pathways (BBM-C, VDM-S, and BBM-C) produced quite similar particle size distribution (see Figure D.4). The particle size distribution for the SM1 samples produced by the three different pathways (see Figure D.8) was also comparable, with the pathway BBM-S producing a slightly coarser material. However, only two test samples from each pathway were analyzed by laser scattering. A larger number of tests are needed to reach a more definitive conclusion, especially given that for each OCT test sample (2.3—2.55 kg), only 3—9 g is analyzed with laser scattering.

The spread of the particle size distribution curves for limestone is smaller compared to SM1 (see Figure D.8 and Figure D.4). This difference could potentially also be the result of the different mineralogy of these two aggregates (see Chapter 4). It could be, for example, that the minerals in the softer limestone can be crushed more homogeneously compared to the harder SM1.

The sieving method/procedure has a strong impact on sieving efficiency. Comparing the particle size measured by laser scattering (Table 8.3 and Table 8.4) to the particle size determined by sieving (Table 7.1) can be used to evaluate the sieving methods (mentioned in Table 7.1) used. The proportion of particles passing the 75 µm sieve can be a way of judging sieving efficiency because it is related to the ability of the sieving method to let finer particles pass through the sieve. For subsamples Lim-1 and SM1-1, ca. 24—40% more particles were found to be <77 µm by laser scattering compared to the particle size found by sieving with the *SWECO Vibrating screen*. For subsamples Lim-2A and Lim-2B, 17.5—20% more particles were found to be <77 µm by laser scattering compared to sieving with the *RETSCH AS 300 or RO-TAP sieve shakes*. Hand sieving (used for subsamples SM1-2A and SM1-2B) showed the smallest difference, with only 4—16% more particles found to be <77 µm by laser scattering. Therefore, hand sieving is the chosen method of sieving in the recommended sample preparation procedure.

The large difference between the particle size as determined by laser scattering compared to sieving for the *SWECO Vibrating screen* could be due to my lack of experience with sample preparation from before, as it

could be that I added too much material on the sieve at the same time or that the sieving did not take long enough time.

It is hard to compare the particle size distribution found by particle size analysis (using *Horiba LA-960*) to the work in Canada because the available OCT literature does not provide information on whether the particle size determined by sieving was later confirmed by other means of particle size analysis. Thus, it is difficult to ascertain the extent to which these results are abnormal compared to the particle size distributions used in Canada.

9.2.3 Sample representativity

The aim of any sample preparation process is to ensure that the produced samples are representative of the material from which they were obtained. Therefore, improper sampling can be determinantal to the reliability of any analysis technique, as shown by Gy's theory of sampling [69]. This theory explains that errors during sampling can arise both from the sampling process itself and from sample preparation (such as the loss of material during grinding). A proper sampling process, according to Gy, must allow all the particles of the material to have the same probability of being included in the sample.

To ensure representativity when using a riffle splitter, the opening of the splitter should be $\leq 1.5\ D_{max}$. This general rule was not always followed, partly due to a lack of experience at the start of the sample preparation, and partly due to lack of suitable splitters. Whenever possible, however, rotary splitters were used. These splitters are more suitable to divide samples with a fine particle size.

A stepwise comminution process (as applied for subsample SM1-2 and MSK-Rich-1) would also contribute to more representative splitting of samples. In stepwise crushing, the subsample is first crushed to pass the 2.5 mm sieve (or similar) before being crushed again and then ground to pass the 147 µm sieve. If the aggregate material is crushed too quickly (i.e., without intermediate steps), representativity might be reduced because some minerals might get excessively crushed compared to other minerals (Benoit Fournier, personal communication, May 2023). The excessively crushed minerals might also be lost as dust. The risk from such "over-crushing" is not necessarily that more fine material is produced, but that certain minerals are over-represented in finer fractions. Homogenous stepwise crushing was therefore implemented in the proposed sample preparation procedure (see Figure F.1 in Appendix F and Appendix G1).

In addition, in the OCT, there is a certain loss of sample representativity. The mass of an OCT sample, according to Annex P [39], is 2.5 kg. However, depending on the particle density of the aggregate, only 2.1—2.5 kg may be needed. Some material is therefore removed from the sample using a stainless-steel spoon. According to Gy, this is a "non-probabilistic" sampling procedure that is especially prone to

sampling bias [69]. The mass of the OCT sample can of course be changed depending on the density of the aggregate, but that would make sample preparation tedious as no standard procedure can be followed.

Another factor affecting sample representativity is the loss of material during sample preparation. The material loss for each subsample can be found in Appendix E Table E.1. Note that the loss of material here does not include the weight reduction due to washing and subsequent drying. Sources of material loss include:

1. Material getting stuck in the crushing and grinding equipment
2. Material getting stuck in gaps in the sieving tower (mainly in the *SWECO Vibrating screen*)
3. Material lost as dust
4. Material accidentally dropped on the floor

Although some loss of material may be inevitable, care was taken during the laboratory work to reduce material loss. For example, as much material as possible was retrieved from inside the grinding equipment and the sieving apparatus.

Early in the pilot testing, the loss of material was significantly high (6.5% for subsample Lim-1). Even more material was lost (up to 18%) from subsample SM1-1 due to a mistake in mounting the sieving apparatus. Later in the pilot testing, material loss was significantly reduced (to ≤5% for subsample SM1-2 and the MSK samples). The move away from using the *SWECO Vibrating screen* can partially explain this reduction in material loss as no significant loss of material was observed when hand sieving or when using the smaller sieve shakers.

9.3 OCT pilot testing

9.3.1 OCT testing procedure

The oxygen consumption testing procedure for the pilot testing was nearly identical to the procedure followed in Canada thanks to the available visual demonstration of the procedure (video from the interlaboratory study [49, 51]; photos and videos from the 2022 Canada-Norway workshop).

Perhaps one of the more important steps to focus on during the preparation of the reaction cell is the mixing of the ground material both before and after water is added. The video from the interlaboratory procedure shows that the mixing is done by hand [51]. No indication is given regarding how long the mixing process should take, only that the material ought to be “well-mixed” at the end of the process. The video also warns against the formation of lumps as they might affect the resulting oxygen consumption. However, what constitutes a “well-mixed” ground material is somewhat subjective. Therefore, and after discussion with

Dr. Andreia Rodrigues during the 2023 Canada-Norway workshop, a 15 min mixing time (by hand) was used for the remaining part of the pilot testing (mainly involving the preparation of the MSK Rich samples). This extended mixing time (15 min) was also included in the recommended procedure for the OCT (Appendix G2).

9.3.2 RH corrections

The oxygen consumption results shown in Section 8.3 are corrected for all ambient conditions (temperature, pressure and RH). Corrections for pressure and temperature are unlikely to influence the oxygen consumption results. In addition, the temperature measurements from the oxygen sensor show that the sensor's temperature increases slightly during the OCT to prevent condensation. This is exactly what the oxygen sensor is designed to do [67]. For all OCT tests in Steps B and C, the OCT software provided the oxygen concentration measurements with and without RH corrections. Therefore, it was possible to calculate how implementing the RH corrections affects the oxygen consumption values. The results show that the RH at the end of the stabilization period (0.5h) is around 89—95%, causing the difference between the corrected and uncorrected oxygen consumption to be ca. 0.15—0.26%. Considering the current oxygen consumption limit of 4%, the effect of RH corrections seems quite marginal. However, measuring RH inside of the reaction cell and implementing RH corrections is a relatively easy and straightforward process. Therefore, it is recommended to measure and correct for RH in future OCT testing to obtain even more reliable results.

9.3.3 OCT results from Step B

SM1 and limestone test samples were prepared with three different sample preparation pathways (shown in Figure 7.2). Two of these pathways (VDM-S and BBM-S) involved the use of steel grinding equipment, while the third pathway (BBM-C) involved only ceramic/tungsten equipment.

Considering the samples prepared with ceramic/tungsten grinding equipment, the oxygen consumption was 0% (<0.44%) for limestone and 3.46% for SM1. These are reasonable results given the total sulfur content (S_T) of the aggregates (0.02 wt. % for the limestone and 0.45 wt. % for SM1) and the detection of pyrrhotite in the SM1 aggregate by DTA.

For both limestone and SM1, the O_2 consumption results from the pathways involving steel equipment are very similar (with a difference of <0.5% oxygen consumed) to the results from the BBM-C pathway (see Section 8.3.1). This similarity preliminarily indicates that iron contamination is not a major concern for OCT testing with the equipment used in this thesis. However, the number of tests is small, and more tests are needed to reach a more definitive conclusion.

El-Mosallamy and Shehata [40] showed that iron contamination can cause an increase of oxygen consumption by as much as 15—36% oxygen consumed (as shown in Figure 2.11 and Figure 2.12). An increase in oxygen consumption of this magnitude was not observed for tests carried out in this study.

As mentioned before, Annex P [39] does not explicitly discourage the use of steel grinding equipment, only cast-iron disks for the disk pulverizer. In addition, the procedure for the interlaboratory study organized by Ulaval does not warn against the use of steel equipment in general, only cast-iron equipment [49, 51]. In fact, steel pulverizing equipment is currently used for sample preparation at Ulaval (Andreia Rodrigues, personal communication, April 2023).

A further preliminary confirmation (though far from definitive) that iron contamination from steel equipment is (currently) not a major concern for the pilot testing is the oxygen consumption for one of the preliminary tests (Prelim-3 in Table 8.1). The tested sample got contaminated by iron due to an unclean jaw crusher, and although the contamination was visible, the oxygen consumption for that test was ≤0.44% (measured to be 0%, but only with the use of one decimal place).

Moving on to the effect of test duration on oxygen consumption, the results shown in Figure 8.4 preliminarily indicate that O_2 consumption increases significantly as the test duration increases. The oxygen consumption more than doubles when comparing the 3.5h to the 16.7h test duration. These results are in agreement with El-Mosallamy et al. [40]. The authors tested aggregates with the OCT for a similar duration (16.5h) and reported a significant increase in the resulting oxygen consumption (see Figure 2.18). In fact, the rate at which the oxygen consumption increases in the work of El-Mosallamy and Shehata (Figure 2.18) is similar to the rate observed in Figure 8.4.

As for the saturation level, limestone was tested with 60% saturation. The resulting oxygen consumption (0.35%) was comparable to the results at 40% saturation. As shown in Section 2.4.5 taken from the specialization project [1], the oxygen consumption for 60% saturation is expected to be much lower compared to 40%. However, the oxygen consumption results for limestone are both close to 0% because the tested limestone is a non-sulfide bearing aggregate. This test, therefore, was not sufficient to examine how the saturation level affects oxygen consumption. Testing a deleterious sulfide-bearing aggregate at a range of different saturation levels could have provided more documentation to the question. Nonetheless, similar to the test carried out during preliminary testing (Step A), the limestone tested at 60% saturation showed the thin film of water as described by Rodrigues et al. [3]. This thin film would most likely inhibit the diffusion of oxygen and therefore the oxidation process in sulfide-bearing aggregates.

9.3.4 OCT results from Step C

The oxygen consumption for MSK 0.9 was 8.75% (see Figure 8.5). The total sulfur content for this aggregate (freshly ground material) was found to be 1.05 wt. % (performed at NBTL). Although significantly above the 4% critical limit, the oxygen consumption is considerably lower compared the values reported in Canada. During the 2022 Canada-Norway workshop on pyrrhotite, Dr. Andreia Rodrigues [59] reported the oxygen consumption for MSK 0.9 to be about 27% (with the parameters recommended by Annex P [39] and particle size 50% <75 μm and 50% 75—150 μm). Lower oxygen consumption (about 23%) was reported by Rodrigues during the 2023 Canada-Norway workshop on pyrrhotite for the *MSK 0.8* aggregate (with a total sulfur content of 0.82 wt. %) [63].

The MSK 0.9 sample tested was not representative as it was not prepared for OCT testing but was rather the leftover material after sample preparation for the accelerated mortar bar expansion test (AMBT) carried out during the spring of 2022. It was first assumed that the lower oxygen consumption was due to this lack of representativity which could have affected the amount of iron sulfides in the sample. However, the analysis of bulk samples showed a total sulfur content of 1.25 wt. % (performed at NBTL) which was even higher than the total sulfur content (1.05 wt. %) found for the same aggregate when it was freshly ground (see Chapter 4). Another possible explanation was discussed during the 2023 Canada-Norway workshop, as the Canadian research team indicated that the material could have already oxidized since it was stored for almost 1.5 years in the particle size <147 μm. To verify this explanation, some of the remaining material from the MSK 0.9 sample (dry) was examined under a stereomicroscope to look for signs of oxidation. However, the analysis yielded no definitive conclusion. Another way to verify the explanation would be to test freshly grounded MSK 0.9 material in the OCT and compare the results. However, no more MSK 0.9 aggregate material was available for the pilot testing with the OCT (one of the limitations of this M.Sc. study).

MSK Rich, with a total sulfur content of 1.84 wt. % (freshly ground material, performed at NBTL), was also tested in the pilot testing. The oxygen consumption for this aggregate was 7.41%, as shown in Figure 8.5. Currently, there are no recent oxygen consumption results from Canada for the MSK Rich aggregate. However, given the higher sulfur content in this aggregate, the oxygen consumption is expected to be higher than 22.1%, which the value reported (average of six tests) in Canada for the MSK aggregate with sulfur content 0.99—1.15 wt. % [3]. The oxygen consumption for MSK Rich is also surprisingly lower than the 8.75% oxygen consumed by the tested MSK 0.9 aggregate with a lower total sulfur content (S_T of 1.25 wt. %).

The MSK Rich aggregate was tested about one week after grinding the aggregate to the required particle size. In addition, the aggregate material was vacuum-sealed soon after grinding. Therefore, for the MSK Rich aggregate at least, pre-oxidation is unlikely to be responsible for the low oxygen consumption.

Even for the tested limestone aggregate, oxygen consumption is lower compared to the results reported by Rodrigues et al. [3] and El-Mosallamy and Shehata [40]. In fact, Rodrigues et al. tested a limestone aggregate (HPL) that had the same total sulfur content (0.02 wt. %) as the tested Norwegian limestone. The oxygen consumption for HPL was 0.95% (average of two tests) and is significantly higher than the oxygen consumption obtained for the Norwegian limestone. Although a plausible explanation for this difference can be aggregate composition (the Norwegian limestone is a pure limestone), these results suggest that the oxygen consumption reported in this study is lower than expected.

One possible reason that could explain part of the low oxygen consumption across the tested aggregates might be the particle size. As shown by El-Mosallamy and Shehata [60] (see Section 2.4.4), finer particles can decrease the amount of oxygen consumed during the OCT. The surprisingly high percentage of particles <39 μm for all samples tested by laser scattering (39—48%) can therefore partly explain the lower oxygen consumption obtained in this pilot testing. Ways of verifying this explanation are described in Chapter 11, Recommended further work. If finer particle size is partly the cause of the low oxygen consumption, then more effective sieving procedures must be considered for future sample preparation.

Other factors responsible for the low oxygen consumption can be the test setup (data logger and OCT software) or other unknown issues related to adopted procedures (sample and reaction cell preparation). Particularly, errors in the data logger or the OCT software, sample representativity, and the effect of washing the aggregate material before crushing ought to be investigated. Due to time constraints, the effect of these factors on oxygen consumption was not examined further in the present study. More specific suggestions for testing the effect of these factors are described in Chapter 11, Recommended further work.

The MSK Rich aggregate was also mixed in with limestone at 25%. The resulting oxygen consumption was around 2.19%, slightly more than one fourth of the resulting O_2 consumption for the pure MSK Rich aggregate. The linear nature of the results agrees with the findings of El-Mosallamy et al. [60]. The authors mixed sand with sulfide ore at 1%, 2%, 5% and 10% and tested the mixtures with the OCT. Although no general linear relationship could be established, the O_2 consumption almost doubled when comparing the mixtures at 1% and 2% sulfide ore, as well as the mixtures at 5% and 10% sulfide ore. The somewhat linear trend for oxygen consumption of the MSK Rich aggregate hints at a possible systemic error resulting in lower oxygen consumption than expected.

As shown in Table 8.5, the 25% MSK Rich 75% limestone mixture was tested with both oxygen sensors. The almost identical results (0.01% standard deviation) provide an early indication of high test reproducibility between these two sensors. This finding indicates that the possible systematic error causing the low oxygen consumption is unlikely to be caused by an issue in the oxygen sensors.

9.4 Proposed sample preparation and OCT procedure

Given the results of this study, and the accumulated experience with sample preparation, it is possible to recommend a sample preparation procedure (shown in Figure F.1). The starting point of the procedure is a representative primary subsample sent by the aggregate producer. In the recommended procedure, "primary subsample" refers to the aggregate mass that will be washed and dried before reducing its particle size. Regarding the primary subsample, the following points should be considered:

- The primary subsample should have a minimum weight of 11 kg. However, the weight of the subsample should not exceed 14—15 kg because better representativity of the aggregate material can be achieved when close to 100% of the subsample mass is analyzed with the various tests listed below and in Figure F.1.
- The primary subsample should be representative of the material produced and sampled from the stockpile, e.g., in the fraction 8/16 mm (or similar).

The aggregate producer can also send a field sample (e.g., 50—100 kg with fraction 8/16 mm or similar). The primary subsample (with a minimum weight of 11 kg) can then be prepared by a combination of quartering the field sample (according to a quartering procedure modified after the sample handling procedure for coarse materials by N. Oberhardt, 2020—see Appendix G1) and half-splitting. Note that the recommended preparation procedure (in Figure F.1 and Appendix G1) does not consider the preparation of material received in larger stones (e.g., in big bags).

Figure F.1 shows how the primary subsample (minimum mass of 11 kg) is treated so that samples are obtained for the following tests:

- The mortar bar expansion test
- Thin section analysis (if appropriate)
- The oxygen consumption test (OCT)
- Total sulfur analysis

The procedure is therefore comprehensive, allowing the producer to send as little as 11-15 kg for all the steps of the Canadian testing protocol, in addition to any thin section analysis. The procedure describes in detail the sample preparation process for the OCT and for total sulfur analysis with bulk samples. Given that the flowchart starts with the minimum mass of the primary subsample (11 kg), the minimum mass needed for each stage of the flowchart is provided in Figure F.1. Starting with a slightly higher mass of the primary subsample therefore allows for more flexibility in the procedure presented.

Given its time and cost efficiency, and the early results indicating very little iron contamination, the VDM-S pathway (Figure 7.2) is incorporated into the proposed sample preparation procedure. Furthermore, the recommended procedure has a focus on sample representativity in all stages of sample preparation. For example, crushing/grinding in the procedure is carried out in a stepwise manner to avoid over-crushing (i.e., the over-representation of certain minerals in some fractions of the material). More specifically, the gap opening in the jaw and disk crushers will be reduced gradually, and the aggregate material will be first crushed to pass the 5 mm and ca. 3.5 mm sieves before being ground further to the size <147 μm.

The full sample preparation procedure can be found in Appendix G1.

The Norwegian OCT procedure is also shown in Appendix G2. This procedure is based on the Canadian OCT procedure described in the interlaboratory study [49, 51] and Annex P [39]. Only slight modifications were needed.

10 Summary and conclusion

Sample preparation, including splitting, crushing and grinding of samples, and the pilot testing of the prepared samples in the oxygen consumption test (OCT) were the two main focus areas for this M.Sc. study.

A literature review was conducted at the start of the master's thesis to understand the cases of concrete degradation due to pyrrhotite, the deterioration mechanism, the standards, testing protocols and regulations for sulfide-bearing aggregates, and finally the development and procedure of the OCT.

Preliminary testing (Step A) with the OCT was carried out with three non-representative limestone subsamples to ensure that the OCT setup is ready for "proper" testing with representative subsamples. The testing showed that the OCT setup is operating as intended. RH inside of the reaction cell reached 100% relatively early during the OCT, indicating the need to calibrate the O_2 sensors in an environment with 100% relative humidity. Even though the effect of RH changes on the oxygen consumption results is marginal, it is recommended to measure and correct for RH during the OCT.

In Step B, three methodologies/pathways of sample preparation were investigated (Figure 7.2) using two Norwegian aggregates (limestone and SM1). The pathways involved the use of either mainly steel grinding equipment (pathways VDM-S and BBM-S) or mainly ceramic equipment (BBM-C). The results show that, overall, the time spent on aggregate preparation was preliminarily found to be affected by the aggregate's hardness and mineralogy, as the preparation of the harder SM1 aggregate took significantly more time compared to the limestone aggregate. Moreover, based on the results of Step B, grinding with pathways VDM-S and BBM-S was found to be the least time consuming (Table 8.2). However, the sample preparation process is still generally too time consuming. Although more tests are needed, the VDM-S and BBM-S pathways did not, preliminarily, cause any significant contamination in the OCT test samples.

When considering time and cost efficiency, in addition to the risk of iron contamination, the preliminary conclusion is that pathway VDM-S is the recommended pathway for later sample preparation. This pathway involves the use of jaw and disk crushers (tungsten plates) for the crushing step and the vibratory disk mill (steel grinding set) for the grinding step.

The particle size distribution of the limestone and SM1 test samples produced by the three different sample preparation pathways was also measured by laser scattering. No large differences were observed between the different pathways. However, the large number of particles <75 µm and particles >150 µm (as measured by laser scattering compared to sieving) hint that the crushing/grinding of the aggregate material might have been inhomogeneous, and that sieving efficiency was not sufficiently high.

The results of the particle size determination by laser scattering also showed that the limestone samples had more particles in the range 39—150 µm compared to the SM1 samples, again showing the importance of the aggregate's hardness for the process of crushing and grinding. Moreover, of all the sieving methods used in this thesis, hand sieving was found to have the smallest difference between the amount of particles <75 µm found by laser scattering as compared to sieving. Therefore, hand sieving is recommended for future sample preparation.

The two Norwegian aggregates, limestone and SM1, showed an oxygen consumption (average of all tests) of 0% (<0.44%) and 3.31%, respectively. This is in agreement with the aggregates' total sulfur content (0.02 wt. % and 0.45 wt. % for limestone and SM1, respectively). In addition, a longer duration of the OCT (16.7h vs 3.5h) resulted in significantly higher oxygen consumption for the SM1 aggregate.

Two Canadian aggregates, MSK 0.9 and MSK Rich, were tested in the OCT in Step C of the laboratory work. The total sulfur content for MSK 0.9 was 1.25 wt. % (leftover material) and 1.05 wt. % (freshly ground material), and for MSK Rich was 1.84 wt. % (freshly ground). The oxygen consumption of MSK 0.9 and MSK Rich was benchmarked against the results obtained at ULaval. The oxygen consumption for the MSK 0.9 and MSK Rich was 8.75% and 7.41%, respectively. Even though above the 4% critical limit, these values are almost a third of the oxygen consumption results obtained in Canada for the MSK aggregate.

Two test samples were prepared by mixing 75% limestone and 25% MSK Rich. Each test sample was tested with one of the oxygen sensors available. The average oxygen consumption was 2.19%, indicating a slightly linear trend when compared to the results of pure MSK Rich. The low standard deviation of the oxygen consumption (0.01%) suggests that the reproducibility of the OCT results between the two sensors is high.

Overall, the results of the MSK 0.9 and MSK Rich aggregates point to a potential source of error that is systematically causing the oxygen consumption values to be lower compared to the Canadian reference values. One of the sources of error could be the higher-than-expected proportion of fine particles (<39 µm and <77 µm) in the test samples found by particle size analysis by laser scattering (*Horiba LA-960*). The challenge of lower-than-expected oxygen consumption needs to be investigated further.

Based on the experience gained in the M.Sc. study, a sample preparation procedure was developed for the OCT in Norway. This procedure takes a comprehensive approach, as the sample sent by the producer is handled such that test samples for the OCT and all other necessary analyses are obtained. A detailed procedure for the oxygen consumption test (OCT) was also developed. The developed OCT procedure is based on Annex P [39], the interlaboratory study [49, 51] and the experience gained with OCT testing during this study.

11 Recommended further work

11.1 Further improvements in sample preparation

The still-too-time-consuming sample preparation procedure created as part of this thesis can be further developed. More experience with sample preparation can prompt the use of new machinery/procedures that most likely will increase the efficiency and, thus, the commercial viability of the OCT. Most available crushing/grinding equipment relevant to the OCT at the IGP Mineral Processing Laboratory was investigated throughout this study. However, purchasing new equipment, or expanding the capabilities of existing equipment, might be a viable option to improve the efficiency of sample preparation. For example, for the vibratory disk mill, the current maximum capacity of the grinding set (steel) available at the IGP Mineral Processing Laboratory is 100 ml. The current tungsten grinding set available has half that capacity. It is possible for the laboratory to purchase a 200 ml grinding set made from steel or a 100 ml set made from tungsten, thus improving the efficiency of sample preparation by making the process less time consuming. In addition, Professor Rolf Arne Kleiv at NTNU suggested the use of larger bench ball mills than used in this study, and/or the use of tungsten carbide grinding balls for these mills (Rolf Arne Kleiv, personal communication, June 2023). The tungsten grinding balls can be expensive, so it is important that their purchase can be justified by significant saving in time consumption on sample preparation.

Other methods and/or equipment for sieving ought to be investigated, especially given the low efficiency of sieving for the samples prepared during this thesis. Given the results from laser scattering (*Horiba LA-960*), hand sieving is particularly promising. A smaller amount of material can be run through the sieves for a longer duration of time than used in this thesis. The particle size of the sieved samples can then be analyzed with *Horiba LA-960* to investigate if an increase if sieving efficiency is achieved.

One of the main possible sources of error for many test procedures, including the OCT, is that the reliability of the final result strongly depends on the representativity of the samples received. Sampling by the producer is not part of the test procedure, even if it will have a significant effect on the obtained results. In the context of the OCT, for example, the producer might sample in a non-representative way. These possible sources of error can be reduced by creating clear guidelines for aggregate producers on how to prepare representative samples to be sent for laboratory testing.

11.2 Further OCT testing

Four aggregate types (two Canadian and two Norwegian) were tested as part of this master's thesis. As discussed in the specialization project [1], testing a larger number of Norwegian aggregates with the OCT is vital for the further development of the critical oxygen consumption limit.

A larger number of OCT tests are also needed to completely rule out iron contamination from the sample preparation pathways BBM-S and VDM-S. In addition, a new sample preparation pathway using only ceramic/tungsten equipment might become available if the 100 ml tungsten grinding set for the vibratory disk mill is purchased.

As discussed in Chapter 9, the oxygen consumption results obtained during this study are systematically lower than the results documented in Canada. Table 11.1 presents some potential sources of error behind the lower O_2 consumption and how these errors can be further investigated.

Table 11.1: List of potential sources of error and ways of verifying whether these errors are partly responsible for the low oxygen consumption during the pilot testing in Norway.

Source of potential error	Potential error	How to investigate?
OCT setup	Systematic error with the data acquisition module	Run 2 OCTs with another data logger (e.g., the HOBO data logger sent from Canada as part of the interlaboratory study)
	Unknown error with the OCT software	To be checked.
Sample preparation	Samples are not representatives	Test two parallel samples from the same aggregate.
	High percentage of fine particles	Test the MSK aggregate with the particle size 75—147 µm only (i.e., remove the particles passing the 75 µm sieve) and check if significantly higher O_2 consumption is obtained.
	Pre-washing of aggregates before crushing causing pre-oxidation	Test a washed and unwashed sample from the same aggregate with the OCT
OCT procedure	Mixing of water and the aggregate material is not thorough enough	Run the OCT with samples mixed with household mixers or similar appliances

Three oxygen consumption tests were carried out with the SM1 aggregate. The resulting oxygen consumption was 3—3.5%, which is close to the current 4% limit set by Annex P [39]. The oxygen consumption of the SM1 aggregate could even be slightly higher (by up to 0.26% oxygen consumed) for two of the tests had it not been for the issue with one of the RH sensors before it was recalibrated. It would be interesting to test this aggregate in the accelerated mortar bar expansion test (Step III in the Canadian

testing protocol [2]). If the expansion of the mortar bars is above the recommended Canadian limit values of Step III, this could potentially indicate that the critical oxygen consumption limit of 4% is not conservative enough.

11.3 A new approach

Performing the OCT with a longer duration and a coarser particle size than recommended by Annex P [39] can potentially solve many of the problems the OCT currently faces. The benefits of testing with a coarser particle size include an increase in the efficiency of sample preparation, while longer duration can widen the gap between the oxygen consumption of deleterious and non-deleterious aggregates. Testing with coarser particle size (75—300 μm) and longer duration (16.5h) was carried out by El-Mosallamy and Shehata [40] with promising results (see Figure 2.18). It would be interesting, however, to test with slightly coarser particle size (e.g., 0—600 μm) and an even longer duration (e.g., 24h) and investigate the effect on oxygen consumption. If reasonable results are achieved, the commercial viability of the OCT can be significantly improved.

After discussion with Professor Rolf Arne Kleiv, another approach was suggested. Instead of creating aggregate layers in the reaction cell where not all of the particles have equal access to oxygen, the material inside the reaction cell can be kept in motion (for example, rotated) during the OCT. The goal of this approach is to make the test less dependent on many parameters and make the surface area of particles the major parameter affecting the oxygen consumption. However, such a new approach would probably take many years in development with many uncertainties lying ahead.

12 References

1. Muhyiddin Y. Discussion of the test parameters for an oxygen consumption test used to measure the pyrrhotite reactivity of sulfide-bearing aggregates [Specialization Project - TKT4550 Konstruksjonsteknikk fordypningsprosjekt]: Norwegian University of Science and Technology (NTNU); 2022.
2. Rodrigues A, Duchesne J, Fournier B, Durand B, Shehata MH, Rivard P. Evaluation protocol for concrete aggregates containing iron sulfide minerals. ACI materials journal. 2016;113(3):349-59.
3. Rodrigues A, Duchesne J, Fournier B. Quantitative assessment of the oxidation potential of sulfide-bearing aggregates in concrete using an oxygen consumption test. Cement & concrete composites. 2016;67:93-100.
4. Moum J, Rosenqvist IT. Sulfate attack on concrete in the Oslo region Journal of the American concrete institute. 1959;56:257-64.
5. Lugg A, Probert D. 'Mundic'-type problems: a building material catastrophe. Construction & building materials. 1996;10(6):467-74.
6. Ayora C, Chinchon S, Aguado A, Guirado F. Weathering of iron sulfides and concrete alteration: Thermodynamic model and observation in dams from Central Pyrenees, Spain. Cement and concrete research. 1998;28(9):1223-35.
7. Schmidt T, Leemann A, Gallucci E, Scrivener K. Physical and microstructural aspects of iron sulfide degradation in concrete. Cement and concrete research. 2011;41(3):263-9.
8. Rodrigues A, Duchesne J, Fournier B, Durand B, Rivard P, Shehata M. Mineralogical and chemical assessment of concrete damaged by the oxidation of sulfide-bearing aggregates: Importance of thaumasite formation on reaction mechanisms. Cement and concrete research. 2012;42(10):1336-47.
9. Zhong R, Wille K. Investigating the Deterioration of Basement Walls Made of Concrete in CT. University of Connecticut, Storrs: Report for the Attorney General of the State of Connecticut; 2016.
10. Rodrigues A. Concrete deterioration due to sulfide-bearing aggregates [PhD thesis]. Québec, Canada: Université Laval; 2016.
11. Jana D. Pyrrhotite Epidemic in Eastern Connecticut: Diagnosis and Prevention. ACI materials journal. 2020;117(1):61-70.
12. Duchesne J, Rodrigues A, Fournier B. Concrete damage due to oxidation of pyrrhotite-bearing aggregate: a review. RILEM Technical Letters. 2021;6:82-92.
13. Jana D. Cracking of residential concrete foundations in eastern Connecticut, USA from oxidation of pyrrhotite. Case Studies in Construction Materials. 2022;16:e00909.
14. Mauk JL, Crafford TC, Horton JD, San Juan CA, Robinson JGR. Pyrrhotite distribution in the conterminous United States, 2020. Report. Reston VA; 2020. Report No.: 2020-3017.
15. Mauk JL, Horton JD. Data to accompany U.S. Geological Survey Fact Sheet 2020-3017: Pyrrhotite distribution in the conterminous United States U.S. Geological Survey data release 2020 [cited 2023 June 14th]. Available from: https://www.sciencebase.gov/catalog/item/5e34a35fe4b0a79317dc25e6.
16. Belzile N, Chen Y-W, Cai M-F, Li Y. A review on pyrrhotite oxidation. Journal of geochemical exploration. 2004;84(2):65-76.
17. Deer WA. An introduction to the rock-forming minerals. 1992.
18. Janzen MP, Nicholson RV, Scharer JM. Pyrrhotite reaction kinetics: reaction rates for oxidation by oxygen, ferric iron, and for nonoxidative dissolution. Geochimica et cosmochimica acta. 2000;64(9):1511-22.
19. Thomas JE, Skinner WM, Smart RSC. A mechanism to explain sudden changes in rates and products for pyrrhotite dissolution in acid solution. Geochimica et cosmochimica acta. 2001;65(1):1-12.

20. Oliveira I, Cavalaro SHP, Aguado A. Evolution of pyrrhotite oxidation in aggregates for concrete. Materiales de construcción (Madrid). 2014;64(316):e038-9.
21. Casanova I, Agulló L, Aguado A. Aggregate expansivity due to sulfide oxidation — I. Reaction system and rate model. Cement and concrete research. 1996;26(7):993-8.
22. Nicholson R, Scharer J. Laboratory Studies of Pyrrhotite Oxidation Kinetics. 1994. p. 14-30.
23. Grattan-Bellew PE, Eden WJ. Concrete Deterioration and Floor Heave Due to Biogeochemical Weathering of Underlying Shale. Revue canadienne de géotechnique. 1975;12(3):372-8.
24. Luo S, Wang Z, Gong Q, Wang D. The role of temperature in thaumasite formation under the immersion of magnesium sulfate solution. Magazine of concrete research. 2022;74(13):672-81.
25. Thomas MDA, Rogers CA, Bleszynski RF. Occurrences of thaumasite in laboratory and field concrete. Cement & concrete composites. 2003;25(8):1045-50.
26. Chinchón-Payá S, Aguado A, Coloma F, Chinchón S. Study of aggregate samples with iron sulfides through micro X-ray fluorescence (μXRF) and X-ray photoelectron spectroscopy (XPS). Materials and structures. 2015;48(5):1285-90.
27. Nordstrom DK, Alpers CN. Geochemistry of Acid Mine Waters. The Environmental Geochemistry of Mineral Deposits: Part A: Processes, Techniques, and Health Issues 6A. Littleton, CO.: Society of Economic Geologists; 1999. p. 133-60.
28. Knipe SW, Mycroft JR, Pratt AR, Nesbitt HW, Bancroft GM. X-ray photoelectron spectroscopic study of water adsorption on iron sulphide minerals. Geochimica et cosmochimica acta. 1995;59(6):1079-90.
29. Multani RS, Waters KE. A review of the physicochemical properties and flotation of pyrrhotite superstructures (4C – Fe7S8/ 5C – Fe9S10) in Ni-Cu sulphide mineral processing. Canadian journal of chemical engineering. 2018;96(5):1185-206.
30. Steger HF. Oxidation of sulfide minerals: VII. Effect of temperature and relative humidity on the oxidation of pyrrhotite. Chemical geology. 1982;35(3):281-95.
31. Kwong ECM. Abiotic and biotic pyrrhotite dissolution [MASc thesis]. Waterloo, Ontario, Canada: University of Waterloo; 1995.
32. Janzen MP. Role of ferric iron, trace metal content, and crystal structure on pyrrhotite oxidation [MSc thesis]. Canada: University of Waterloo; 1996.
33. Kwong YTJ, Swerhone GDW, Lawrence JR. Galvanic sulphide oxidation as a metal-leaching mechanism and its environmental implications. Geochemistry: Exploration, Environment, Analysis. 2003;3:337 - 43.
34. Shuey RT. Semiconducting ore minerals. 1975;4: p. 415.
35. Ekmekçi Z, Demirel H. Effects of galvanic interaction on collectorless flotation behaviour of chalcopyrite and pyrite. International journal of mineral processing. 1997;52(1):31-48.
36. Rand DAJ. Oxygen reduction on sulphide minerals. Journal of electroanalytical chemistry and interfacial electrochemistry. 1977;83(1):19-32.
37. Danielsen SW, Hagelia P, Wigum BJ, De Weerdt K, Aasly K, Lindgård J, et al. Magnetkis i betongtilslag. Betydning for betongs bestandighet. Statens vegvesen (Norwegian Public Road Adminstration); 2019. Report No.: 463.
38. Rodrigues A, Duchesne J, Fournier B. A new accelerated mortar bar test to assess the potential deleterious effect of sulfide-bearing aggregate in concrete. Cement and concrete research. 2015;73:96-110.
39. Canadian Standards Association. CSA A23.1:2019. Annex P (informative) - Impact of sulphides in aggregate on concrete behaviour and global approach to determine potential deleterious reactivity of sulphide-bearing aggregates. Mississauga, Ontario, Canada 2019.
40. El-Mosallamy M, Shehata MH. Tests for oxidizable sulfides in aggregates: Applicability and limitations. ACI materials journal. 2020;117(2):229-40.

41. Duchesne J, Fournier B, Francoeur J. Study of the Deterioration of Concrete Incorporating Sulfide-Bearing Aggregates. Sixth International Conference on Durability of Concrete Structures. University of Leeds, Leeds, West Yorkshire, LS2 9JT, United Kingdom2018.
42. Moore CM, Strack CM, Moser RD, McMahon GW. Proposed Testing and Research Approach for Pyrrhotite-Induced Concrete Deterioration. Washington, DC: Engineer Research and Development Center (ERDC), U.S. Army Corps of Engineers; 2018.
43. ASTM International. ASTM C295. Standard Guide for Petrographic Examination of Aggregates for Concrete. West Conshohocken, PA 2019.
44. ASTM International. ASTM C157. Standard Test Method for Length Change of Hardened Hydraulic-Cement Mortar and Concrete. West Conshohocken, PA 2017.
45. Ytterdal SG. Lessons learned from the Follo Line Project – Pyrrhotite: a showstopper for reuse of TBM material as concrete aggregate. Magnetkis i betongtilslag (NPRA reports) Appendix 4. Oslo, Norway 2018.
46. Lindstad H. Introduction to pyrrhotite in concrete aggregates [Specialization Project - TKT4550 Konstruksjonsteknikk fordypningsprosjekt]: Norwegian University of Science and Technology (NTNU); 2021.
47. Fure Ø. Characterisation of pyrrhotite-bearing concrete aggregates using conventional techniques in combination with SEM-based Automated Mineralogy [Master's thesis]. Trondheim, Norway: Norwegian University of Science and Technology (NTNU); 2021.
48. Lindgård J. Pyrrhotite: Experiences from pilot-testing in Norway with the Mortar Bar Test (MBT) Canada-Norway workshop on the Impact of pyrrhotite on the durability of concrete structures; Oct, 2022; Quebec City, Canada.
49. Pyrrhotite Project - Interlaboratory Study - Document 1 - General Instructions of Phase I. Université Laval; 2023.
50. Pyrrhotite Project - Interlaboratory Study - Document 2 - Determination of Sulphide Sulphur Content of Concrete Aggregates (Ts). Université Laval; 2023.
51. Pyrrhotite Project - Interlaboratory Study - Document 3 - Detection of the Oxidation Potential of Sulphide-Bearing Aggregates by an Oxygen Consumption Test (OCT). Université Laval; 2023.
52. European Committee for Standardization. EN 12620:2002+A1. Brussels, Belgium 2008.
53. Standard Norge. NS-EN 12620:2002+A1:2008+NA:2016 Nasjonalt tilegg NA:2016 - Tilslag for betong 2016.
54. Candian Standards Association. CSA A23.1-14/A23.2-14: Concrete Materials and Methods of Concrete Construction/Test Methods and Standard Practices for Concrete. Mississauga, ON, Canada 2014.
55. ASTM International. ASTM C294. Standard Descriptive Nomenclature for Constituents of Concrete Aggregates. West Conshohocken, PA 2019.
56. Elberling B, Nicholson RV, Reardon EJ, Tibble R. Evaluation of sulphide oxidation rates: a laboratory study comparing oxygen fluxes and rates of oxidation product release. Revue canadienne de géotechnique. 1994;31(3):375-83.
57. Elberling B, Nicholson RV. Field determination of sulphide oxidation rates in mine tailings. Water Resour Res. 1996;32(6):1773-84.
58. ICT International. Apogee Soil Oxygen SO-200 Series: Fast Response: ICT International [cited 2023 Jan 27th]. Available from: https://ictinternational.com/products/apogee-soil-oxygen-so-200-series/apogee-soil-oxygen-so-200-series-fast-response/.
59. Rodrigues A. Oxygen Consumption Test Optimization. Canada-Norway workshop on the Impact of pyrrhotite on the durability of concrete structures; Oct 2022; Quebec City, Canada.
60. El-Mosallamy M, Shehata MH. Effects of Sample Preperation on the Results of the Oxygen Consumption Test Used to Evaluate Oxidation Potential of Sulfide-Bearing Aggregate. CSCE Conference; Vancouver, BC, Canada 2017. p. 1-10.

61. Marcelino AP, Calixto JM, Gumieri AG, Caldeira CL, Delbem ID, Ferreira MC. A feasible evaluation protocol to determine the most reactive sulfide-bearing aggregate for use in concrete. Construction & building materials. 2020;242:118031.
62. Guirguis B, Shehata MH. A new screening test to evaluate the presence of oxidizable sulphide minerals in coarse aggregates. Construction & building materials. 2017;154:1096-104.
63. Rodrigues A. Oxygen consumption test (OCT): Effect of variability due to sample preparation and the effect of various proportions pyrrhotite. Canada-Norway workshop on the impact of pyrrhotite on the durability of concrete structures; May 2023; Reykjavik, Iceland.
64. Wills BA, Napier-Munn T. Wills' Mineral Processing Technology - An Introduction to the Practical Aspects of Ore Treatment and Mineral Recovery (7th Edition). 2006:148.
65. Retsch GmbH. How to get the best results with the Vibratory Disc Mill RS 200 - Tips and tricks Retsch GmbH. Retsch-Allee 1-5, 42781 Haan, Germany.
66. FRITSCH Milling and Sizing. FRITSCH Planetary Mills classic line 2013 [cited 2023 June 24th]. Available from: https://www.youtube.com/watch?v=5ShOAS3EGGU.
67. Apogee Instruments. Owner's manual. Oxygen sensor. Models: SO-110, SO-120, SO-210, and SO-220. Logan, Utah, USA 2022.
68. E+E Elektronik. RH sensor - Data sheet [Internet]. [cited 2023 June 13th]. Available from: https://www.epluse.com/fileadmin/data/product/ee06/datasheet_EE06.pdf.
69. Gy PM. The sampling of particulate materials — A general theory. International Journal of Mineral Processing. 1976;3(4):289-312.

Appendix A: Test matrix

Table A.1: The originally envisioned test matrix for the pilot testing with the oxygen consumption test (OCT). The steps of laboratory work were different and focused more on mixing aggregates and varying the OCT parametes. The satuartion levels and the particle size distributions in Step 4 were as suggested by the specialization project.

	Aggregate	**Mass available**	**Particle size**	**Saturation level**	**Ground material height [mm]**	**Headspace [mm]**	**Duration [h]**	**Porosity**
Step 1: Preliminary testing	Limestone	185 kg	50% <75 µm, 50% 75—150 µm	40%	100	100	3.5	50%
Step 2a: Annex P test parameters - No mixing of aggregates	Limestone	185 kg	50% <75 µm, 50% 75—150 µm	40%	100	100	3.5	50%
	MSK 0.9	2.5 kg	<147 µm	40%	100	100	3.5	50%
	MSK 0.2	20.1 kg	50% <75 µm, 50% 75—150 µm	40%	100	100	3.5	50%
	MSK Rich	18.2 kg	50% <75 µm, 50% 75—150 µm	40%	100	100	3.5	50%
Step 2b: Annex P test parameters - MSK mixed with limestone	MSK 0.2 mixed with limestone at 25%, 50% and 75%	-	50% <75 µm, 50% 75—150 µm	40%	100	100	3.5	50%
	MSK Rich mixed with limestone at 25%, 50% and 75%	-	50% <75 µm, 50% 75—150 µm	40%	100	100	3.5	50%
Step 3: Testing Norwegian aggregates	SM1	120+ kg (fraction 0/32 mm)	50% <75 µm, 50% 75—150 µm	40%	100	100	3.5	50%
	Norite	-	50% <75 µm, 50% 75—150 µm	40%	100	100	3.5	50%
Step 4: Changing test parameters	25% MSK 0.2, 75% limestone	-	50% <75 µm, 50% 75—150 µm	25%, 35%	100	100	3.5	50%
	25% MSK Rich, 75% limestone	-	Particle sizes (1, 2, 3a and 3b)[1] recommended by the specialization project from last semester	40%	100	100	3.5	50%

[1] **1**: (75—150 µm), **2**: (33% <75 µm, 33% 75—150 µm, 33% 150—300 µm), **3a**: top layer (<75 µm), bottom layer (75—150 µm) and **3b**: top layer (75—150 µm), bottom layer (<75 µm)

Table A.2: The revised test matrix showing the oxygen consumption tests carried out throughout the present study.

	Aggregate	**Particle size**	**Saturation level**	**Ground material height [mm]**	**Headspace [mm]**	**Duration [h]**	**Porosity**
Step A Preliminary testing	Limestone	<142 µm, <125 µm	40%, 60%	75, 100	100, 125	3.5	-
Step B Non-steel grinding equipment	Limestone	27% <77 µm, 73% 77—142 µm	40%, 60%	100	100	3.5	50%
	SM1	37% <77 µm, 63% 77—142 µm	40%	100	100	3.5	50%
Step B Steel grinding equipment	Limestone x2	50% <75 µm, 50% 75—147 µm	40%	100	100	3.5	50%
		44% <75 µm, 56% 75—147 µm					
	SM1 x2	44% <75 µm, 56% 75—147 µm	40%	100	100	3.5, 16.7	50%
		46% <75 µm, 54% 75—147 µm					
Step C Benchmarking against Canadian results	MSK 0.9	<147 µm	40%	100	100	3.5	50%
	MSK Rich	50% <75 µm, 50% 75—147 µm	40%	100	100	3.5	50%
	(25% MSK Rich, 75% limestone) x2	33% <75 µm, 67% 75—147 µm	40%	100	100	3.5	50%

Appendix B: Sample preparation flowcharts

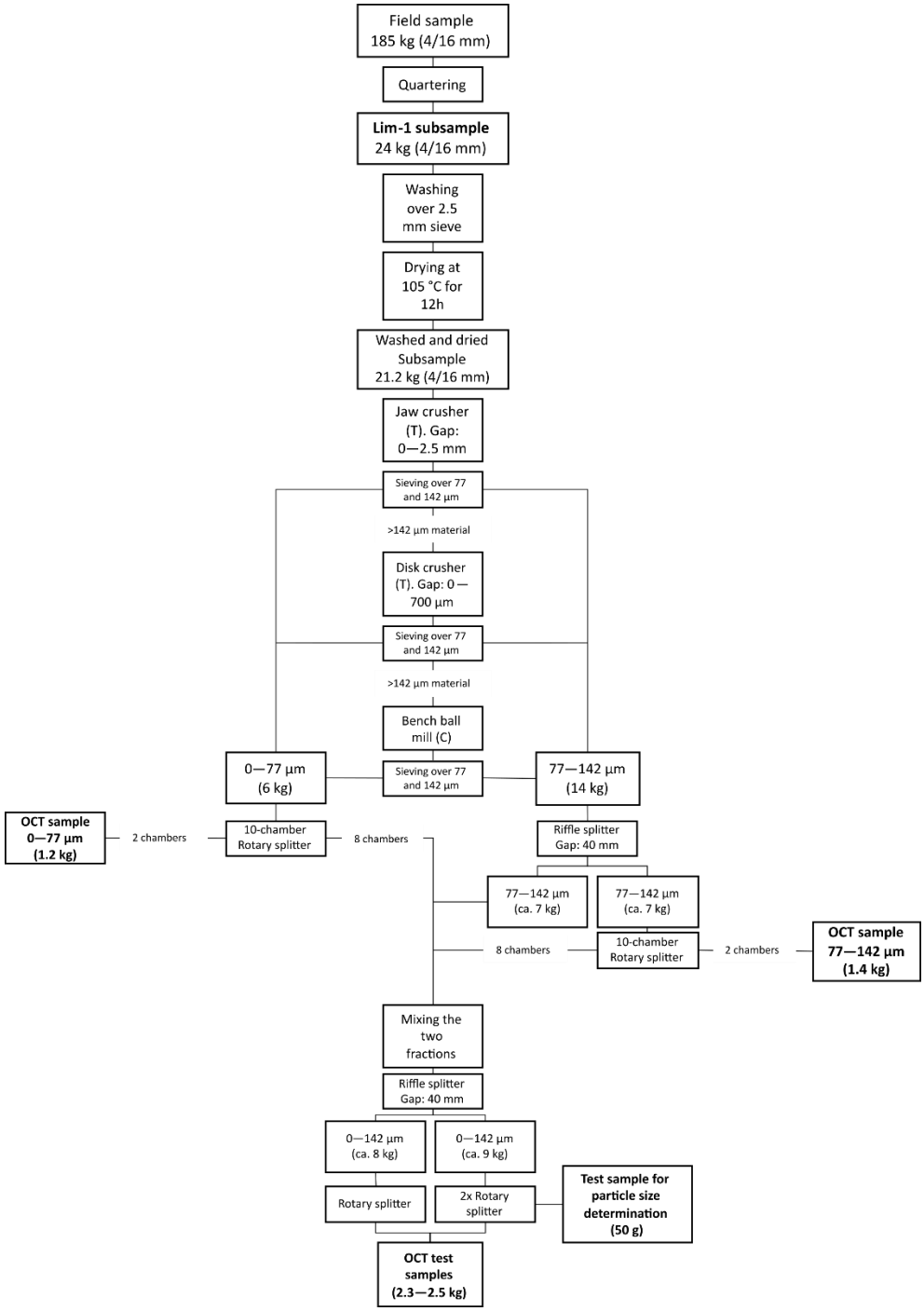

Figure B.1: The flowchart shows the sample preparation process (pathway BBM-C) of the limestone subsample Lim-1. (T): tungsten carbide equipment. (S): steel equipment. (C): ceramic equipment.

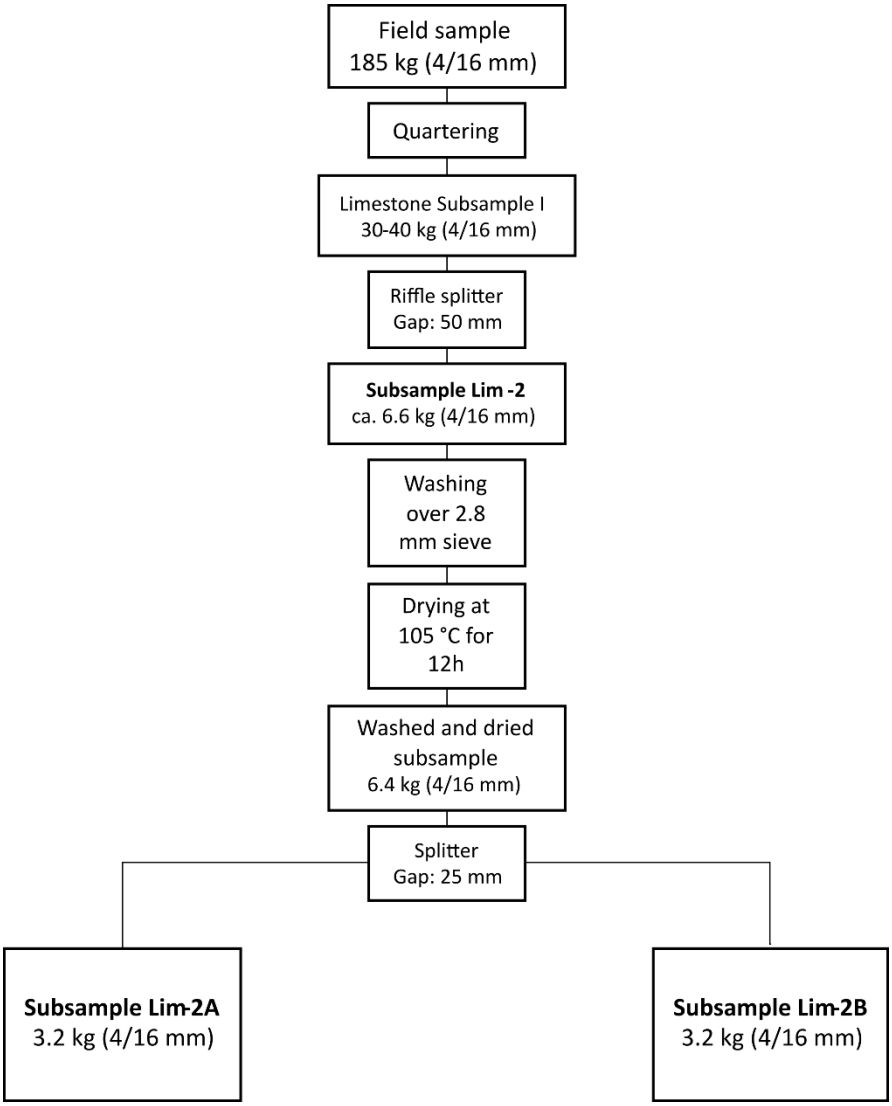

Figure B.2: The flowchart shows how the limestone subsamples Lim-2A and Lim-2B were obtained.

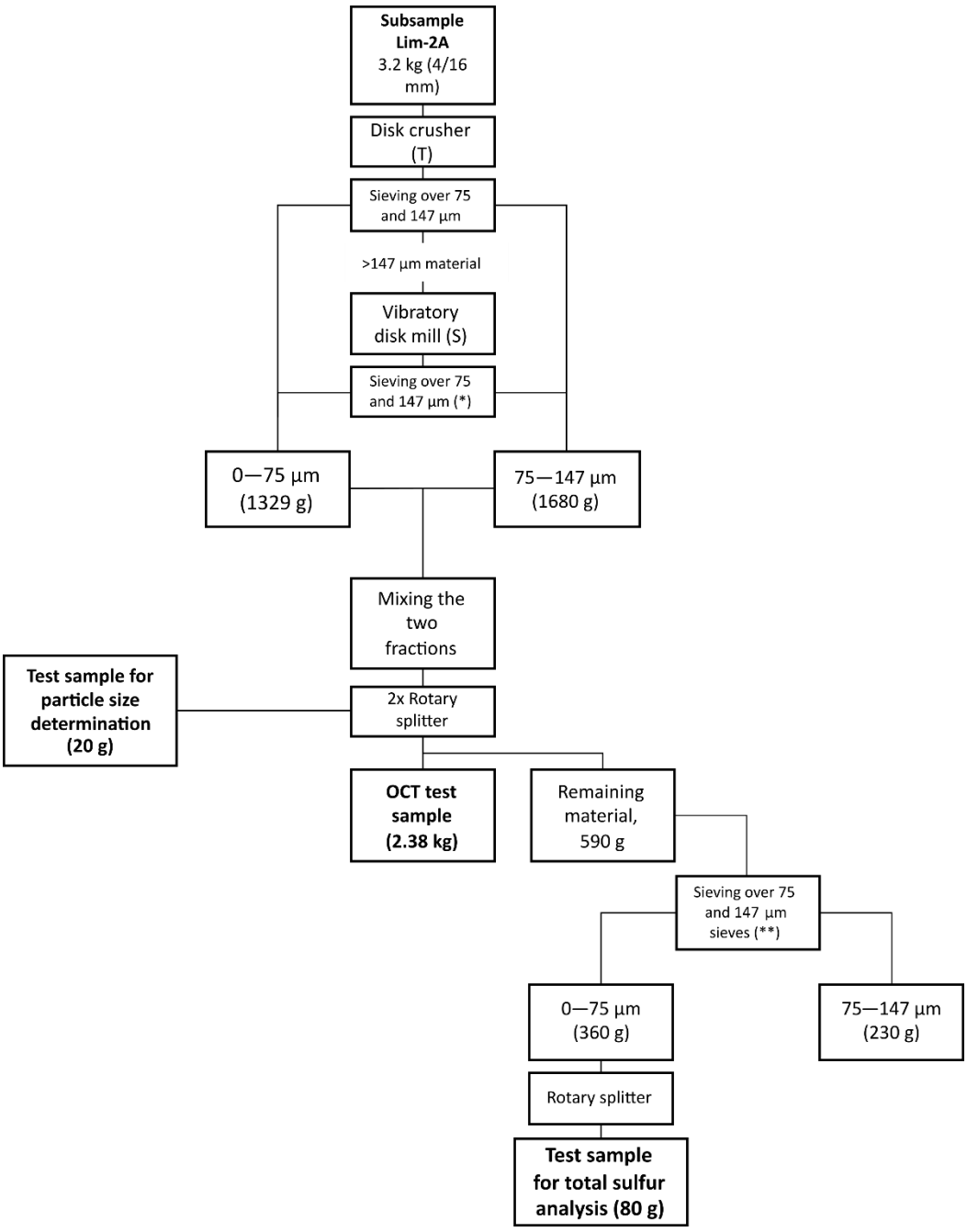

Figure B.3: The flowchart shows the sample preparation process for subsample Lim-2A (VDM-S pathway). (T): tungsten carbide equipment. (S): steel equipment. (C): ceramic equipment. (*) Sieved using the *RETSCH AS 300* Sieve shaker. (**) Sieved by hand.

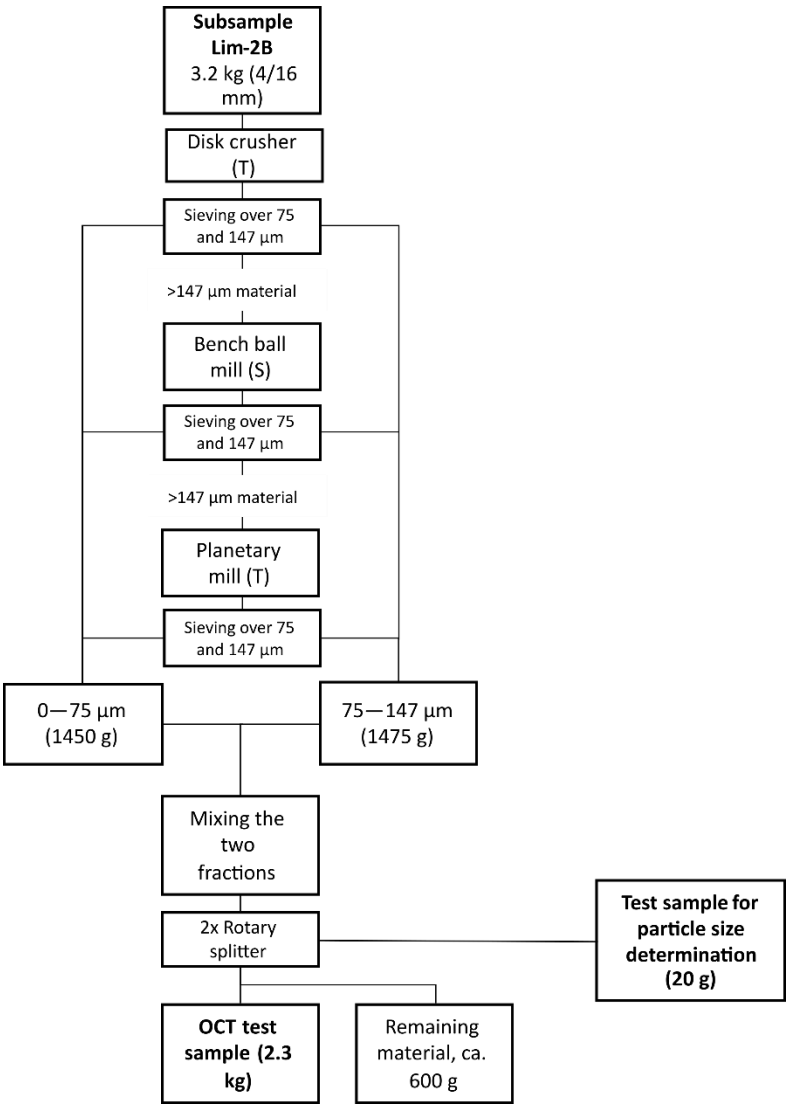

Figure B.4: The smaple preparation process of subsample Lim-2B (BBM-S pathway). (T): tungsten carbide equipment. (S): steel equipment. (C): ceramic equipment.

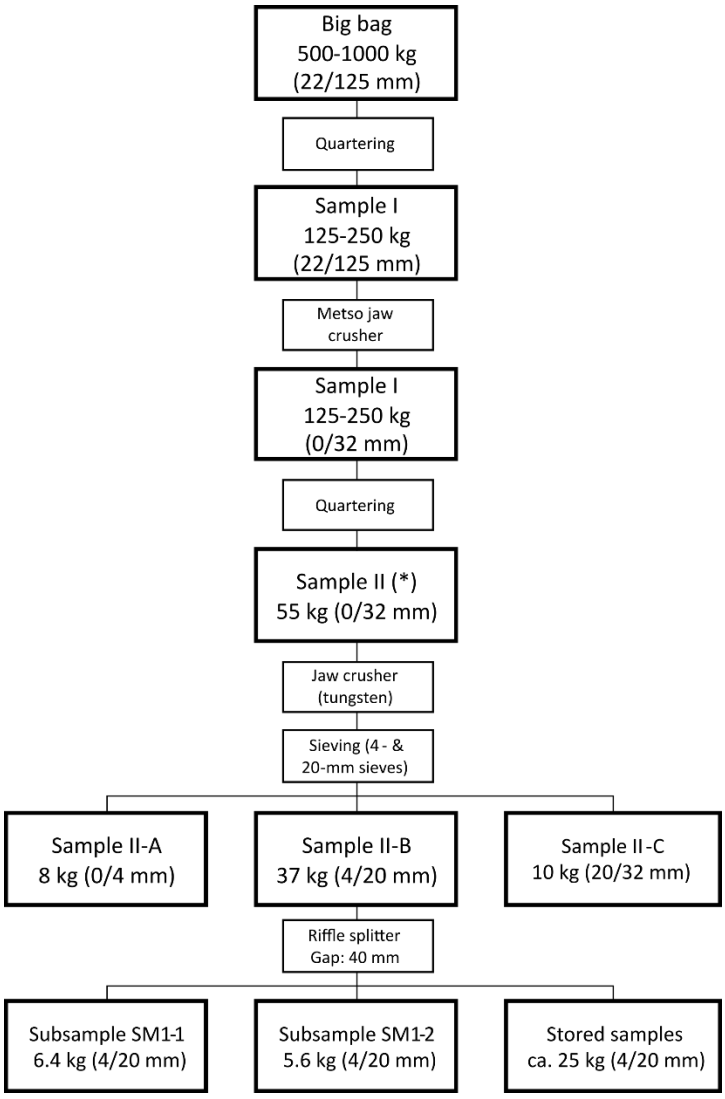

Figure B.5: The flowchart shows how the subsamples SM1-1 and SM1-2 (4/20 mm) was obtained. (*) The previous steps were carried out before the start of this M.Sc. study.

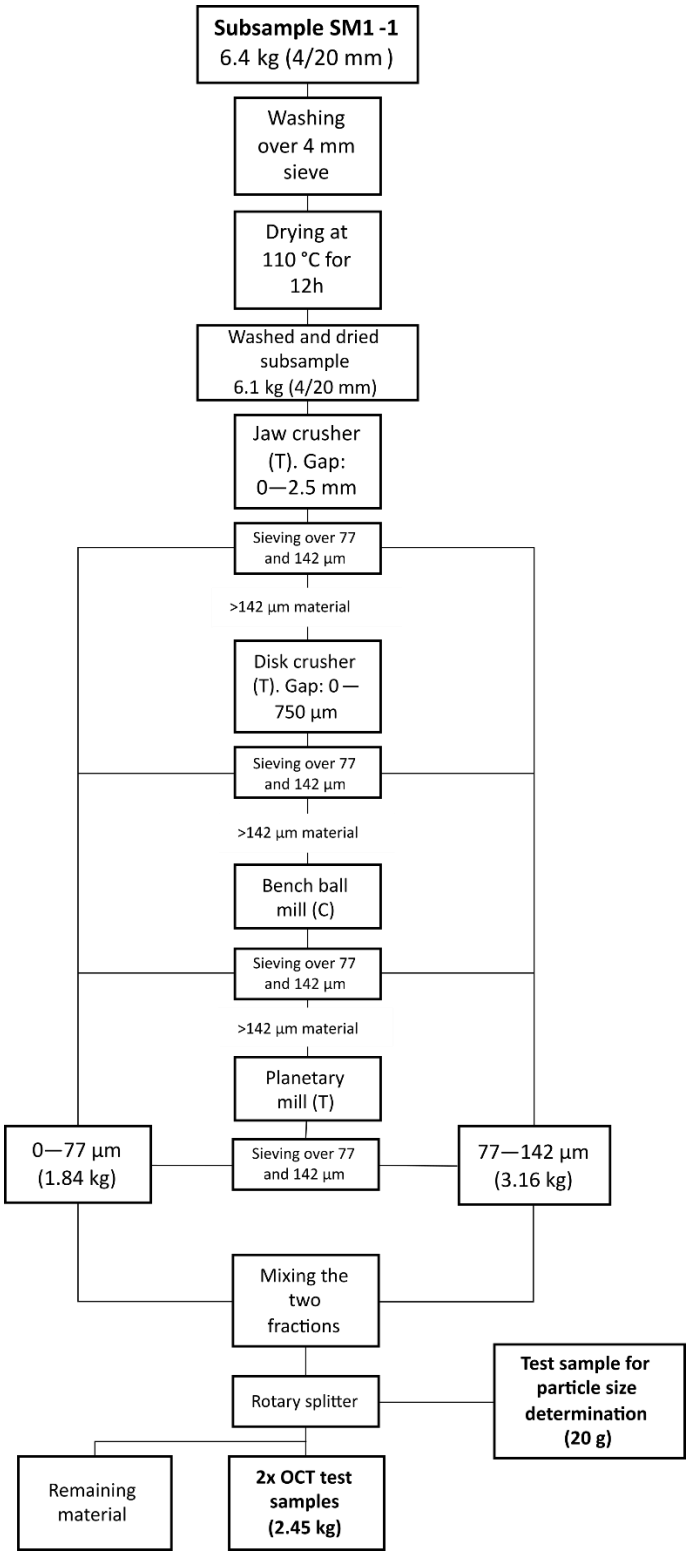

Figure B.6: The sample preparation process of subsample SM1-1 to reach the target size of <142 µm (BBM-C pathway). (T): tungsten carbide equipment. (S): steel equipment. (C): ceramic equipment.

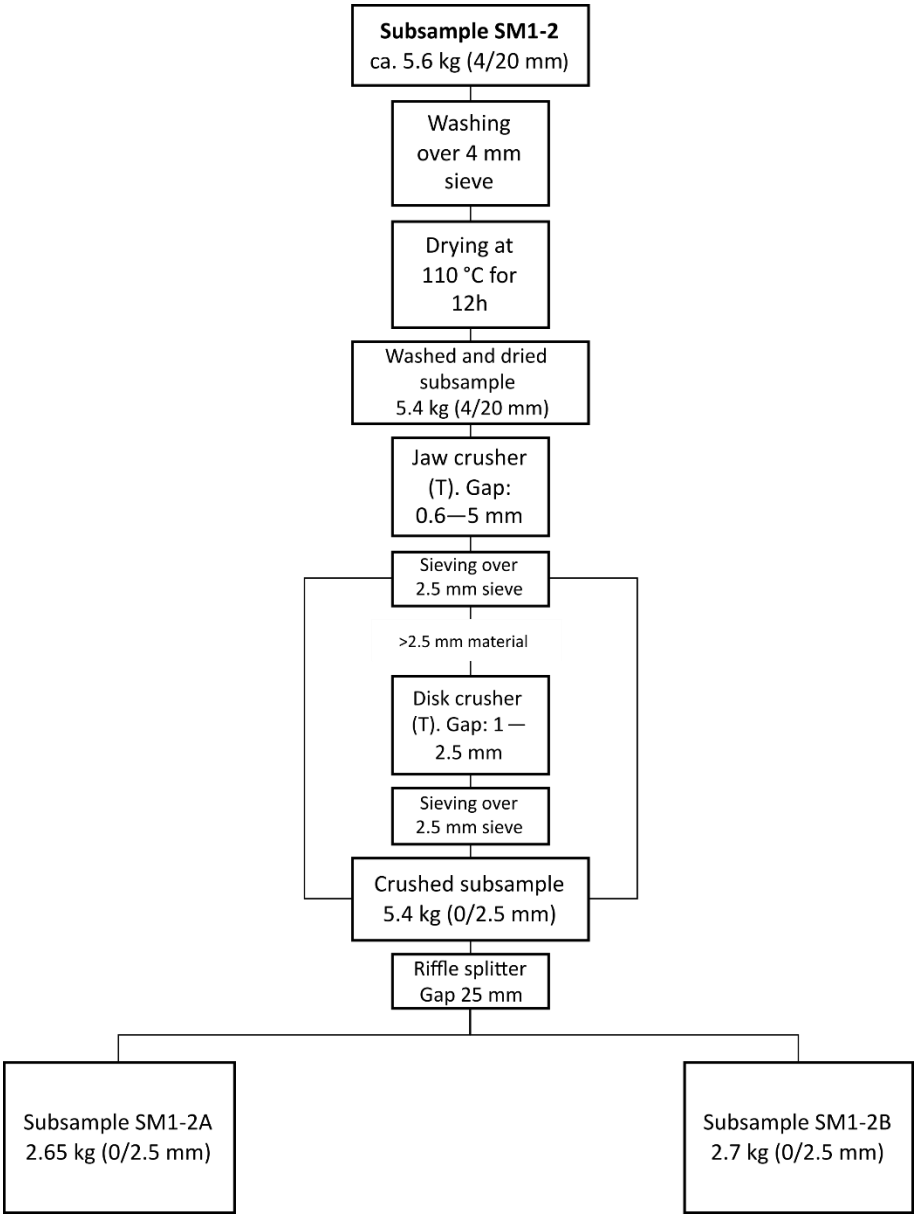

Figure B.7: The flowchart shows the preparation process of subsample SM1-2 until riffle splitting the material into subsample SM1-2A and SM1-2B. (T): tungsten carbide equipment. (S): steel equipment. (C): ceramic equipment.

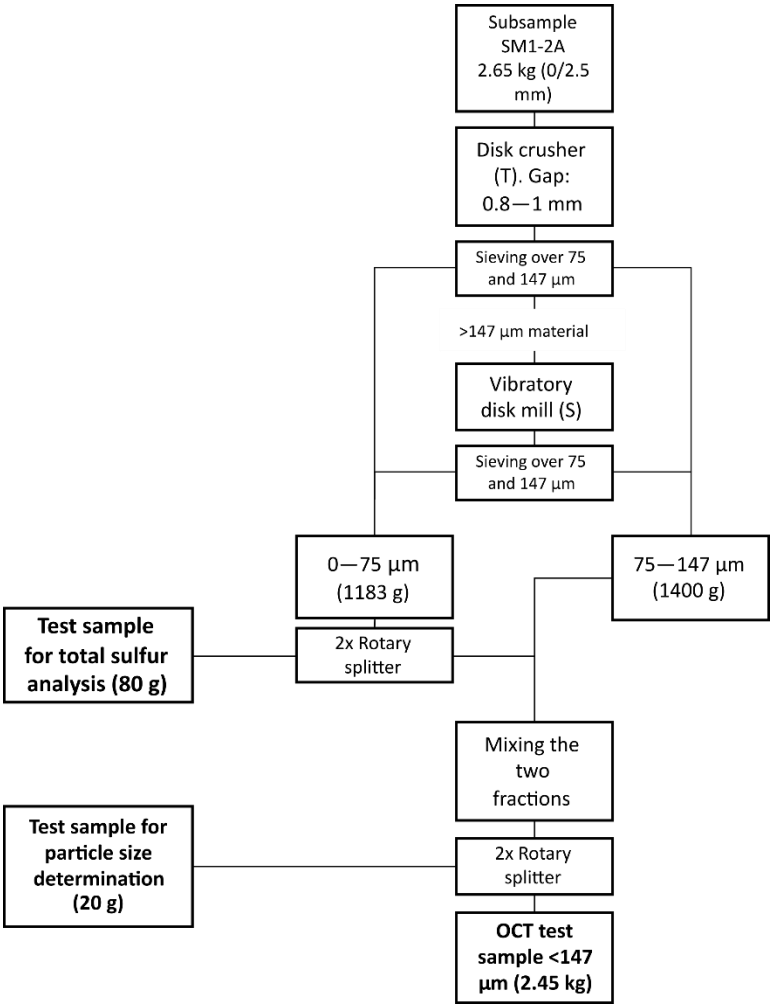

Figure B.8: The flowchart shows the preparation process (pathway VDM-S) of the subsample SM1-2A. (T): tungsten carbide equipment. (S): steel equipment. (C): ceramic equipment.

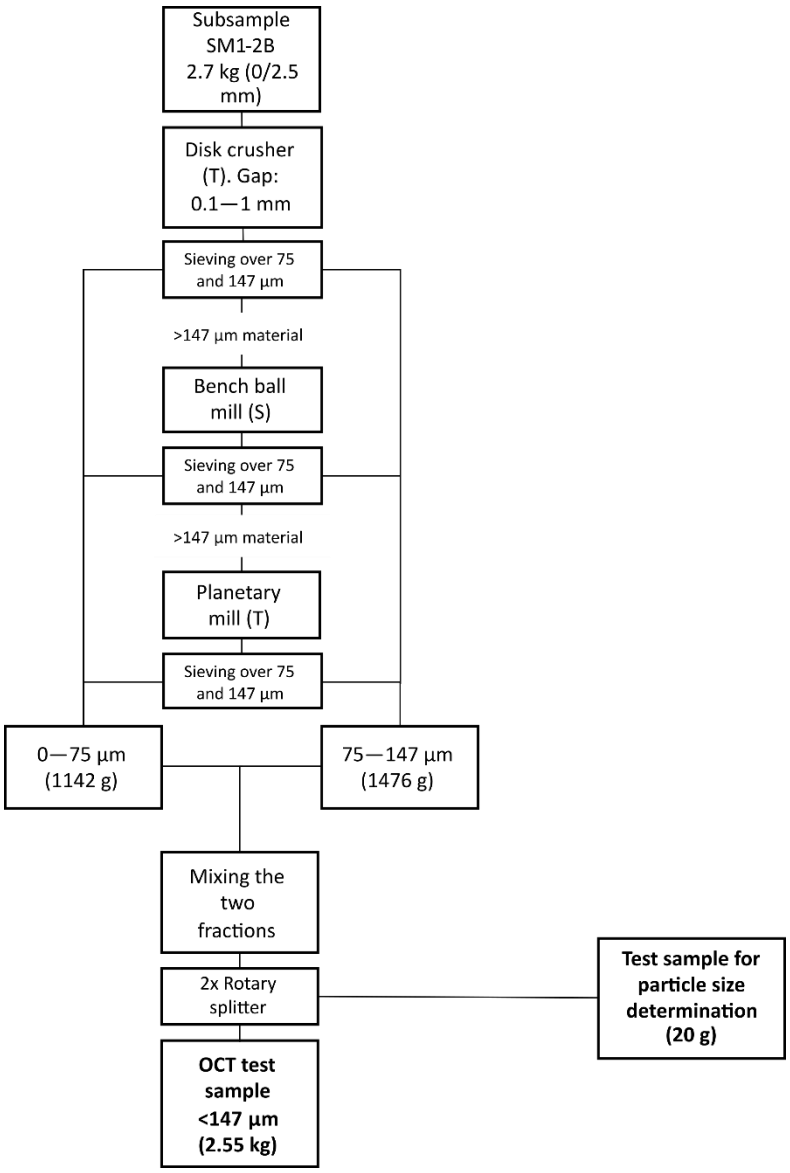

Figure B.9: The preparation methodology for subsample SM1-2B. The pathway used for this subsample was BBM-S. (T): tungsten carbide equipment. (S): steel equipment. (C): ceramic equipment.

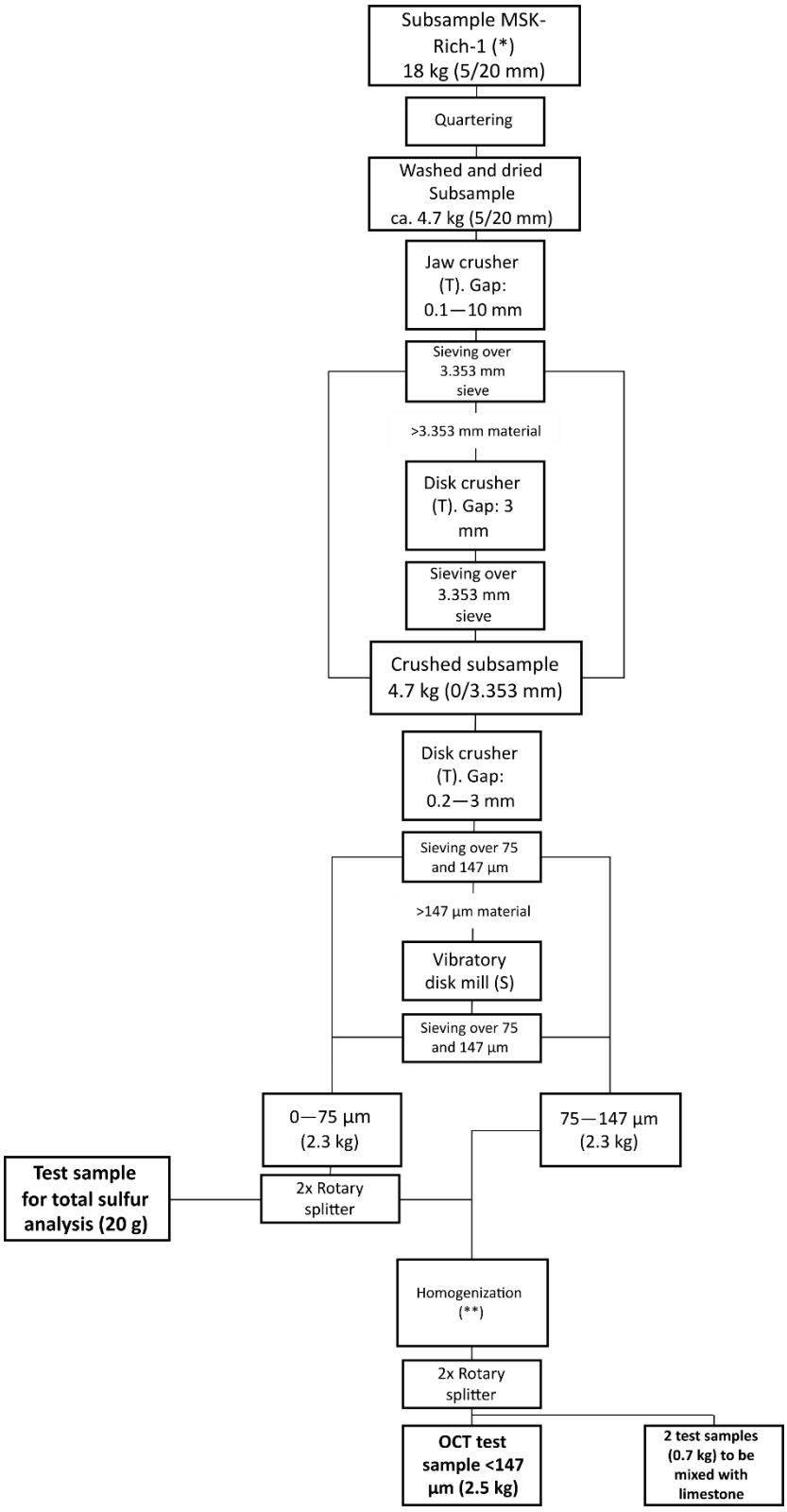

Figure B.10: The preparation methodology of subsample MSK-Rich-1 with the pathways VDM-S. (T): tungsten carbide equipment. (S): steel equipment. (C): ceramic equipment. (*) The subsample was washed and dried. (**) Homogenization was carried out by passing the material through a riffle splitter for a total for five times.

Appendix C: Time consumption

Table C.1: The time consumed by sample preparation (rough estimate). Time spent on splitting, washing and drying is not considered. Sample preparation at SINTEF was carried out by a trained laboratory technician.
**Remaining aggregate mass with a particle size >147 µm (or >2.5 mm for †)) that is fed to the crushing or grinding equipment. For an example explaining this table, see Section 8.2.

Subsample (pathway)	Mass** [kg]	Fraction [mm]	Equipment	Location of equipment	Operator	Time spent
Lim-1 (BBM-C)	21.2	4/16	Jaw crusher (tungsten).	Coarse crushing - NTNU	The author	3h
	15.6	<2.5	Disk crusher (tungsten)	Coarse crushing - NTNU	The author	3h
	3	<1	Bench ball mill (ceramic)	Fine crushing - NTNU	The author	17.5h
				Total time spent:		**23.5h**
SM1-1 (BBM-C)	6.1	4/20	Jaw crusher (tungsten)	Coarse crushing - NTNU	The author	3h
	5.6	<2.5	Disk crusher (tungsten)	Coarse crushing - NTNU	The author	2h
	3.17	<1	Bench ball mill (ceramic)	Fine crushing - NTNU	The author, SINTEF	23h
	0.13	<0.5	Planetary mill (tungsten)	Fine crushing - NTNU	SINTEF	1h
				Total time spent		**29h**
Lim-2A (VDM-S)	3.2	4/16	Disk crusher (tungsten)	Knuserommet - SINTEF	SINTEF	1h
	2.36	<1	Vibratory disk mill (steel)	Knuserommet - SINTEF	SINTEF	4-5h
				Total time spent		**5-6h**
Lim-2B (BBM-S)	3.2	4/16	Disk crusher (tungsten)	Knuserommet - SINTEF	SINTEF	1h
	1.4	<1	Bench ball mill (steel)	Fine crushing - NTNU	The author	5-6h
	0.07	<0.5	Planetary mill (tungsten)	Fine crushing - NTNU	The author	1h
				Total time spent		**7-8h**
SM1-2	5.4	4/20	Jaw crusher (tungsten)	Coarse crushing - NTNU	SINTEF	3h
	<5.4†	<4	Disk crusher (tungsten)	Knuserommet - SINTEF	SINTEF	2h
SM1-2A (VDM-S)	2.65	<2.5	Disk crusher (tungsten)	Knuserommet - SINTEF	SINTEF	1h
	1.78	<1	Vibratory disk mill (steel)	Knuserommet - SINTEF	SINTEF	8-9h
SM1-2B (BBM-S)	2.73	<2.5	Disk crusher (tungsten)	Knuserommet - SINTEF	SINTEF	4h
	0.86	<1	Bench ball mill (steel)	Fine crushing - NTNU	SINTEF	3h
	0.13	<0.5	Planetary mill (tungsten)	Fine crushing - NTNU	SINTEF	1h
				Total time spent:		**22-23h**
MSK Rich-1 (VDM-S)	4.65	5/20	Jaw crusher (tungsten)	Coarse crushing – NTNU	SINTEF	2h
	4.65	<3.353	Disk crusher (tungsten)	Knuserommet - SINTEF	SINTEF	2h
	3.21	<1	Vibratory disk mill (steel)	Knuserommet - SINTEF	SINTEF	11h
				Total time spent		**15h**

Appendix D: Particle size distribution curves

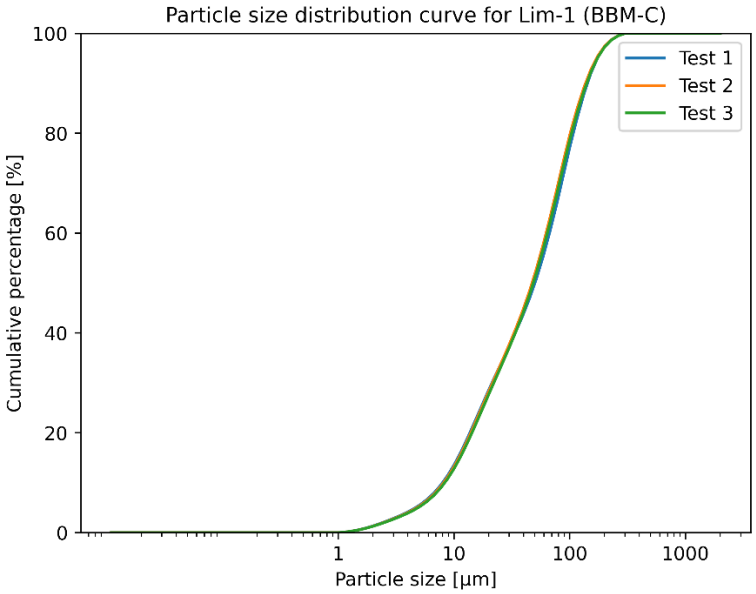

Figure D.1: The particle size distribution curves for the test sample Lim-1 (pathway BBM-C) found by laser scattering (*Horiba LA-960*). The result of each tested specimen (1—3 g) is referred to as Test 1, 2 and 3.

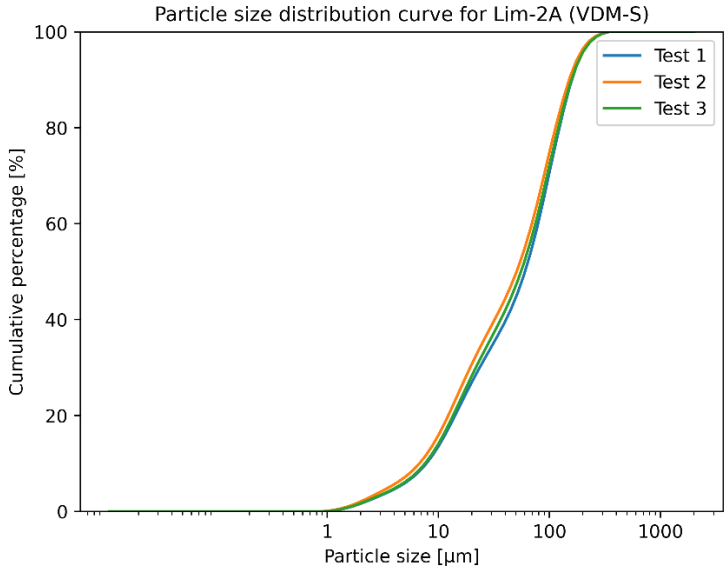

Figure D.2: The particle size distribution curves for the test sample Lim-2A (pathway VDM-S) found by laser scattering (*Horiba LA-960*). The result of each tested specimen (1—3 g) is referred to as Test 1, 2 and 3.

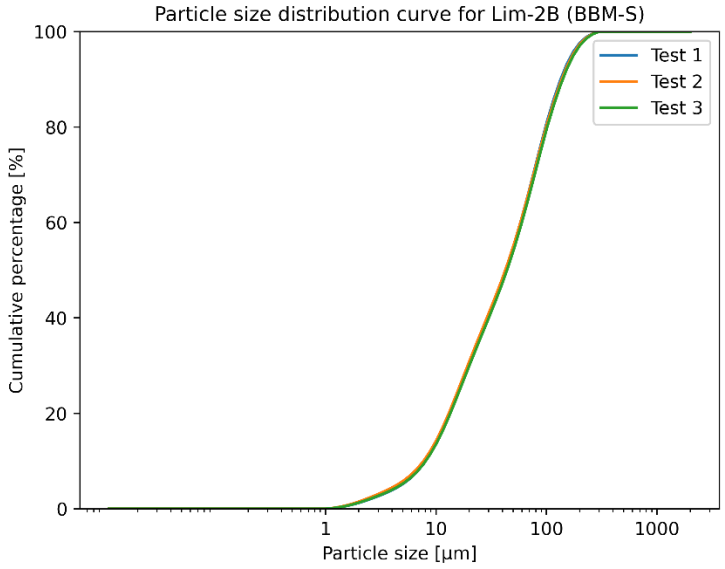

Figure D.3: The particle size distribution curves for the test sample Lim-2B (pathway BBM-S) found by laser scattering (*Horiba LA-960*). The result of each tested specimen (1—3 g) is referred to as Test 1, 2 and 3.

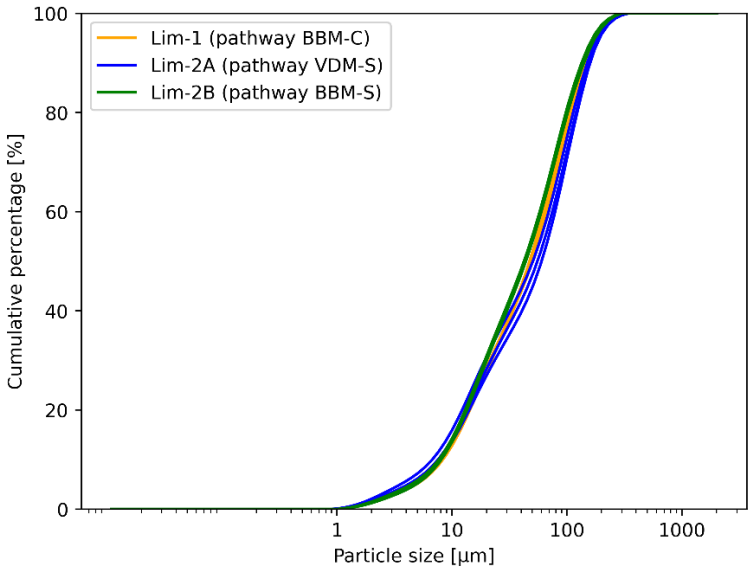

Figure D.4: The particle size distribution for all the limestone test samples. Three curves are plotted for each test sample representing tests 1, 2 and 3 introduced in the previous figures.

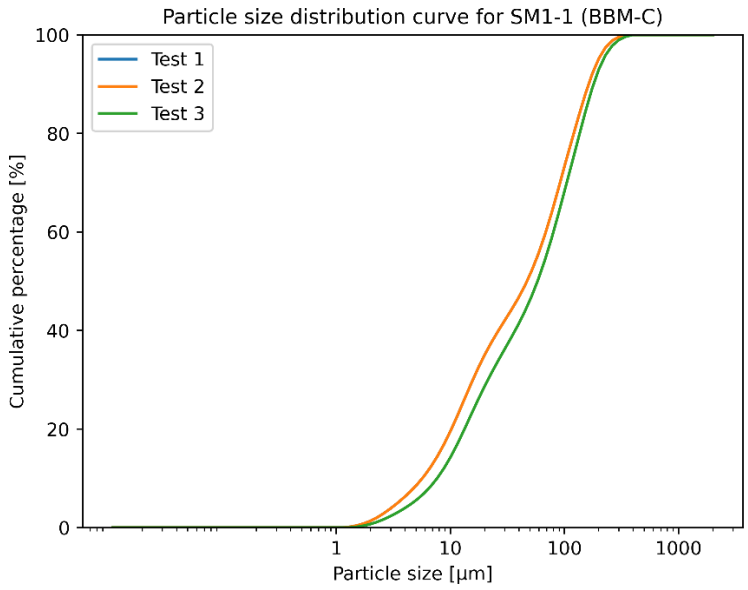

Figure D.5: The particle size distribution curves for the test sample SM1-1 (pathway BBM-C) found by laser scattering (*Horiba LA-960*). The result of each tested specimen (1—3 g) is referred to as Test 1, 2 and 3.

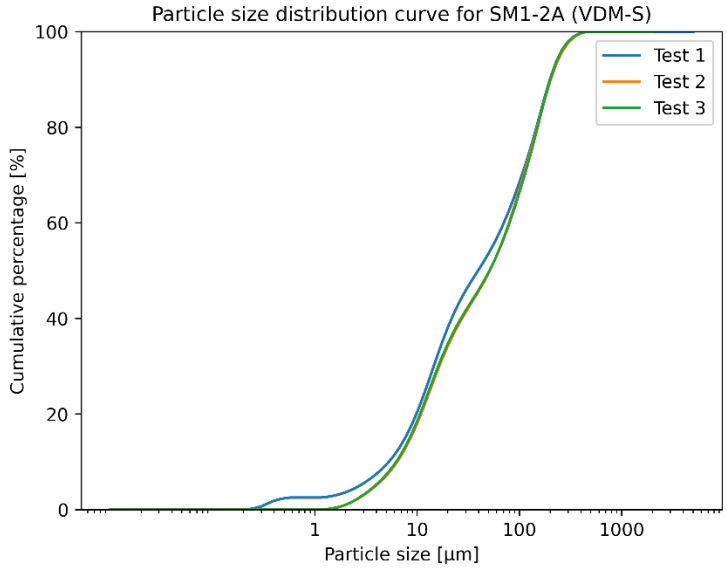

Figure D.6: The particle size distribution curves for the test sample SM1-2A (pathway VDM-S) found by laser scattering (*Horiba LA-960*). The result of each tested specimen (1—3 g) is referred to as Test 1, 2 and 3.

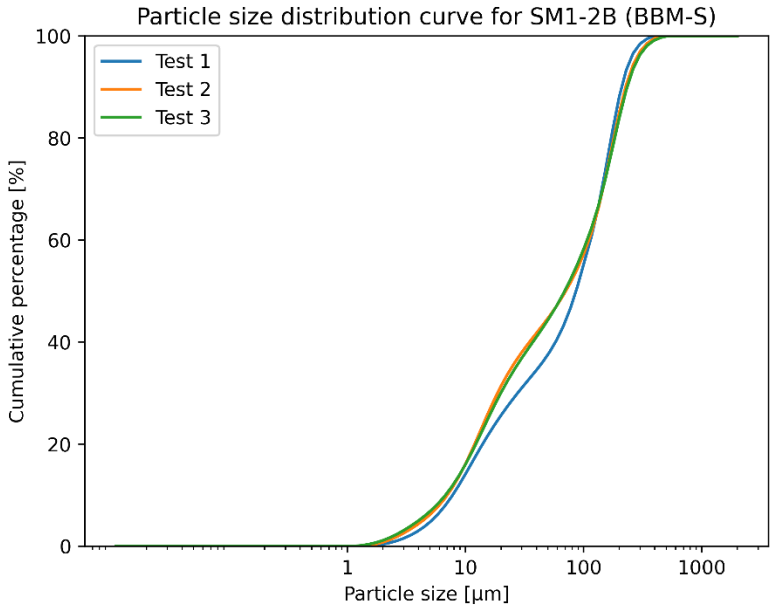

Figure D.7: The particle size distribution curves for the test sample SM1-2B (pathway BBM-S) found by laser scattering (*Horiba LA-960*). The result of each tested specimen (1—3 g) is referred to as Test 1, 2 and 3.

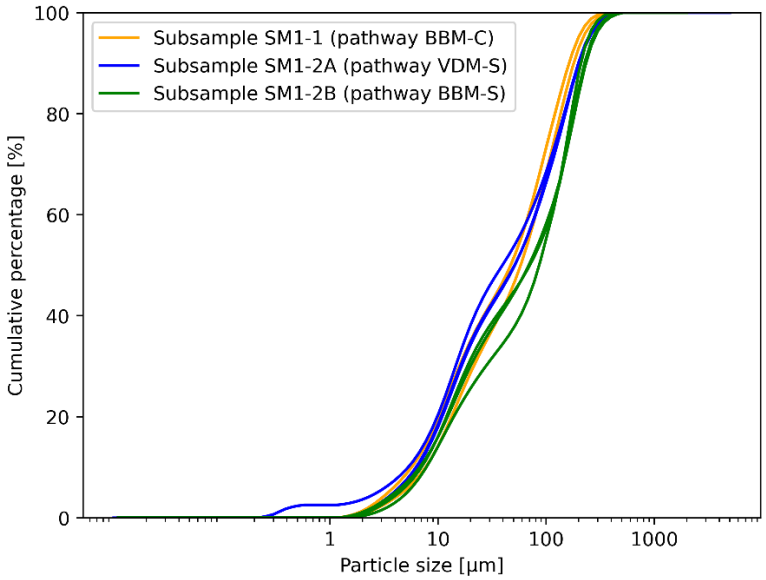

Figure D.8: The particle size distribution for all the SM1 test samples. Three curves are plotted for each test sample representing tests 1, 2 and 3 introduced in the previous figures.

Appendix E: Material loss

Table E.1: The table shows the amount of material lost for each subsample prepared as part of the present study. The loss of material is calculated based on the washed and dried subsample mass.

Subsample	**Aggregate**	**Sample preparation pathway in Figure 7.2**	**Material loss as percentage of washed and dried subsample mass**
PreLim-1	Limestone	-	-
PreLim-2	Limestone	-	-
PreLim-3	Limestone	-	11.7%
Lim-1	Limestone	BBM-C	6.5%
Lim-2A	Limestone	VDM-S	6%
Lim-2B	Limestone	BBM-S	8.6%
SM1-1	SM1	BBM-C	18%
SM1-2A	SM1	VDM-S	2.4%
SM1-2B	SM1	BBM-S	4.2%
MSK-Rich-1	MSK Rich	VDM-S	4.4%

Appendix F: Flowchart of proposed sample preparation procedure

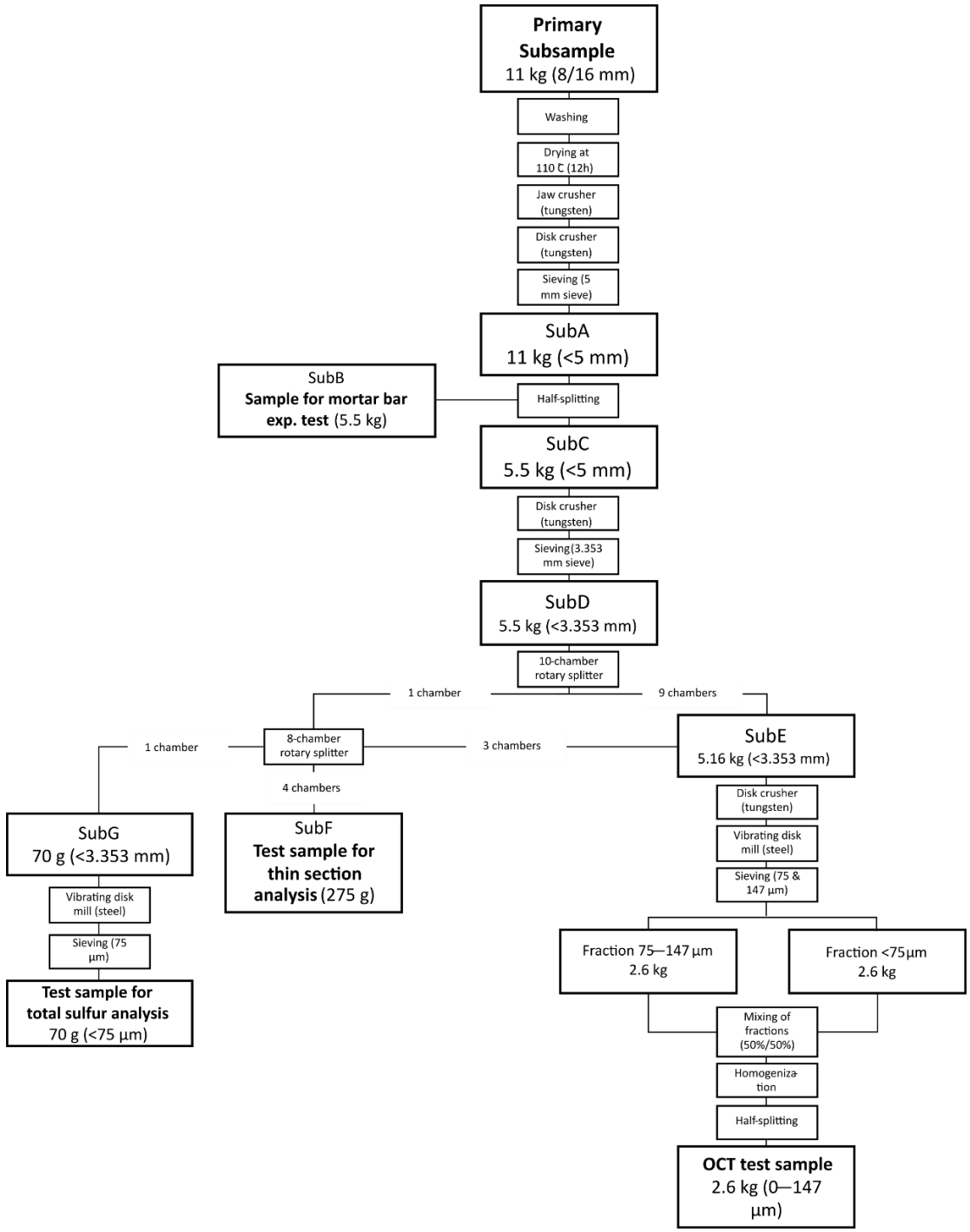

Figure F.1: The figure shows the recommended sample preparation procedure. SubA referrs to the subsample after washing, drying and crushing to a D_{max} of 5 mm. SubB and SubC denote the subsamples formed when subsample SubA is divided in half. The subsample SubD referrs to the subsample SubC after crushing to a D_{max} of 3.353 mm. SubE, SubF and SubG are subsamples formed when dividing SubD in a 10- and an 8-chamber rotary splitters.

Appendix G: Proposed sample preparation (G1) and OCT procedure (G2)

Sample preparation procedure

1. Scope

The following procedure describes the sample preparation for total sulfur analysis (Step I) and the oxygen consumption test, OCT (Step II) of the Canadian testing protocol (Rodrigues et al. (2016)) for sulfide-bearing aggregates. The sampling of material to be further prepared for the mortar bar expansion test (Step III) and for any thin section analysis is also illustrated. Therefore, the procedure shows how one sample from the aggregate producer can be prepared for all tests of the Canadian testing protocol.

2. Documentation and references

The following sources have been used in the development of this procedure:

1. Canadian Standards Association. CSA A23.1:2019. Annex P (informative) - Impact of sulphides in aggregate on concrete behaviour and global approach to determine potential deleterious reactivity of sulphide-bearing aggregates. Mississauga, Ontario, Canada 2019.
2. Rodrigues A, Duchesne J, Fournier B. Quantitative assessment of the oxidation potential of sulfide-bearing aggregates in concrete using an oxygen consumption test. Cement & concrete composites. 2016;67:93-100.
3. Rodrigues A, Duchesne J, Fournier B, Durand B, Shehata MH, Rivard P. Evaluation protocol for concrete aggregates containing iron sulfide minerals. ACI materials journal. 2016;113(3):349-59.
4. Pyrrhotite Project - Interlaboratory Study - Document 1 - General Instructions of Phase I. Université Laval; 2023.
5. Pyrrhotite Project - Interlaboratory Study - Document 2 - Determination of Sulphide Sulphur Content of Concrete Aggregates (Ts). Université Laval; 2023.
6. Pyrrhotite Project - Interlaboratory Study - Document 3 - Detection of the Oxidation Potential of Sulphide-Bearing Aggregates by an Oxygen Consumption Test (OCT). Université Laval; 2023.
7. Internal procedure: Vacuum packing of dry powders. Kamila Zablocka. 2023.
8. Internal procedure: Sample handling procedure for coarse materials. N. Oberhardt. 2020 (see Attachment 2).

3. Equipment

The following list is chosen based on the available equipment at IGP (Department of Geoscience and Petroleum) at NTNU. Similar equipment can be used.

- 42.2 cm (*SWECO*) sieves with the following sieve openings:
  - 16 mm
  - 8 mm
  - 2.5 mm
- 20.7 cm sieves with the following sieve openings:
  - 5 mm
  - 3.353 mm (or sieve with a similar opening, for example 3.5 mm)
  - 147 µm

    - 75 µm
- 3-4 stainless steel trays.
- A ventilated oven (for drying at 110 ˚C)
- *RETSCH BB100* jaw crusher, to be only used with **tungsten plates**.
- *FRITSCH disk mill pulverisette 13* (hereafter referred to as "disk crusher"), to only be used with **tungsten disks**.
- *RETSCH Vibratory Disk Mill RS 200* with 100 ml steel grinding set (hereafter referred to as "vibratory disk mill").
- 10-chamber rotary splitter
- 8-chamber rotary splitter
- Small splitter (opening 25 mm)
- Riffle splitter
- Plastic bags
- Scale (accuracy ±1 g)
- Vacuum sealer

The material should be fed to the crushing equipment (jaw and disk crusher) continuously to ensure homogenous crushing/grinding.

Prior to use, all equipment to be used in this procedure must be cleaned with water and/or compressed air.

4. Safety procedures

If the necessary precautions are not followed, safety risks in this procedure can include the risk of inhaled dust, physical injury or hearing damage. Make sure the necessary PPE (dust mask, laboratory coat, safety glasses, hearing protection and appropriate gloves) are used when preparing samples. When crushing, grinding or splitting samples, make sure that the working area is well-ventilated.

5. Procedure

Throughout this procedure, any loss of material should be avoided as much as possible.

Attachment 1 Figure 1 (and steps 1 and 2 below) illustrates how a larger sample from the producer (in this **example**, 88 kg with fraction 8/16 mm) can be treated to produce a primary subsample of 11 kg (to be further treated in Figure 2).

Note that the weights provided in steps 1 to 2 below are used as an example. A different starting field sample (with fraction 8/16 mm or similar) can be used as long as a representative subsample (denoted as *primary subsample*) with a weight of 11—15 kg is obtained.

1. Obtain a representative sample of 22 kg (sample 2 in Figure 1) from the field sample (88 kg) following a quartering procedure modified after an internal procedure (the sample handling procedure for coarse materials by Nikolas Oberhardt (2020)). Attachment 2 shows how this procedure can be adapted for this step.

2. Divide sample 2 into two parallel samples (samples 3 and 4) using a small splitter (opening 25 mm).

The following steps describe the processing of **sample 3** (hereinafter referred to only as "primary subsample"). The processing of the primary subsample is shown in Attachment 1 Figure 2.

Note that the remaining part of the procedure assumes that the weight of the primary subsample is 11 kg (minimum weight). The weights given below are provided as minimum weights for each step.

3. Spread 1-2 kg of the primary subsample on the 2.5 mm sieve. Spray the material with water.
4. Place the washed material in a container.
5. Repeat steps 3 and 4 until the entire primary subsample is washed.
6. Place the washed subsample in multiple clean stainless-steel trays. Place the trays in a ventilated oven at 110 ˚C for 12 hours so that the subsample reaches constant mass.
7. Place the washed and dried primary subsample in a container and mix properly.
8. Crush the subsample with the *RETSCH BB100* jaw crusher. Use a gap size of **10 mm**.
9. Sieve (by hand) the crushed material over the 5 mm sieve.
10. Crush the fraction >5 mm in the jaw crusher. Reduce the gap size gradually and record the new one.
11. Repeat steps 9 and 10 for a total of **5 passes** through the jaw crusher. Reduce the gap size gradually with each pass until the minimum gap of the jaw crusher is reached.
12. Make sure to recover any material stuck in the jaw crusher.
13. Weigh the primary subsample and record the weight.
14. Let the material >5 mm pass through the disk crusher. Use the gap size **5 mm**.
15. Sieve (by hand) the crushed material over the 5 mm sieve.
16. Crush the material remaining >5 mm again in the disk crusher. Reduce the gap size and record the new gap size.
17. Repeat steps 15 and 16 **until no material is retained on the 5 mm sieve**. Reduce the gap size gradually with each pass. The primary subsample, now reduced to the particle size <5 mm will now be referred to as SubA.

18. Recover any material stuck in the disk crusher.

19. Feed the entire SubA material (the crushed primary subsample) to a 10-chamber rotary splitter. The primary subsample will be divided in half with each five sampling cups making up one subsample (SubB or SubC).

20. Store SubB (with a weight of 5.5 kg) in a closed container and give the container the following name:
    [Aggregate name] (<5 mm) sample for mortar bar test [date of splitting process].
    Note: the minimum mass needed for this step is 5 kg.

Only subsample **SubC** (5.5 kg) will be processed further in this procedure.

21. Grind the mass of SubC (5.5 kg) with the disk crusher. Use the gap size **3 mm**.

22. Sieve (by hand) the crushed material over the 3.353 mm sieve (or sieve with a similar sieve opening).

23. Crush the fraction >3.353 mm again in the disk crusher. Reduce the gap size and record the new gap size.

24. Repeat steps 22 and 23 **until no material is retained on the 3.353 mm sieve**. Reduce the gap size gradually with each pass. The SubC material, now reduced to the particle size <3.353 mm will now be referred to as SubD.

25. Recover any material stuck in the disk crusher.

26. Feed subsample SubD to the 10-chamber rotary splitter. Empty 9 of the chambers (sampling cups) in a large container.

27. Divide the material in the remaining sampling cup from step 26 in an 8-chamber rotary splitter. After the splitting process, each sampling cup in the 8-way rotary splitter should have around 70 g of material. The material from 4 sampling cups should be mixed to form subsample SubF (to be used in **thin section analysis**). The fifth cup will make up subsample SubG (to be processed further for **total sulfur analysis**). The last three cups should be mixed with the material in the large container from step 26 forming subsample SubE (5.16 kg).

28. Record the weight of subsample SubE. The weight should be approx. 5.16 kg.

The next few steps describe how **SubE** is processed.

29. Crush the mass of SubE (5.16 kg) with the disk crusher. Start with the gap size **1 mm**.

30. Sieve (by hand) the ground material over the 147 µm and 75 µm sieves.

31. Place the material passing through the 147 µm and 75 µm sieves **immediately into separate sealed plastic bags** (one plastic bag for each fraction). The plastic bags can be reopened when more material is added.

32. If the weight of the fraction <75 µm exceeds the weight of the fraction 75—147 µm, then increase the gap size of the disk crusher. Record the new gap size.

33. Crush the material >147 µm in the disk crusher. Reduce the gap size and record the new one.

34. Repeat steps 30-33 until the material has passed through the disk crusher **10 times** (or until the disk crusher is no longer effectively crushing the material). Make sure to reduce the gap size gradually (until the **minimum gap size** is reached for the final two passes).

35. Recover all the material stuck inside of the disk crusher.

36. Record the weight of the fractions >147 µm, 75—147 µm and <75 µm.

37. Add 100 g (or less) of the fraction >147 µm to the grinding set of the vibratory disk mill. Grind the material with the mill, and record the following parameters: runtime, RPM and amount of material added.

38. Sieve (by hand) the ground material over the 147 µm and 75 µm sieves.

39. Repeat step 31.

40. If the weight of the fraction <75 µm exceeds the weight of the fraction 75—147 µm, then decrease the runtime or the RPM. Record the new runtime and RPM.
    Note: try to select the RPM and the runtime so that they are kept constant throughout the grinding process

41. Repeat steps 37-40 **until the entirety of the material passes the 147 µm sieve**.

42. Record the weight of the fractions 75—147 µm and <75 µm.

43. Place the two fractions 0—75 µm and 75—147 µm in the same container and mix well.

44. Let the mixed material pass through a riffle splitter 5 times. In this step, the sample will not be divided, but the material is passed through the splitter for further homogenization of the fractions.

45. Feed the material into a 10-chamber rotary splitter. 5 sampling cups (chambers) shall make up one **OCT test sample** (A or B). Each specimen should have a mass of about 2.6 kg.
    Note: the absolute minimum aggregate mass needed for the OCT is calculated according to equation 1 in Appendix G2 (OCT procedure).

46. If the OCT specimens will be tested more than one week after their preparation, they should be vacuum sealed. The internal procedure "Vacuum packing of dry powders" can be followed.
    Note: the machine used for vacuum packing by the pyrrhotite project is similar but works slightly differently compared to the default machine in the vacuum packing procedure. Make sure to read the instructions of the machine used by the pyrrhotite project for correct vacuum sealing.

Note that if samples from two different aggregates are to be mixed to make up one OCT test sample, then the aggregate mixture must pass through a riffle splitter 5 times for additional homogenization.

The next few steps deal with the processing of SubG

47. Add subsample SubG to the grinding set of the vibratory disk mill. Grind the material with the mill, and record the following parameters: runtime, RPM and amount of material added.

48. Sieve subsample SubG over the 75 µm sieve.

49. Grind the material retained on the 75 µm sieve in the vibratory disk mill until 100% of subsample SubG passes the 75 µm sieve.

Attachment 1

Appendix G1: Recommended sample preparation procedure

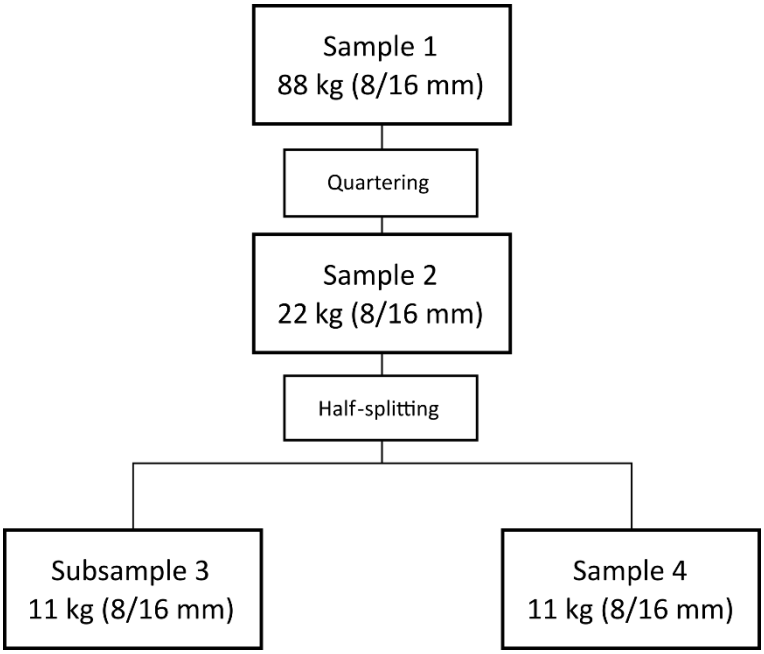

Figure 1: The sample preparation pathway. Part 1 (steps 1-2 in the procedure above). See Attachment 2 for how the quartering process is carried out.

Appendix G1: Recommended sample preparation procedure

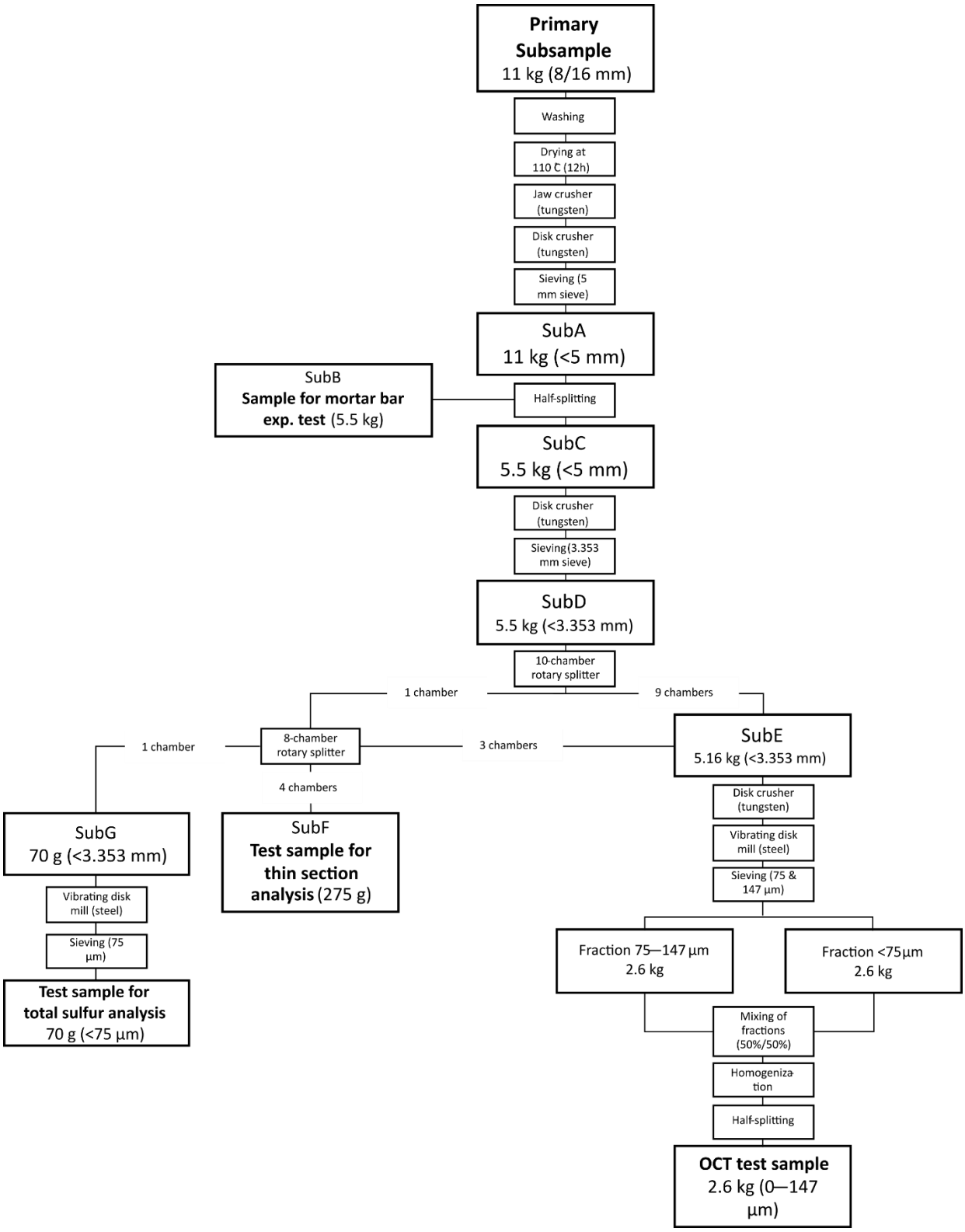

Figure 2: Part 2 of the sample preparation pathway (steps 3 to 45 in the procedure).

Attachment 2

Sample quatering overview

88 kg field sample

1. 1/4 splitting

4 samples 22 kg each

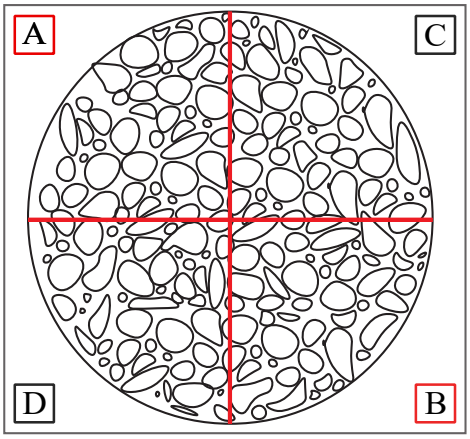

Sample spread out in unilayer on ground

Sample C and D kept for later analysis

Samples A and B form a new circle

2. 1/4 splitting of samples A and B

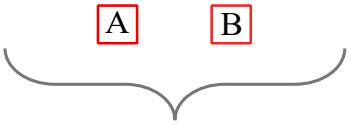

4 samples 11 kg each

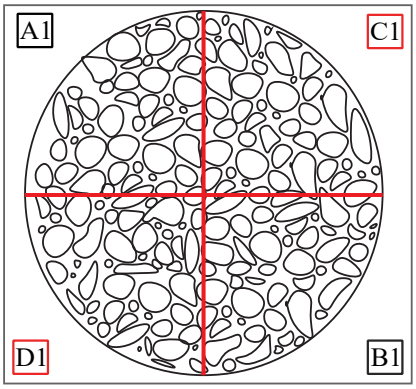

Samples A1 and B1 are kept for later analysis

Samples C1 and D1 are mixed to form the sample 2 (22 kg)

Sample 2 is then divided in half by a splitter to samples 3 and 4

Modified after "Sample handling procedure for coarse materials N. Oberhardt, 2020"

Oxygen consumption test procedure

1. Scope

The following procedure describes how the oxygen consumption test (OCT) is carried out. The OCT constitutes Step II in a Canadian testing protocol for sulfide-bearing aggregates.

The purpose of the OCT is to find out how much oxygen is consumed by a mixture of aggregate material and water. Aggregates containing significant amounts of sulfide minerals (particularly pyrrhotite) are expected to oxidize and consume more oxygen than aggregates free or containing very little sulfide minerals.

2. Documentation and references

The following sources have been used in the development of this procedure:

1. Canadian Standards Association. CSA A23.1:2019. Annex P (informative) - Impact of sulphides in aggregate on concrete behaviour and global approach to determine potential deleterious reactivity of sulphide-bearing aggregates. Mississauga, Ontario, Canada 2019.
2. Rodrigues A, Duchesne J, Fournier B. Quantitative assessment of the oxidation potential of sulfide-bearing aggregates in concrete using an oxygen consumption test. Cement & concrete composites. 2016;67:93-100.
3. Rodrigues A, Duchesne J, Fournier B, Durand B, Shehata MH, Rivard P. Evaluation protocol for concrete aggregates containing iron sulfide minerals. ACI materials journal. 2016;113(3):349-59.
4. Pyrrhotite Project - Interlaboratory Study - Document 1 - General Instructions of Phase I. Université Laval; 2023.
5. Pyrrhotite Project - Interlaboratory Study - Document 3 - Detection of the Oxidation Potential of Sulphide-Bearing Aggregates by an Oxygen Consumption Test (OCT). Université Laval; 2023.

3. Equipment and materials

- Acrylic reaction cell (200 mm in height, 146.5 mm in diameter). The two reaction cells purchased by SINTEF from Canada are shown in Figure 1.
- Oxygen sensor (Apogee SO-110).
- RH sensor (EE06-FT1A1).
- Data acquisition module (ADAM-4017) and power unit. These are provided in the compact box shown in Figure 2.
- Steel pestle (see Figure 3).
- Large plastic or stainless-steel tray.
- Stainless-steel spoon.
- Small scoop.
- Plastic bags.
- Scale (accuracy ±1 g).
- Deionized water.
- Plastic beakers (200—1000 ml).

- Silicon grease by VWR Chemicals (art. number: 6674.0050).
- Polystyrene case of the appropriate height (shown in Figure 4).
- Timer (to be set for 15 min).

All equipment to be used in this procedure must be properly cleaned before use to avoid any contamination of the tested samples.

4. Safety measures

The use of PPE (particularly gloves, dust mask and laboratory coat) is necessary to avoid any adverse health effects while conducting the OCT.

5. Necessary aggregate mass and added water mass

See the master thesis, Section 2.3.3.5, for the full detailed equations for the necessary amount of aggregate mass and added water. Equations (1) and (2) below are calculated for the reaction cells that are available in the SINTEF Concrete Laboratory and assume a porosity of 50%.

The OCT test sample (from the sample preparation procedure in Appendix G1) has a mass of 2.6 kg. However, the aggregate mass required for the OCT will be less than 2.6 kg. This necessary amount of aggregate material and deionized water (to be later mixed with the aggregate material) can be calculated from equations (1) and (2), respectively:

$$\text{Required aggregate mass} = [843 \times \rho_{agg}] \quad (1)$$

$$\text{Required water mass} = [843 \times S_{gm}] \quad (2)$$

S_{gm} is called the saturation level and is normally set at 40% (i.e., S_{gm} =0.4) unless explicitly stated. Using equation 2, at 40% saturation, the amount of water needed is 337 g.

ρ_{agg} is the particle density of the aggregate in (g/cm^3) to be found in the CE-declaration of the aggregate or determined through the pycnometer method (according to NS EN 1097-6).

6. Procedure

1. Turn on the computer next to the reaction cells. Make sure that the computer is connected to the internet.
   Note: make sure the computer does not turn off or go into sleep mode throughout the duration of the test.

2. Open the OCT software on the computer. Make sure the upper part of the interactive interface is green (a red color, as shown in Figure 5, indicates that the sensors are not connected to the computer).

3. Make sure that the software is displaying the oxygen concentration values (rather than 0.0) in the red box shown in Figure 5.

4. Empty the OCT test sample (2.6 kg) in a plastic or stainless-steel tray.

5. Using a stainless-steel spoon, remove excess aggregate material from the tray until the aggregate mass specified by equation 1 is reached. Store the excess aggregate material is a sealed plastic bag.

6. Mix the OCT test sample well using your hands. Mixing the aggregate material is necessary to avoid any segregation of the fractions <75 μm and 75—147 μm.

7. Add the mass of deionized water (as calculated in equation 2) to the tray with the aggregate material.

8. Mix the aggregate material and water by hand properly for 15 min. The mixing should produce a homogenous material (avoid lumps).

9. Use a small scoop to add half of the mixture to the reaction cell.

10. Use the steel pestle to apply pressure and compact the mixture until a thickness of 50 mm is achieved (as shown in Figure 6).

11. Add the other half of the mixture to the reaction cell.

12. Compress with the steel pestle until the second layer reaches a thickness of 50 mm. The two layers combined should have a thickness of 100 mm (shown in Figure 7).
    Note: Make sure the surface of the second layer is as even as possible.

13. Add the silicone grease to the top surface of the cell before placing the lid (shown in Figure 8). The silicone grease should be applied uniformly across the entire top surface of the reaction cell.

14. Close the lid of the cell and tighten the screws.

15. Place the polystyrene case around the reaction cell.

16. On the OCT program in the computer, click on “NEW TEST”. Fill in the required information.

17. Click on “START TEST”.

18. The program will now collect the data points from the sensors for 3.5 hours.
    Note 1: Make sure the computer does not turn off or go into sleep mode throughout the duration of the test.
    Note 2: You do not need to click on “STOP TEST” when the test ends because the OCT software automatically stops the test after 210 minutes.

19. To manually calculate the oxygen consumption for the test, use the following formula:

$$O_2 \text{ consumption } [\%] = \frac{O_2 \text{ concentration (at 0.5h)} - O_2 \text{ concentration (at 3.5h)}}{O_2 \text{ concentration (at 0.5h)}} \times 100 \quad (3)$$

Figure 1: The two reaction cells used for the OCT testing at SINTEF.

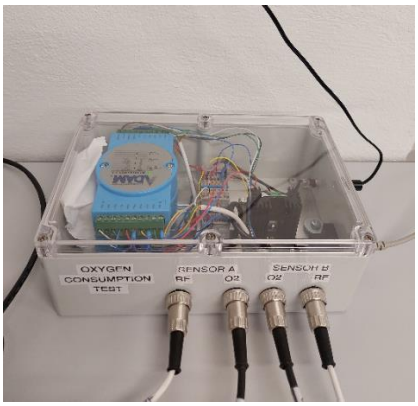

Figure 2: The compact box containing the power unit and the data acquisition module.

Figure 3: The steel pestle used for compacting the aggregate material prior to OCT testing.

Figure 4: The polystyrene case (and its blue base) used to thermally insulate the reaction cells during the OCT.

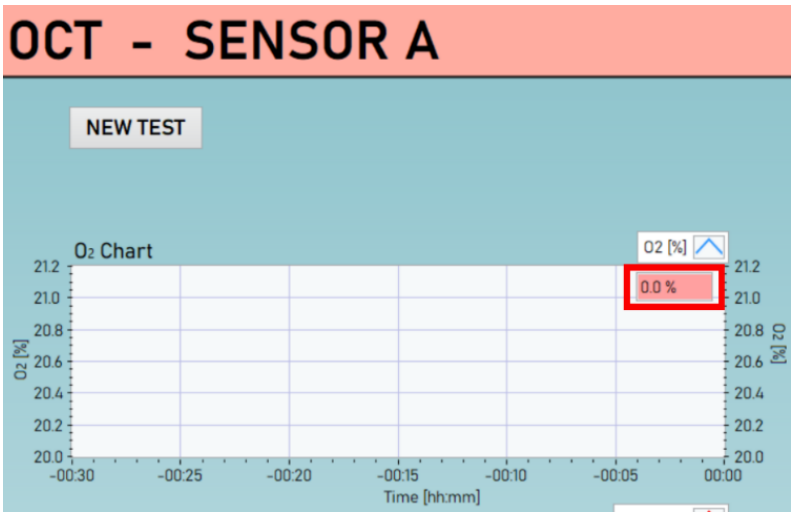

Figure 5: The interface of the OCT software.

Figure 6: The reaction cell after one layer of the aggregate-water mixture (thickness of 50 mm) is added and compacted.

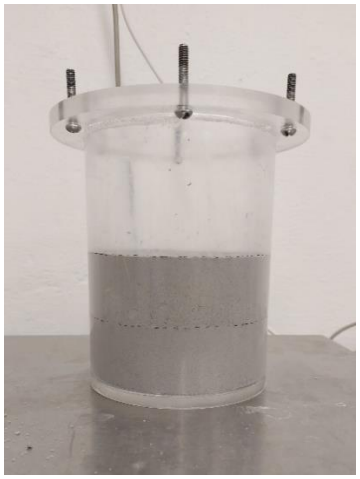

Figure 7: The reaction cell after the mixture of water and aggregate material is added to the cell in two compacted layers with a 100 mm in total thickness.

Figure 8: The picture shows how silicon grease should be applied on the top surface of the reaction cell.

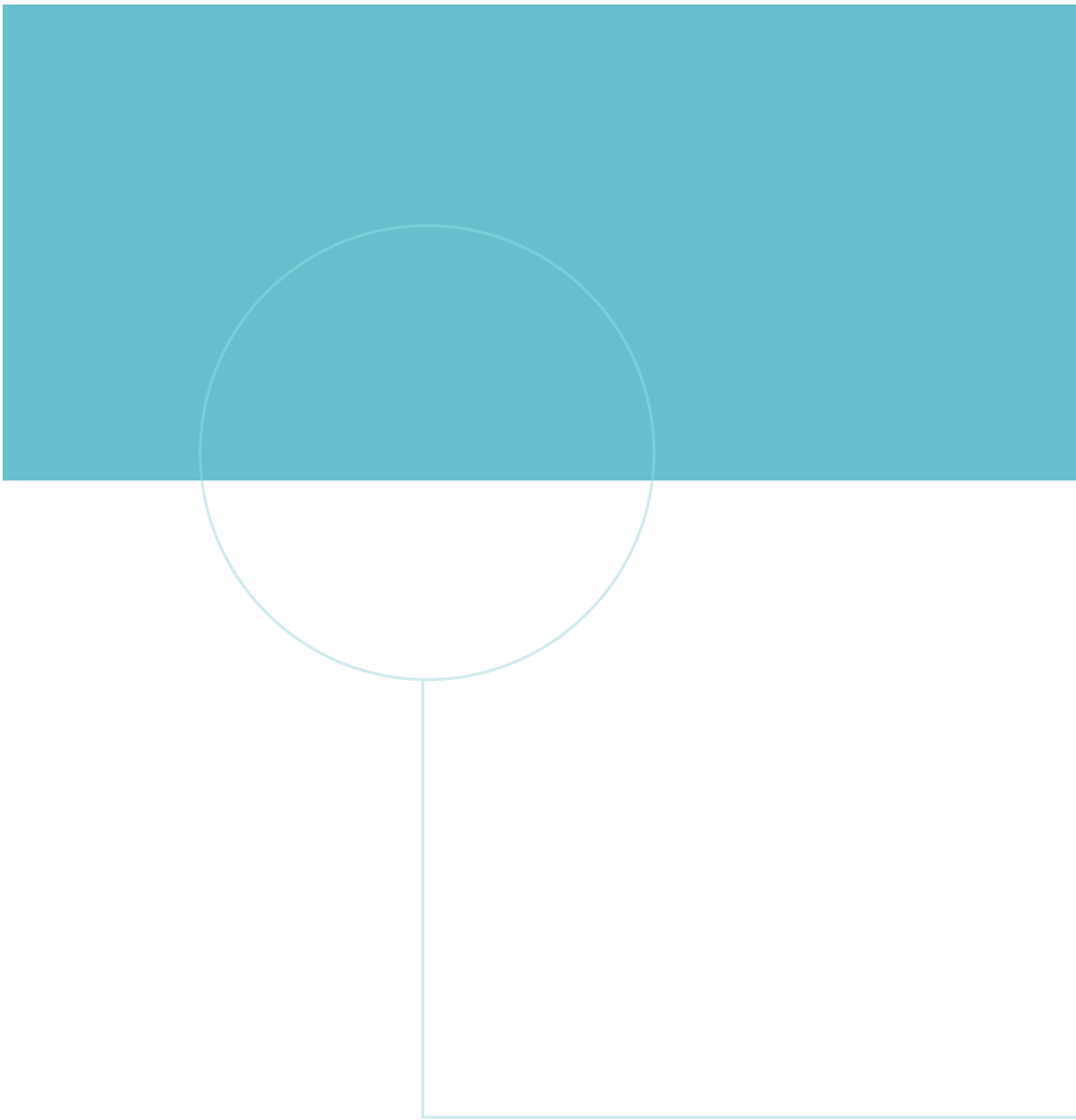

NTNU

Norwegian University of
Science and Technology